ROADVIEW

Robust Automated Driving in Extreme Weather

Project No. 101069576

Deliverable 3.4

Library of validated physics-based parameterised noise models

WP 3 – Validated sensor and sensor noise models for synthetic environments

Authors	Pak Hung Chan (WMG), Jonathan Robinson (WMG), Daniel Gummadi (WMG), Yuri Poledna (THI), Valentina Donzella (WMG)
Lead participant	WMG
Delivery date	30/08/2024
Dissemination level	Public
Type	Other

Version 1.0

Co-funded by the European Union

Innovate UK

Co-funded by the European Union. Views and opinions expressed are however those of the author(s) only and do not necessarily reflect those of the European Union or European Climate, Infrastructure and Environment Executive Agency (CINEA). Neither the European Union nor the granting authority can be held responsible for them. Project grant no. 101069576.

UK participants in this project are co-funded by Innovate UK under contract no.10045139.
Swiss participants in this project are co-funded by the Swiss State Secretariat for Education, Research and Innovation (SERI) under contract no. 22.00123.

Revision history

Author(s)	Description	Date
Pak Hung Chan (WMG), Jonathan Robinson (WMG), Daniel Gummadi (WMG), Yuri Poledna (THI), Valentina Donzella (WMG)	Draft deliverable v0.3	12/08/2024
Martin Sanfridson (RISE)	Review of v0.3	14/08/2024
Pak Hung Chan (WMG), Yuri Poledna (THI), Valentina Donzella (WMG)	Update v0.4	16/08/2024
Amine Ben-Daoued (CE)	Review of v0.4	19/08/2024
Pak Hung Chan (WMG), Yuri Poledna (THI), Valentina Donzella (WMG)	v1.0 Complete	27/08/2024
Mario Ceccarelli (accelCH), Sara Mostafavi (accelCH)	Formatting and formal check	30/08/2024

Contents

List of Figures

List of Tables

Partner short names

THI	Technische Hochschule Ingolstadt
CE	Centre d'études et d'expertise sur les risques, l'environnement, la mobilité et l'aménagement
RISE	RISE Research Institutes of Sweden AB
WMG	The University of Warwick
accelCH	accelopment Schweiz AG

Abbreviations

AAD	**Assisted and Automated Driving**
ACDC	Adverse Conditions Dataset with Correspondences
AI	Artificial Intelligence
D	Deliverable
DNN	Deep Neural Network
DSD	Droplet Size distribution
DSS	Denoise Snow Score
EM	Electromagnetic
FID	Frechet Inception Distance
FMCW	Frequency Modulated Continuous Wave
FR-IQA	Full Reference Image Quality Assessment
FSIM	Feature Similarity Index Measure
HAAR-PSI	Haar Perceptual Similarity Index
HD	Hausdorff Distance
IEEE	Institute of Electrical and Electronics Engineers
ISP	Image Signal Processing
IW-SSIM	Information Content Weighted SSIM
KID	Kernel Inception Distance
LiDAR	Light Detection and Ranging
LISA	LiDAR Light Scattering Augmentation
LWC	Liquid Water Content
MDE	Mean Distance Error
MMDE	Maximum Mean Distance Error

MOR	Meteorological Optical Range
NCAP	New Car Assessment Program
NR	No Reference
PC	Point Cloud
PDD	Puy de Dome
PSNR	Peak Signal to Noise Ratio
RADAR	Radio Detection And Ranging
RCS	Radar Cross Section
REHEARSE	adveRse wEatHEr datAset for sensoRy noiSe models
RGB	Red-Green-Blue
RGGB	Red-Green-Green-Blue
RMSE	Root Mean Squared Error
SDM	Shahbeigi-Donzella metric
SNR	Signal to Noise Ratio
SR-SIM	Spectral residual based similarity
SURF	Speeded Up Robust Features
T	Task
VSI	Visual saliency-induced index
WP	Work Package

Executive summary

Objectives

The objective of this deliverable is to describe the development and validation of physics-based adverse weather noise models that affect the performance of automotive perception sensors. Moreover, the deliverable also aims to explain the process of creating and selecting the right metrics to support the validation process, and how they have been applied to the data produced by the noise models generated in this task (i.e. T3.4) and in T3.3. (i.e. data-driven models) to compare them with the real sensor data generated in the REHEARSE dataset (adveRse wEatHEr datAset for sensoRy noiSe models) (i.e. T3.2).

The developed models are designed to be integrated into any simulation pipeline, and for this project specifically into the ROADVIEW simulation pipeline (i.e. T3.7), supporting the virtual testing and more in general X-i-L testing of the ROADVIEW automated driving pipeline, or any automated driving pipeline. This deliverable created validated parametric physics-based adverse noise models tailored for automotive camera, LiDAR (Light Detection and Ranging), and 4D-RADAR (Radio Detection And Ranging). They will be used in Work Package (WP) 7 to test the robustness of the perception, actuation and control in adverse weather.

Methodology and implementation

The developed adverse weather noise models build on state-of-the-art models, with novel contributions. Independently from the sensor type (i.e. camera, LiDAR or 4D-RADAR) they consume ideal sensor data (either simulated of produced by real sensors in ideal conditions) and weather information (e.g. rain, droplet size distribution, rain rate, etc.) and produce as the output ‘noisy’ data, in exactly the same format of the input data, so they can be consumed by the perception algorithm without any further modifications. To validate the models, a series of image quality assessment metrics, point cloud metrics and qualitative assessments have been selected, adapted and applied to evaluate and compare the effect of the noise in the real world and simulated through the models. Several different metrics have been selected to cover different aspects of data degradation (e.g. changes in spatial contain, in the frequency domain, etc.).

Outcomes

This task has produced validated adverse weather (i.e. rain, fog, and snow) models tailored to camera, LiDAR and 4D-RADAR for automotive. Moreover, a library of image quality assessment metrics and point cloud metrics has been created and some of them have been investigated as predictive tools for the performance of perception algorithm using sensor data. The produced models have been validated against real data and compared to data-driven models. These results will feed into T3.5 to consider and combine noise models including internal sensor noises, occlusions, surface effects, etc.

Next steps

The developed models will be optimised for real-time performance and integrated into the simulation pipeline in WP7 to test the ROADVIEW system. Additionally, the developed adverse noise models will be considered in T3.5 for compounding of noise models. We are also currently in the process of writing 3-4 collaborative journal papers to disseminate the main scientific innovations produced by the newly developed models and metrics.

1 Introduction

The project ROADVIEW aims to demonstrate that the robustness under weather conditions of automated vehicles can be safely enhanced using X-i-L (everything-in-the-loop) testing. To support suitable testing, validated physics-based adverse weather noise models for perception sensors are created in T3.4 and can be incorporated into Carla and other simulators.

To reduce the simulation-to-reality gap, the ideal sensor data produced by a simulator should be affected by different sources of noise depending on the scenario to be tested. This task tackles the addition of adverse weather, namely rain, snow and fog, as a source of noise onto real or simulated (from now on 'ideal') sensor data generated by automotive camera, light detection and ranging (LiDAR) and imaging radio detection and ranging (Imaging RADAR). The developed models in this task consider real-world sensor and weather parameters to generate the noise, allowing for fine control over the noise and for reproducing measured weather events.

This report will also tackle validation of the produced data-driven (T3.3) and physics-based (T3.4) noise models using the real world from the REHEARSE dataset (ROADVIEW T3.2, Figure 1a). Validation of the created noise models against real-world data is key to ensure that the predicted behaviour in simulated tests can be trusted and reflects the sensor's behaviour in the real world. In this report, the effect of adverse weather is quantified using image quality assessment (IQA) metrics and newly proposed and adapted point cloud (PC) metrics. The degraded data generated from the ROADVIEW data-driven model (ROADVIEW T3.3, Figure 1b) and ROADVIEW physics-based model (ROADVIEW T3.4, Figure 1c) are compared against the real data (REHEARSE dataset, ROADVIEW T3.2, Figure 1a).

a) REHEARSE Emulated Fog (10 m) b) Data-Driven fog model (Heavy) c) Physics-Based model (10 m)

Figure 1: Sample weather images under the influence of fog generated using different techniques

This report is separated into 7 core chapters. Firstly, chapter 2 presents the implementation of the models and how they fit in the simulation pipeline for ROADVIEW. The following chapter, chapter 3, presents the parameterisation of the weather, specifically the drop size distribution (DSD) for the considered phenomena. The three subsequent chapters (Ch. 4, 5, 6) present the details of the created models for camera, LiDAR and Imaging RADAR respectively. They are followed by the comparison and validation of the models (Ch. 7). Finally, key conclusions from this task are presented, the future work and how this work feeds into other parts of the ROADVIEW project.

The weather noise models created in this task are made available on the ROADVIEW GitHub:
https://github.com/roadview-project/Physics_Based_Weather_Models.

2 Implementation

This chapter describes where the developed noise models will be implemented in the ROADVIEW pipeline, Figure 2. To design the weather noise models to be agnostic to the simulation platform and real sensor specifications and models, the developed models are designed to consume the output of real sensor data (before further sensor signal processing). A generalised flow process, starting from the simulator (e.g. Carla or CarMaker) or existing datasets where the 'ideal' sensor data will be passed into the noise models, is shown in Figure 3.

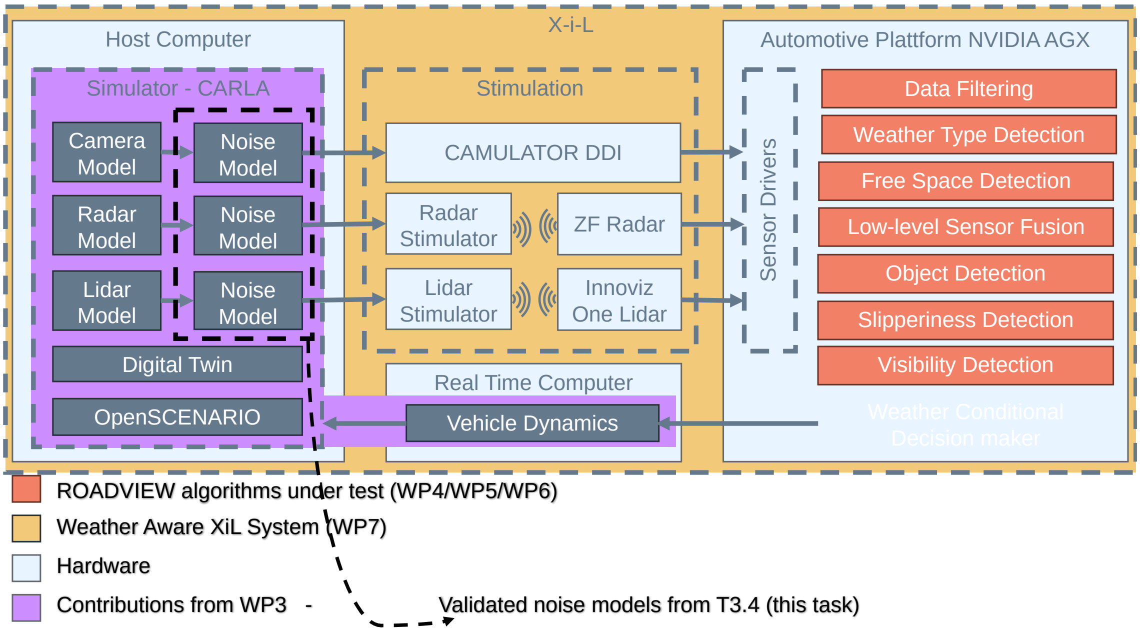

Figure 2: A diagram demonstrating how the noise models fit within the ROADVIEW simulation testing pipeline

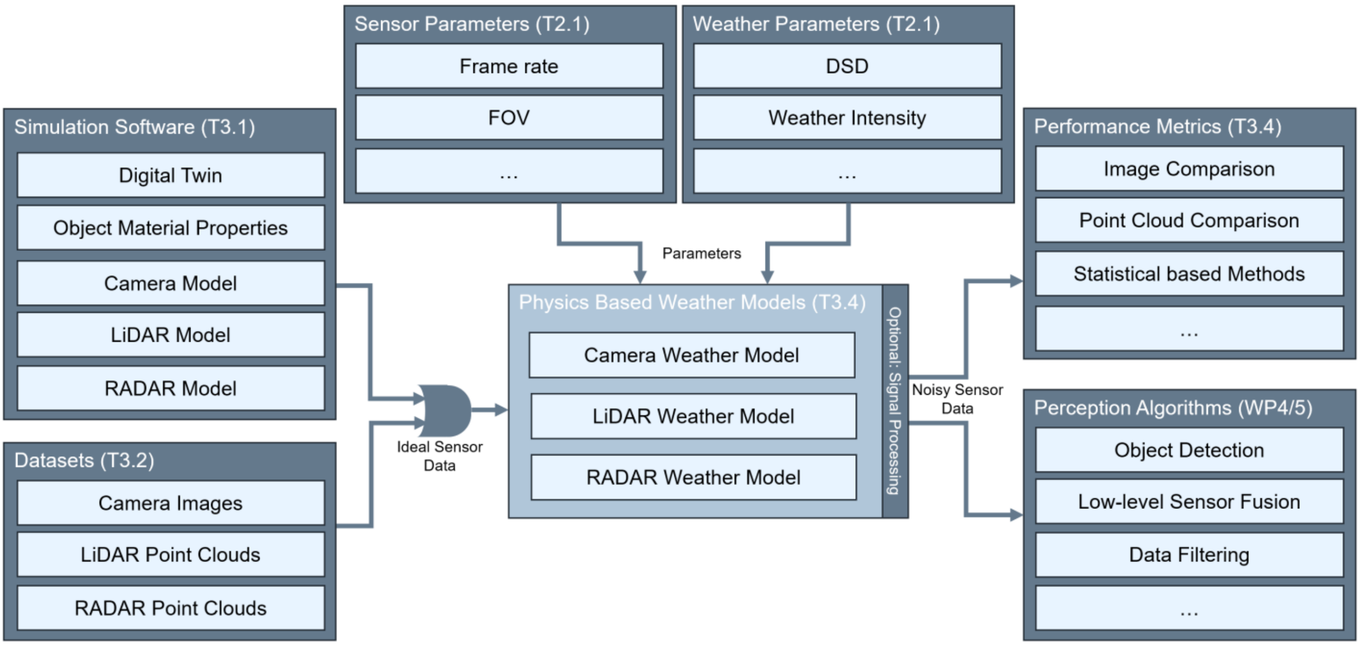

Figure 3: A flow diagram to show the inputs and outputs of the developed ROADVIEW weather model

2.1 Camera

Camera is a passive sensor composed of an array of pixels and photodiodes capturing the visible light wavelengths. Adverse weather conditions are part of the driving environment, affecting the light intensity captured by the photodiode. A colour filter array (usually a 2x2 pattern) limits the ranges of wavelengths which hit the photodiode (pixel), enabling a specific colour intensity to be captured by every pixel. At this stage, the image is still a single-channel intensity image known as the Bayer image. In the simulation process, the camera noise model is designed to apply noise at the output of the simulated camera model (ideally as a Bayer image), prior to any image signal processing (ISP) (which creates correlation between pixel values and might introduce artefacts). The output of the noise model can then be directly used or passed through an ISP to create visually pleasing images.

To simulate the real effect of the noise, the sensor and weather parameters are considered in the created weather noise models, see Chapter 4 for more details. The developed models are focused on the weather manifestation in the air, i.e. the falling raindrops, suspended fog particles, and the falling snowflakes. Assumptions made in the model are listed below:

- The scene considers daytime with no localised light sources.
- Only gravity acts upon the particles.
- Falling particles are travelling at terminal fall speed.
- There is no lens distortion.
- The camera is pointed parallel to the ground.

The model may be further developed in the future to address some of the assumptions. Additionally, parts of the work on this task will be complemented by ROADVIEW T3.5 to compound different noise models, for example adding surface effects into the noise model.

2.2 LiDAR

The LiDAR weather models are designed to modify existing 'ideal' point clouds outputted from the sensors or simulated environment. The data captured by LiDAR are stored and transmitted as a point cloud, where each data point contains location coordinates as well as any other information captured such as reflected intensity. Hence, by applying weather noise to the point cloud we ensure that the LiDAR weather models are agnostic to the type of LiDAR sensor. The 'ideal' point cloud along with sensor and weather parameters is used by the ROADVIEW LiDAR weather models to adjust the points position and intensity and/or remove/add points depending on the interactions between each beam and the weather particles in the air.

The output of the LiDAR weather model is an adjusted point cloud representative of the effect of rain, fog or snow. The original and adjusted point clouds can be compared with PC metrics to quantify the noise added.

2.3 RADAR

The output of the imaging RADAR is in the form of a 3D point cloud. Each point in the RADAR point cloud contains the location of the point combined with information from RADAR technology such as power, speed and radar cross section (RCS). The implementation of the RADAR noise models is similar to the implementation for the LiDAR.

Due to the novelty of the imaging RADAR in automotive, there is not an imaging RADAR model in Carla or CarMaker at the time of this report. Hence, WMG along with THI developed an imaging RADAR model incorporated into the Carla simulator.

3 Adverse Weather Precipitation Distributions

The ROADVIEW project aims to ensure robust operation under harsh weather conditions. A breakdown of how weather conditions affect the perception sensors has been previously presented in ROADVIEW Deliverable 2.1 (Warg, et al., 2024).

This section will provide an overview into the drop size distribution (DSD) of adverse weather, used in the proposed noise models. The DSD presents the number and probability of different droplet sizes at a weather intensity in a point/volume of space and time. This information is key for the physics-based weather noise models to appropriately consider the effects on the sensor output based on their field of view and resolution.

The following distribution equations are commonly parameterised to describe the DSD of different weather phenomena, the variables will be clarified in the following subchapters:

- Exponential Model

$$N(D) = N_0 e^{-\Lambda D}$$

- Gamma Distribution

$$N(D) = N_0 D^{\mu} e^{-\Lambda D}$$

- Log-Normal Distribution

$$N(r) = \frac{N_0}{r\sigma\sqrt{2\pi}} \cdot e^{-\frac{(\ln(r)-\ln(\bar{r}))^2}{2\sigma^2}}$$

3.1 Rain

Many works modelling rain have deployed existing distributions to generate their noise. Most works applied the distribution presented by Marshall and Palmer, see Table 1 (Marshall & Palmer, 1948). The emulated rain's drop size distribution recorded in the REHEARSE dataset at both the Carissma outdoor facility and CEREMA PAVIN platform can both also be approximated to follow the Marshall-Palmer distribution (Poledna Y. , Drechsler, Donzella, & Chan, 2024).

Table 1: Rain DSD used in different existing works

Author	Equation Used	Parameterisation	Comments
Garg et al., (Garg & Nayar, 2007) **Kilic et al., (Kilic, et al., 2021)** **Berk et al., (Berk, et al., 2019)** **De Charette et al., (De Charette, Taburo, Barnum, & Rowe, 1-10)**	Exponential	$N_o = 8000$ $\Lambda = 4.1 \cdot R^{-0.21}$ $D = diameter\ of\ raindrop$	This is the Marshall-Palmer distribution parameters for rain (Marshall & Palmer, 1948). R denotes the rain rate in mm/h.
Rasshofer et al., (Rasshofer, Spies, & Spies, 2011)	Gamma	$N_0 = \frac{\gamma \rho b^{\frac{\alpha+1}{\gamma}}}{\Gamma\left(\frac{\alpha+1}{\gamma}\right) \cdot 2^{\alpha}}$ $\mu = \alpha$ $b = \frac{\alpha}{\gamma (D_c/2)^{\gamma}}$ $\Lambda = -\mathrm{b}\frac{D^{\gamma-1}}{2^{\gamma}}$ $D = diameter\ of\ raindrop$	This implementation of the gamma distribution uses 4 core parameters which will need to be defined: $\alpha, \gamma, \rho, D_c$, where D_c is the droplet radius with maximum probability. Γ denotes the gamma function. Parameters of these variables are provided in (Rasshofer, Spies, & Spies,

			2011) for different types of rain.

3.2 Fog

Many works simulating fog on images bypass the need to consider the DSD of fog, opting instead for an empirical model, directly translating the visibility to the noise (attenuation).

Table 2 presents some distributions of fog presented in literature, but the parameters are dependent on the formation of the fog.

Table 2: Fog DSD used in different existing works

Author	Equation Used	Parameterisation	Comments
Rasshofer et al., (Rasshofer, Spies, & Spies, 2011) **Kilic et al., (Kilic, et al., 2021)**	Gamma	$N_0 = \frac{\gamma \rho b^{\frac{\alpha+1}{\gamma}}}{\Gamma\left(\frac{\alpha+1}{\gamma}\right) \cdot 2^{\alpha}}$ $\mu = \alpha$ $b = \frac{\alpha}{\gamma (D_c/2)^{\gamma}}$ $\Lambda = -\mathrm{b}\frac{D^{\gamma-1}}{2^{\gamma}}$ $D = diameter\ of\ raindrop$	The two works display the equation slightly differently but follow the same equation. The variables are defined the same the rain Gamma equation. Parameters of these variables are provided in (Rasshofer, Spies, & Spies, 2011) for different types of fog.
Bernardin et al., (Bernardin, Colomb, Egal, & Boreux, 2010)	Log-Normal	$N_0 = 1330$ $-\ln(\tilde{r}) = 0.44$ $\sigma = 0.59$	The parameters have been specifically parameterised for a fog visibility of 52 m.

3.3 Snow

Snow modelling have been explored by different works. Several works reference the snow DSD presented by Sekhon and Srivastava, however with slightly different cited parameters (Sekhon & Srivastava, 1970). Additionally, Brandes et al. have captured the distribution of snow events over a period and defined a relation using the Gamma distribution. Table 3 presents the different parameters used in the different works. For all the parameters, R denotes the precipitation rate in mm/h.

Table 3: Snow DSD used in different existing works:

Author	Equation Used	Parameterisation	Comments
Rasshofer et al., (Rasshofer, Spies, & Spies, 2011)	Exponential	$N_0 = 7600 \cdot R^{-0.87}$ $\Lambda = 2.55 \cdot R^{-0.48}$	Reference from Gunn and Marshall (Gunn & Marshall, 1958)
Rasshofer et al., (Rasshofer, Spies, & Spies, 2011)	Exponential	$N_0 = 5000 \cdot R^{-0.94}$ $\Lambda = 2.29 \cdot R^{-0.45}$	Referenced from Sekhon and Srivastava (Sekhon & Srivastava, 1970)
Von Bernuth et al., (Alexander, Volk, & Bringmann, 2019)	Exponential	$N_0 = 2500 \cdot R^{-0.94}$ $\Lambda = 2.29 \cdot R^{-0.45}$	Referenced from Sekhon and Srivastava (Sekhon & Srivastava, 1970)

Teufel et al., (Teufel, Volk, Von Bernuth, & Bringmann, 2022)			
De Charette et al., (De Charette, Taburo, Barnum, & Rowe, 1-10)	Exponential	$N_0 = 3800 \cdot R^{-0.87}$ $\Lambda = 25.5 \cdot R^{-0.48}$	Referenced from Gunn and Marshall (Gunn & Marshall, 1958)
Brandes et al., (Brandes, Ikeda, Zhang, Schönhuber, & Rasmussen, 2007)	Gamma	$N_0 = 5000 \cdot R^{-1.2}$ $\mu = -0.00499\Lambda^2 + o.798\Lambda - 0.666$ $\Lambda = 2.27 \cdot (T_0 - T)^{0.18}$	**The parameters are fitted based on recorded snow events in Colorado between 2003 and 2005. Parameterised DSD for a specific time is presented in** Table 4.

Table 4: Recorded parameters for specific snow rates during a Colorado snowstorm (Brandes, Ikeda, Zhang, Schönhuber, & Rasmussen, 2007)

Snow Rate (mm/h)	N_0	μ	Λ
2.59	7.18×10^1	-0.78	0.35
2.70	1.39×10^3	-0.90	1.40
3.03	2.33×10^4	1.23	2.25

3.4 DSD used in physics-based models

This chapter presented different drop size distributions for rain which can be inserted into the developed parametric physics-based weather models to better describe the specific observed phenomena. In this report, the following DSD was used to parameterise the DSD.

- Camera
    - Rain – Marshall-Palmer distribution using exponential equation
    - Fog – CE parameterised Normal distribution
    - Snow – Brandes et al. parameterised Gamma distribution
- LiDAR
    - Rain – Marshall-Palmer distribution using exponential equation
    - Fog – Gamma distribution by Rasshofer and adapted for ROADVIEW
    - Snow – Gunn and Marshall parameters presented by Rasshofer using exponential distribution
- RADAR
    - Rain – Marshall-Palmer distribution using exponential equation
    - Fog – Normal distribution for Bernardin et al. parameters adapted for ROADVIEW
    - Snow – Marshall-Palmer distribution using exponential equation

These DSD distributions were selected based on the requirements for the validation of the models. The rain and fog models are compared against the REHEARSE dataset. The emulated weather has been estimated to be similar to Marshall-Palmer for rain and the DSD for fog has been provided (Poledna Y. , et al., 2024). For snow, DSD are not provided by the datasets used for validation. Hence DSD used by other similar works have been used. However, the Gunn and Marshall exponential yielded odd results with the camera and hence a real measured DSD is used for camera.

The design of the physics-based models means that any distributions can be substituted into the model.

Table 5: Measured DSD from the emulated fog from the REHEARSE dataset

Visibility	N	$\ln(\tilde{r})$	σ
10	6108.49	0.48	0.73
20	3.559.64	0.36	0.78
30	2754.15	0.33	0.74
50	3189.71	0.23	0.66

4 Camera Model

4.1 Rain

4.1.1 Background

Camera captures the image over a short period of time, i.e. exposure time. Falling rain speed is significant in this context and results in streaking of the drop as it travels in the duration of the exposure time. Garg et al. presented their research on the appearance of rain streaks on images, using a mixture of physics-based equations (e.g. to determine the length) and data-driven methods (e.g. to determine the dynamism of the streak) (Garg & Nayar, 2007). Automotive camera research involving simulation of rain generates their appearance based on Garg et al.'s work (Pang, Wang, Xiq, Meng, & Xu, 2024) (Teeti, et al., 2022) (Tremblay, Halder, De Charette, & Lalonde, 2021) (Hospach, Mueller, Rosenstiel, & Bringmann, 2016). However, as deep neural network capabilities advance, a trend of using machine learning networks to generate the desired effects is growing, or a mixture of techniques is used, see Table 6 summarising some recently published work.

Table 6: A comparison of recent works on rain modelling on images. ML is machine learning-based and P is physics-based

Author	Basis	Modelling Techniques	Validation
Pang et al., 2024 (Pang, Wang, Xiq, Meng, & Xu, 2024)	ML, P	• Rain kernel generating streak using parameters for shape, orientation, length and width • Rain map defining location based on a sparsity factor parameter • A merging model to combine generated mask (from map and kernel) with input image	• Visual comparison against Rain100L (synthetic dataset) • Assess quality of generated image using Frechet Inception Distance (FID), Kernel Inception Distance (KID), Peak Signal to Noise Ratio (PSNR) and SSIM
Teeti et al., 2022 (Teeti, et al., 2022)	ML	• Use of CycleGAN re-trained with images containing droplets to generated images	• Assessed the FID of the generated images
Tremblay et al., 2021 (Tremblay, Halder, De Charette, & Lalonde, 2021)	ML, P	• Physics based model for creation of streaking based on (Garg & Nayar, 2007) • Transforming image to visually represent the scene during rain conditions (e.g. with wet surface, darker sky) with CycleGAN	• Visual comparisons against real images and images from other rain models • User studies with participants, subjective assessment
Hospach et al., 2016 (Hospach, Mueller, Rosenstiel, & Bringmann, 2016)	P	• Reconstruction of scene in OpenGL • Uniform distributed rain according to Marshall-Palmer • Streak based on velocity, shutter speed, drop size • Colour set as white with opacity of 0.5	• Sobel filtering • Canny edge detection • Harris corner detection • Histogram evaluation • Speeded Up Robust Features (SURF) feature detection

In existing works, the validation of the noise generated by the models against real data has been minimal, using a mixture of visual comparisons, and simple image quality assessment metrics such as PSNR and SSIM.

These works presented models which apply the noise on 3-colour channel RGB (Red-Green-Blue) images. However, external environmental noise will have an implication on the Bayer image, i.e. on the light intensity captured per pixel that will be then processed by the sensor ISP.

4.1.2 Key Equations

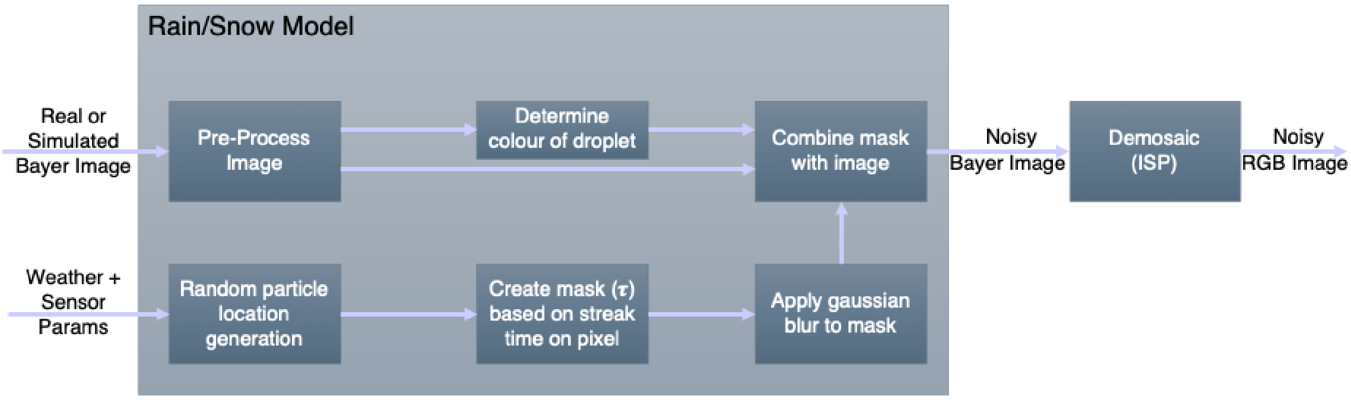

Figure 4: Flow diagram of the particle model for rain and snow.

Figure 4 shows the pipeline for the model based on a particle system to apply rain. The raindrop's intensity on an image ($I_{noise,Rain}$) was determined by Garg et al. as a function of the colour of the raindrop and refraction due to the luminance (Garg & Nayar, 2007).

$$I_{noise,Rain} = 0.94 \cdot I_{Raindrop} + 0.06 \cdot Luminance$$

The colour of the raindrop ($I_{Raindrop}$) is based on the content of the scene, and raindrops have a field of view (FoV) of ~165º (Garg & Nayar, 2007)]. Based on the colour filter per pixel (i.e. either R, G, or B), the average intensity per colour is calculated. The luminance values are extracted from the tables presented in (pIXWLsHAM, 2020) based on the lighting condition of the scene.

$$I_{Raindrop|R,G,B} = \frac{\sum I_{|R,G,B}}{n_{|R,G,B}}$$

Based on the DSD, the total number of rain droplets per unit volume is calculated. The ratio of the drop sizes is preserved, and the droplets are randomly distributed in a volume based on the FoV of the sensor using a uniform distribution. Every droplet in the camera FoV and depth (i.e. not behind an object, see appendix 10.4) is projected into a pixel position.

To create a mask for applying the weather noise, three parameters are computed. This includes the number of horizonal pixels which a raindrop acts upon (based on the droplet size (D) and distance (R)), the length (vertical pixels) of the streak (based on droplet size, distance, velocity ($v(D)$ in pixels per second) and exposure time (ε)), and the time of the droplet affecting a pixel (τ) relative to the exposure time. The raindrop is assumed to remain spherical during the fall, i.e. $pix(D,R)_{hor} = pix(D,R)_{vert}$. A gaussian blur is applied to the mask to simulate the blurring effect due lens focus and depth of field (Hospach, Mueller, Rosenstiel, & Bringmann, 2016).

$$pix(D,R)_{hor} = \frac{D}{(2 * R * \tan(0.5FoV_{hor}))/cam\_res_{hor}}$$

$$v_{rain}(D,R) = \frac{3.78 * D^{0.67}}{pix(D,R)_{vert}}$$

$$pix(D,R)_{streak} = (v(D,R) * \varepsilon) + pix(D,R)_{vert}$$

$$\tau = \begin{cases} 1, & pix(D,R)_{streak} \leq 1 \\ (1 + pix(D,R)_{vert})/(v(D,R) * \varepsilon), & 1 < pix(D,R)_{streak} \end{cases}$$

Finally, the determined mask from the generated raindrops and the colour based on the original image is combined with the Bayer image to form the noisy image.

$$I_{output,rain} = (1 - \tau) * I_{input,bayer} + (\tau) * I_{noise,rain}$$

4.1.3 Sample Images

The model has been applied to images from the REHEARSE dataset, Figure 5 (Poledna Y. , Drechsler, Donzella, & Chan, 2024). Below is a sample image when applying the rain model at different rain rates to the scene with the New Car Assessment Program (NCAP) vehicle facing 45º at 28 m distance in clear weather. For visualisation, the contrast was reduced to better visualise the noise generated in the sky and in front of the vehicle. Further discussion and validation of the model is presented in Chapter 7. A video composed of the generated noise in different weather will be made available on https://www.youtube.com/@ROADVIEWProject.

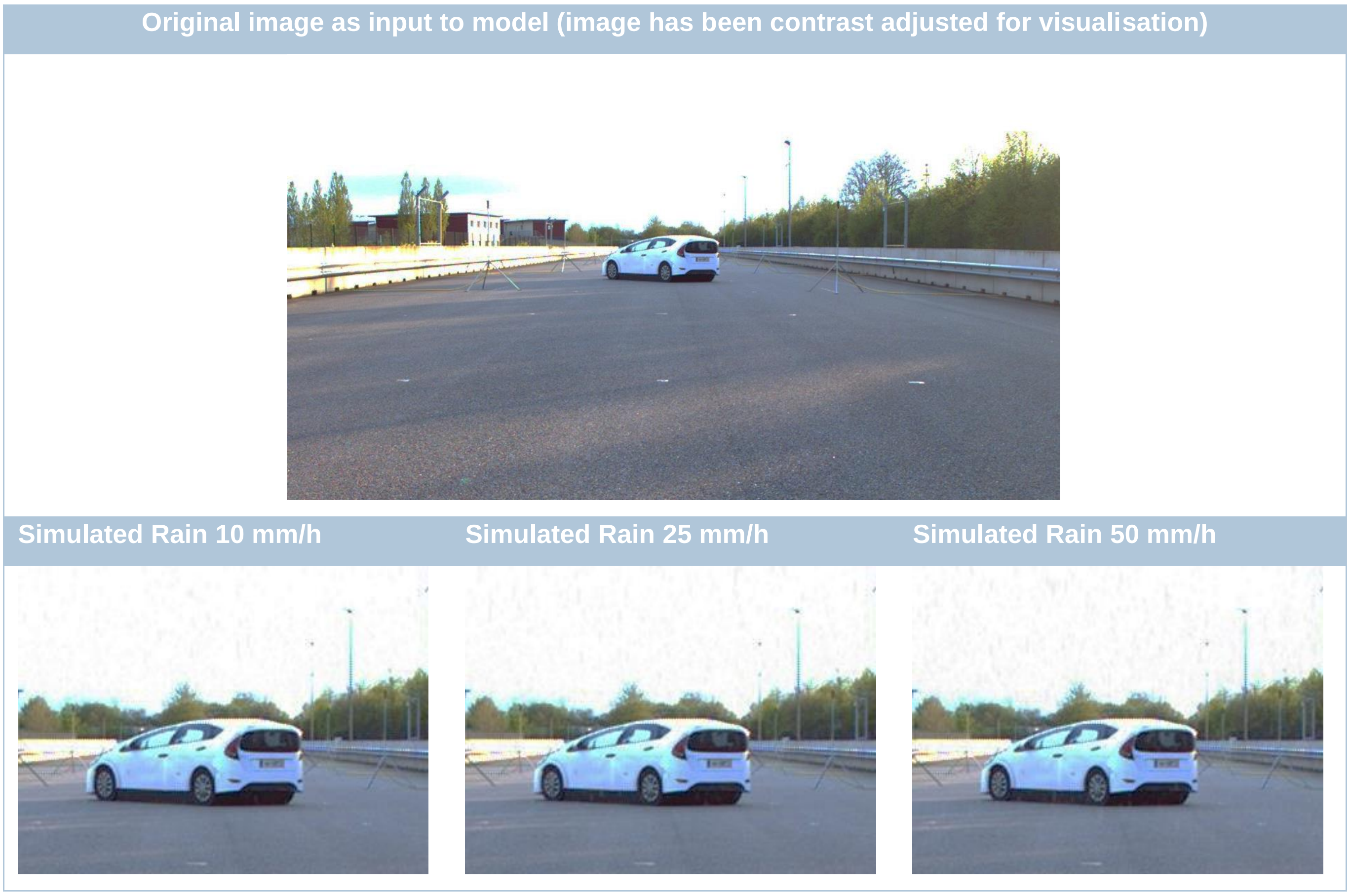

Figure 5: Examples of the simulated rain using the physics-based model. Images have been contrast adjusted by the same amount for better visualisation.

4.2 Fog

4.2.1 Background

There are several works exploring the effect of fog on automotive camera's downstream tasks by simulated fog on existing images, Table 7. Generally, these works have used Koschmieder's theory (Mai, Duthon Pierre, Khoudour, & Velastin, 2021) (Sakaridis, Dai, & Van Gool, Semantic foggy scene understanding with synthetic data, 2018). Other works have also explored the use of ray tracing with radiative transfer equations to computer the extinction theory (Ben-Daoued, Duthon, & Bernardin, 2023).

$$\sigma_{ext,Koschmieder} \approx \frac{2.996}{Visibility}$$

Table 7: A comparison of recent works on fog modelling on images. E is empirically based and P is physics-based.

Author	Basis	Modelling Techniques	Validation
Mai et al., 2021 (Mai, Duthon Pierre, Khoudour, & Velastin, 2021)	E	• Uses Koschmieder's principle • Assumes global illumination in the scene	• None performed
Sakaridis et al., 2022 (Sakaridis, Dai, & Van Gool, Semantic foggy scene understanding with synthetic data, 2018)	E	• Uses Koschmieder's principle	• Visual inspection
Ben-Daoued et al., 2021 (Ben-Daoued, Duthon, & Bernardin, 2023)	P	• Attenuation based on Mie theory/radiative transfer equation • Developed simulator with ray tracing to determine interactions with fog droplets	• Visual comparison against real fog images • Comparison of pixel line intensities in an area • Comparison of object contrast

The validation of generated fog images has been minimal in the works presented. There have been some visual comparisons performed against real collected images. Attempts at quantifying the effects have been performed by comparison of pixel line intensities and contrast of specific areas in the image against real collected images.

4.2.2 Key Equations

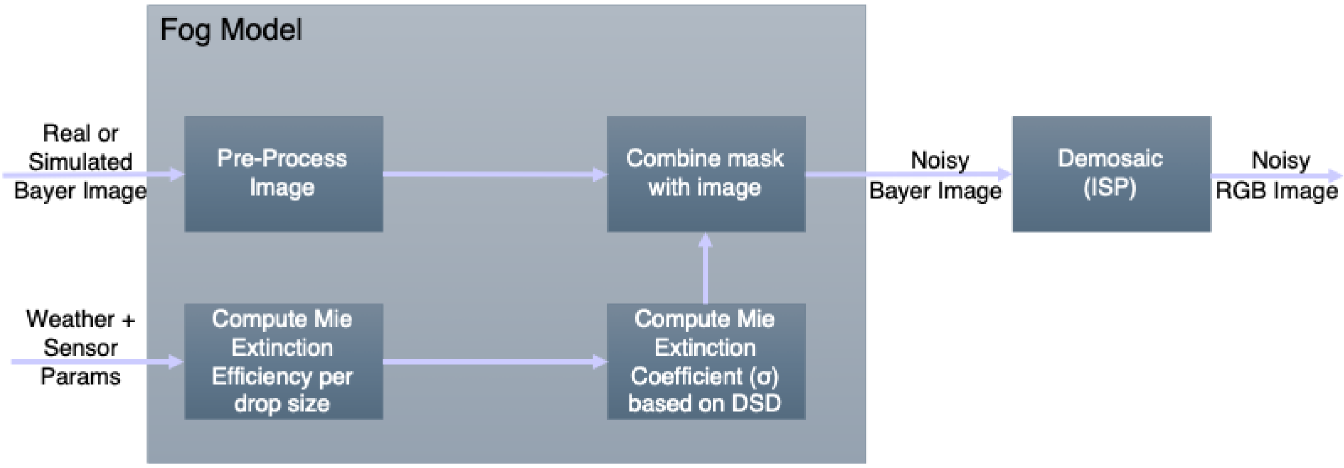

Figure 6: Flow diagram of the fog model

The flow diagram of the fog model is presented in Figure 6. Fog particles are suspended in the air, and they can be considered as stationary for the exposure time. Hence in the general noise equation, $\tau = 1$ and the output is based on the colour of the fog.

$$I_{output,fog} = (1-1)I_{input} + (1)I_{noise,fog}$$

$$I_{noise,fog} = e^{-\sigma_{ext}*D} * I_{input,Bayer} + (1 - e^{-\sigma_{ext}*D}) * Luminance$$

Similar to the rain model, the luminance is determined from (pIXWLsHAM, 2020). The depth has been determined using a modified nddepth network to provide absolute values (Shao, Oei, Chen, Wu Xingming, & Li, 2023). To determine the extinction coefficient, the implementation of Mie theory from Hong Du was used (Du, 2024). Together with a range of sizes based on the drop size distribution provided by the REHEARSE dataset, the extinction efficiency is calculated per drop size per wavelength using the Riccati-Bessel Functions. The extinction efficiency is then combined with the DSD to determine the extinction coefficient.

4.2.3 Sample Images

The images in Figure 7 demonstrate the generated foggy images on a clear image from the REHEARSE dataset with the NCAP vehicle target at 15 m in CE PAVIN platform. The simulated fog rates match the emulated fog visibilities captured in the REHEARSE dataset. Discussions and validation are presented in Chapter 7.

Original image as input to model

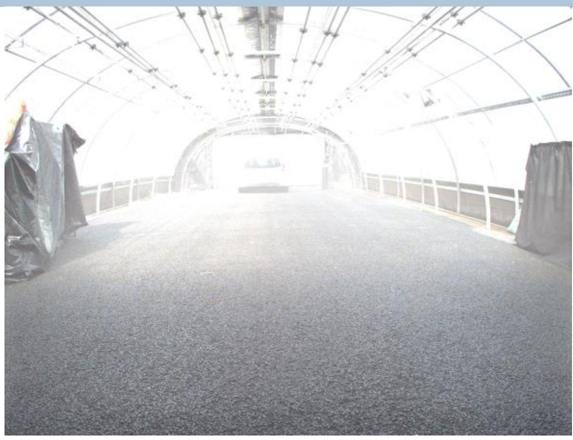

Simulated Fog 50 m | **Simulated Fog 30 m**

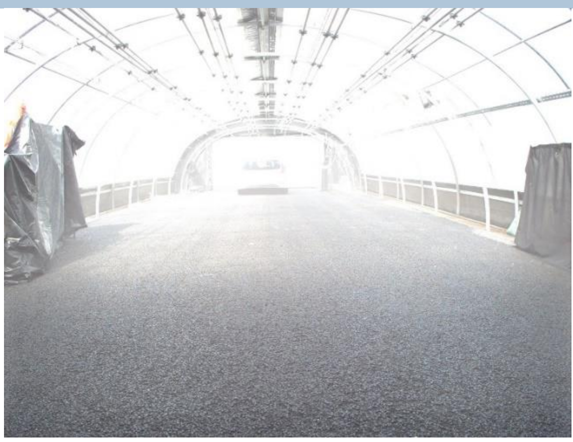

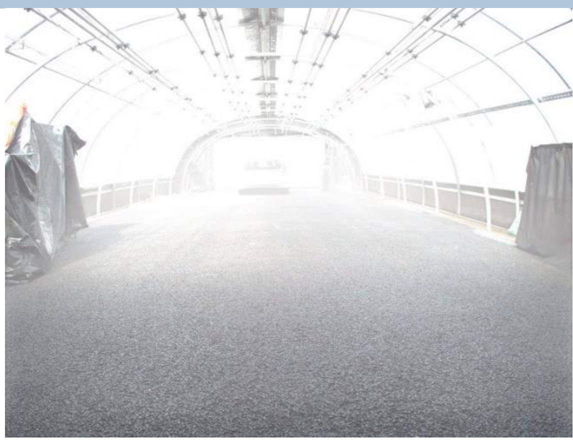

Simulated Fog 20 m | **Simulated Fog 10 m**

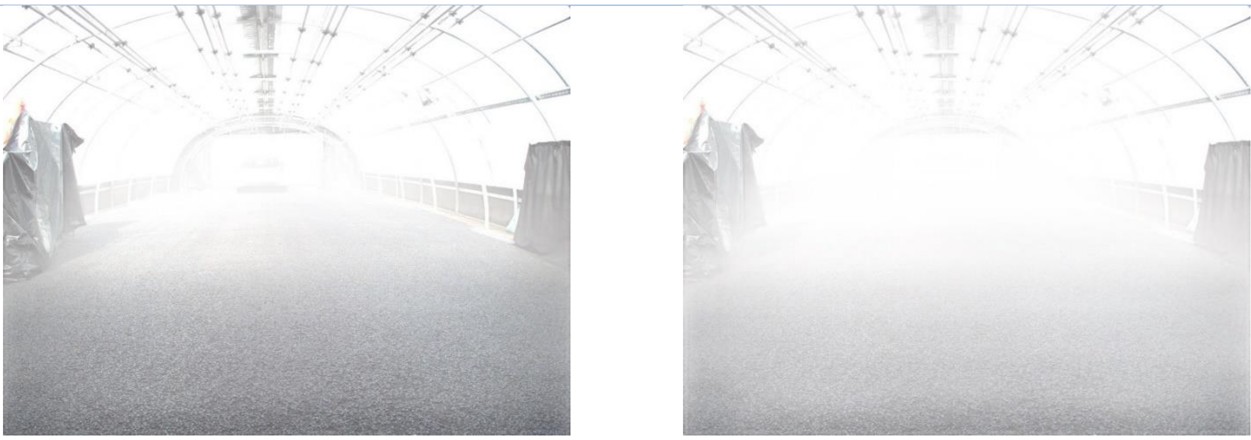

Figure 7: Examples of the simulated fog using an image with the NCAP vehicle at different visibilities using the physics-based model

4.3 Snow

4.3.1 Background

There is a lack of accurate physics-based models of falling snow in literature. Recent works have explored creating paired data with and without falling snow, see

Table 8. However, these works created the paired data using image editing software to produce 'visually' realistic looking falling snow.

Table 8: A comparison of recent works on snow modelling on images. ML is Machine Learning, E is Empirical and P is Physics-Based

Author	Basis	Modelling Techniques	Validation
Rothmeier et al., 2024 (Rothmeier, Huber, & Knoll, 2024)	ML, E	• Synthesised snow cover images using generative AI with commands • Augmented the images with falling snow using a simplistic empirical model by Hendrycks et al. (Hendrycks & Dietterich, 2019)	• Visual filtering of generated images • Assessed the variety of generated images against other datasets using Learned Perceptual Image Patch Similarity (LIPIPS)
Von Bernuth et al., 2019 (Con Bernuth, Volk, & Bringmann, 2019)	E	• Reconstruct image in OpenGL to apply the snow noise • Particle sizes based on snow rate and DSD	• Visual comparison against author collected data of the same scene
Chen et al., 2021 (Chen, et al., 2021)	E	• Falling snow generated based on photoshop tutorial coupled with gaussian blurring	• None performed
Moeslund et al., 2005 (Mpoeslund, Madsen, Aagaard, & Lerche, 2005)	P	• 3D modelling of snowflake in computer graphics • Snow composed of randomly joined triangles • Considers different natural forces acting on the snowflake	• Visual judgement from the author

Similar to the works for rain and fog, these works have performed superficial validation of the models. Visual comparison against real images is by far the most common validation method used.

4.3.2 Key Equations

The snow model follows the methodology of the rain model, see Figure 4, and parameterised based on the physics of snowflakes instead of the raindrops. Although snow falls slower than raindrops of the same size and is less likely to create streaks, the rain model methodology is still applicable as it appropriately considers parameters defining the streak length. Depending on lighting conditions and external factors acting on the snow, streaks can still occur. Additionally, by keeping the same model backbone, it is quicker to make changes and keep both weather models up to date. Specifically, the parameters: DSD (using the gamma distribution for the measured DSD in a Colorado snowstorm), the terminal velocity of the snowflake and the colour of the snowflake are adjusted. Under daylight conditions, snow is highly reflective, saturating the pixel intensity capturing the snow. Hence, the colour of the snow has been set as $I_{snow} = 255$.

$$N_{Gamma,snow}(D) = N_0 * D^{\mu} * e^{-\lambda D}$$

$$v_{snow}(D) = 2 * (10 * D)^{0.31}$$

4.3.3 Sample Images

Paired snow data is not available in the initial release of the REHEARSE dataset. Instead, the noise model is applied to clean images from the Adverse Conditions Dataset with Correspondences (ACDC) dataset (Sakaridis, Dai, & Van Gool, ACDC: The Adverse Conditions Dataset with Correspondences for Semantic Driving Scene Understanding, 2021). The ACDC dataset contains matched frames captured under clear conditions and during different weather events such as snow, rain and fog. Figure 8 presented an image with simulated snow using the presented model. Discussions and validation of the snow model is presented in Section 7.

Original image as input to model

Simulated Snow 2.59 mm/h	Simulated Snow 2.70 mm/h	Simulated Snow 3.03 mm/h

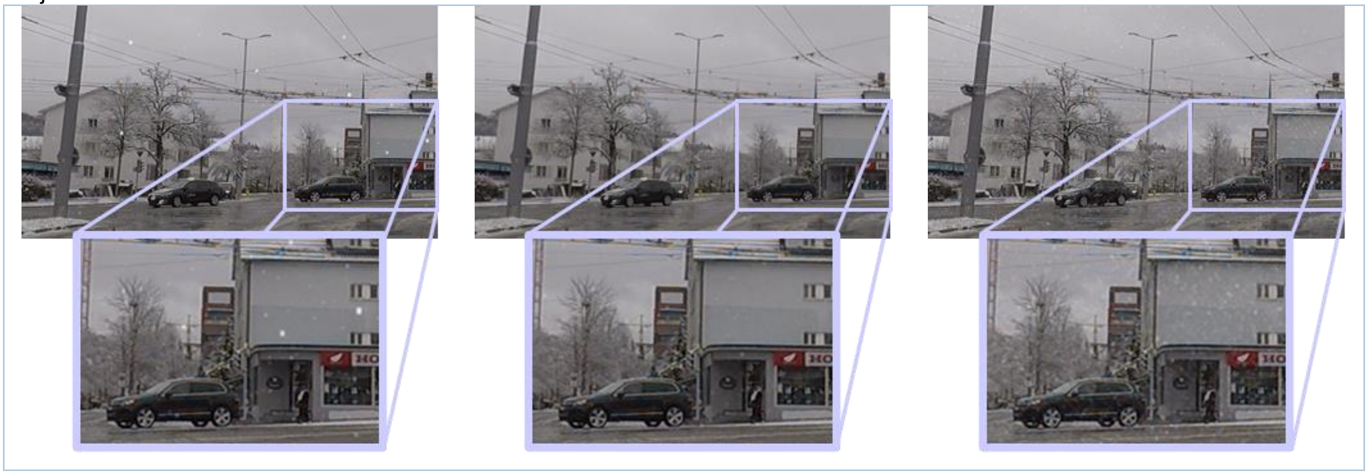
Figure 8: Example cropped images from the ACDC dataset with different snow intensities generated using the physics-based model

4.4 Key Innovation of proposed camera models

The developed ROADVIEW models present a significant advancement with respect to the state of the art, as described below.

- The variation of the colour per pixel due to snow, rain, and fog is applied to the Bayer image, i.e. on the real collected light intensity per pixel.
- The effect of the droplets on each pixel is calculated based on the specific light wavelength of the colour filter on each pixel of the Bayer patter (e.g. RGGB, RCCB, etc.).
- Processing of raw 'Bayer' image by an ISP pipeline, to generate RGB images.
- Validation of Noise Models with real collected data and paired 'ideal' vs. 'noisy' frames, see Chapter 7.
- The models consider appropriately the drop size distribution and the camera parameters.
- For snow, the model considers the distribution and speed of the snow to create the visual mask for applying the noise.

Moreover, there are recent works investigating the direct use of Bayer images in downstream perception tasks (Li, et al., 2024) (Wei, et al., 2023). So, the output noisy images from the ROADVIEW models can be either used as Bayer images in these novel algorithms, or they can be passed through an image signal processing (ISP) algorithm for processing in the RGB colour space.

5 LiDAR Model

5.1 Background

There are many different works exploring the modelling of adverse weather on LiDAR, see Table 9.

Table 9: Recent works on adverse weather modelling for automotive LiDAR

Author	Weather Model	Model Techniques Referenced	ROADVIEW Innovation and adaptations
Rasshofer et al., 2011. (Rasshofer, Spies, & Spies, 2011)	Rain, Fog, Snow	Extinction and back scatter coefficient integrals. Presents different power return equations for "hard" and "soft" targets	Modified the LiDAR power equation to output returned energy (Q_{EXT} and Q_B) based on Mie Theory for accurate rain/fog noise modelling.
Haider et al., 2024 (Haider, et al., 2023)	Rain, Fog	Recursive Method for calculating the extinction and backscattering efficiencies Q_{EXT} and Q_B based on Mie Theory	Developed an efficient iterative approach for calculating Q_{EXT} and Q_B for both rain and fog noise models. Backscatter coefficient in Haider et al modified according to Rasshofer et al.
Kilic et al., 2021. (Kilic, et al., 2021)	Rain, Fog	**Both Rain and Fog:** LiDAR points adjusted based on received power thresholds. **Rain only:** drop reflectivity	Calculated energy threshold based on specific LiDAR maximum intensity. Revised calculation for number of drops – current method obtains Poisson distribution sampled drops per beam volume. Accounting for drops in beams without detections in 'ideal' data (rain and fog).
Hahner et al., 2021. (Hahner, Sakaridis, Dai, & Van Gool, 2021)	Fog	General integrals for hard and soft target returned fog drop power/energy	Added efficient vectorised calculation for returned drop energy integral using trapezium rule. Used returned hard and soft target energies with maximum energy threshold to adjust point ranges.
Garbner et al., 2009. (Grabner & Kvicera, 2009)	Fog	Fog DSD based on local water content	Developed a novel fog drop size distribution that is a function of fog visibility distance
Hahner et al., 2022. (Hahner, et al., 2022)	Snow	General integrals for returned snowflake power/energy	Developed a new method to calculate number of snowflakes in a beam aligning with WMG's rain and fog model.

5.2 Rain

5.2.1 Key Equations

The ROADVIEW model uses energy rather than power. To determine the energy, the number of signal photons that can be captured by the LiDAR is used.

$$E = I * h\frac{c}{\lambda}$$

where I is the intensity, h is the Planck constant, c is the speed of light, and λ is the wavelength of the electromagnetic beam generated by the specific LiDAR.

The first step of the model is to determine the number of raindrops in the beam's path for each beam in the point cloud, based on the real rain distribution (Espineira, Robinson, Groenewald, Chan, & Donzella, 2021). Specifically, the number of raindrops per beam is calculated based on the beam parameters and the DSD of rain. The beam is assumed to be cylindrical without divergence similar to (Hahner, Sakaridis, Dai, & Van Gool, 2021) This is used as the mean for the Poisson distribution and sampling from this to get the probabilistic number of drops from each beam.

$$V_{Beam} = \begin{cases} \pi r_{beam}^2 R_{Obj}, & R_{obj} \in \mathbb{R} \\ \pi r_{beam}^2 R_{Max}, & else \end{cases}$$

$$\mu = V_{Beam} \int_{D_{Min}}^{D_{Max}} N(D)\ dD$$

$$p(n) = \frac{\mu^n}{n!} e^{-n}$$

After obtaining the probable number of drops in the beam path, the energy returned from each drop can be calculated, based on the distance to the generated drop. The energy returned by each drop can then be calculated, see below, where D_{Drop} is the drop diameter, sampled from the DSD, α is the extinction coefficient given by the equation presented below, T_H is the pulse width of the LiDAR beam and $\rho_{Drop} = \left|\frac{n-1}{n+1}\right|^2$ is the drop reflectivity given by Fresnel as per (Kilic, et al., 2021), n being the refractive index of water. This energy calculation has used the power equation given in (Kilic, et al., 2021) and multiplied by the pulse width T_H to convert to energy. The raindrop with the highest energy returned is stored with its position/distance. The energy of the originally detected object (if existing) needs to be reduced to adjust for the rainy medium. This is calculated below where the reduction in energy received from the object is a relationship between the extinction coefficient and the round-trip distance.

$$E_{Drop} = T_H \cdot \frac{\rho_{Drop}\, e^{-2\alpha R_{Drop}}}{R_{Drop}^2} \cdot \min\left\{\left(\frac{D_{Drop}}{2 \cdot r_{beam}}\right)^2, 1\right\}$$

$$E_{Obj,modified} = E_{Obj} \cdot e^{-2\alpha R_{Obj}}$$

The equation for the extinction coefficient α is given in below which has been adapted from (Rasshofer, Spies, & Spies, 2011) to have reduced limits as per the maximum and minimum drop sizes.

$$\alpha = \frac{\pi}{8} \int_{D_{Min}}^{D_{Max}} D^2\, Q_{Ext}(D) N(D)\, dD$$

$Q_{Ext}(D)$ has been calculated according to (Haider, et al., 2023), where $x = \frac{\pi D_{Drop}}{\lambda}$, $m = \Re(n)$, $N_{Max} = x + 4x^{\frac{1}{2}} + 10$, $r_n(mx) = \frac{\Psi_{n-1}(mx)}{\Psi_n(mx)}$ and $\Psi_n(x)$ and $\zeta_n(x)$ are the Ricatti-Bessel functions of the first and second kind.

$$Q_{Ext}(D) = \frac{2}{x^2} \sum_{n=1}^{N_{Max}} (2n+1) \cdot \Re(a_n + b_n)$$

$$a_n = \frac{\left(\frac{r_n(mx)}{m} + \frac{n\left(1 - \frac{1}{m^2}\right)}{x}\right)\Psi_n(x) - \Psi_{n-1}(x)}{\left(\frac{r_n(mx)}{m} + \frac{n\left(1 - \frac{1}{m^2}\right)}{x}\right)\zeta_n(x) - \zeta_{n-1}(x)}$$

$$b_n = \frac{r_n(mx) m \Psi_n(x) - \Psi_{n-1}(x)}{r_n(mx) m \zeta_n(x) - \zeta_{n-1}(x)}$$

The energy of the stored drop ($\boldsymbol{E_{Drop}}$) is then compared to the attenuated energy of the object ($\boldsymbol{E_{Obj}}$) and both are compared to the LiDAR energy detection threshold ($\boldsymbol{E_{Threshold}}$) to determine if: the original point is detected, but with attenuated signal; a rain droplet is detected instead; the beam is too attenuated and cannot be detected anymore, see pseudo code below. The model, in its current format, does not contain multiple returns, it only considers the strongest of the possible returns in the beam path, but in the future this aspect can be further updated. The model also accounts for the size of the droplet to evaluate the return, however, as mentioned above the beam is assumed to be cylindrical as in previous models, as LiDAR beam divergence is designed to be quite small (Hahner, Sakaridis, Dai, & Van Gool, 2021). However, beam divergence can have an implication in the medium and far range and this will be accounted for in future releases of the model.

If $E_{Drop} > E_{Obj}$ & $E_{Drop} > E_{Threshold}$:

Original point is moved to position of rain drop

$I_{Drop} = (E_{Drop} / T_H)/A_{Receiver}$

Else If $E_{Obj} < E_{Threshold}$ & $E_{Drop} < E_{Threshold}$:

Point is removed from the point cloud.

Intensity value is set to zero

Else

Point remains

Intensity value remains (but it is attenuated with respect to the original 'ideal' return)

End

5.2.2 Point Clouds

Samples of the rain noise model applied to the REHEARSE THI outdoor track ideal point clouds are shown in Figure 9. It is clearly visible that in both model and real rainy data, the number of points in the point cloud is significantly reduced with respect to the original 'ideal' point cloud. However, in the simulated model there are more rain noise points in the close range. It is likely that the signal processing in the Ouster LiDAR filtered sporadic points due to rain, but this processing is not performed in the LiDAR model.

Original "Dry" Point Cloud	Original Rain Point Cloud	Rain Model Point Cloud
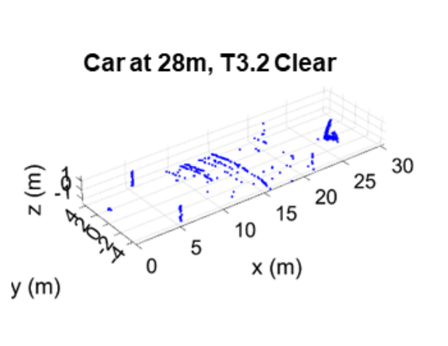	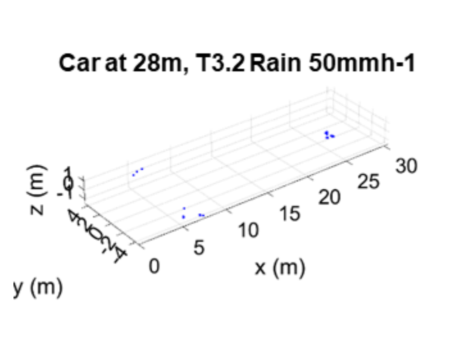	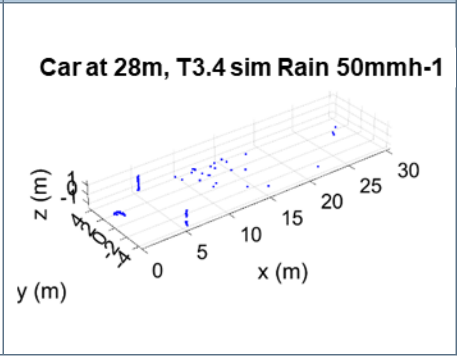

Figure 9: Comparison of emulated and physics-based simulated rain on LiDAR point cloud in the THI outdoor test track

5.3 Fog

5.3.1 Key Equations

As with the rain model, intensity is converted to energy in the same manner as above and for the same reasons. The method of determining the number of fog droplets in the beam's path is the same as for raindrops however the maximum and minimum droplet sizes and DSD have been changed to be representative of fog instead of rain. The gamma distribution has been used for fog as per (Rasshofer, Spies, & Spies, 2011).

$$N(D) = \frac{\gamma \rho b^{\frac{\alpha_{fog}+1}{\gamma}}}{\Gamma\left(\frac{\alpha_{fog}+1}{\gamma}\right)} \left(\frac{D}{2}\right)^{\alpha_{fog}} e^{-b\left(\frac{D}{2}\right)^{\gamma}}$$

$$b = \frac{\alpha_{fog}}{\gamma \left(\frac{D_c}{2}\right)^{\gamma}}$$

where $\Gamma(x)$ is the Gamma function, D_c is the droplet size of maximum probability and α_{fog}, ρ, and γ are to be parameterised.

To parameterise α_{fog}, ρ, and γ, Rasshofer et al. set these values according to different types of fog. However, for assisted and automated driving (AAD) functions there is a limited number of environments where the systems could be operated. Hence for ROADVIEW proposed model, a single type of fog (Advection) has been parameterised. The above equation is combined with equations described in Grabner and Kvicera to convert visibility of the fog directly to α_{fog}, ρ, and γ for use in the DSD (Grabner & Kvicera, 2009). Setting the effective radius, $r_e = 10\mu m$ as per Grabner and Kvicera and $\gamma = 1$ as per the two types of advection fog in Rasshofer et al. The following equations converts visibility to Liquid Water Content (LWC) and determine parameters for the Gamma distribution (Rasshofer, Spies, & Spies, 2011; Grabner & Kvicera, 2009).

$$LWC = 36.489 * Visibility^{-1.1407}$$

$$\alpha_{fog} = \frac{3\gamma \left(\frac{D_c}{2}\right)^{\gamma} \left(\frac{D}{2}\right)^{\frac{1}{\gamma}}}{r_e - \gamma \left(\frac{D_c}{2}\right)^{\gamma} \left(\frac{D}{2}\right)^{\frac{1}{\gamma}}}$$

$$\rho = \frac{(3 * 10^6) LWC \left(\frac{\alpha_{fog} + 3}{r_e}\right)^{\alpha_{fog}+4} \Gamma\left(\frac{\alpha_{fog} + 1}{\gamma}\right)}{4\pi\Gamma(\alpha_{fog} + 4)\gamma \left(\frac{\alpha_{fog}}{\gamma \left(\frac{D_c}{2}\right)^{\gamma}}\right)^{\alpha_{fog}+1}}$$

The extinction and backscatter coefficients have been calculated via the same method as the rain model and the method of changing the points dependent on energy returned is the same as the rain model. The equations to calculate the energy of the drop and the energy of the object in the presence of Fog drops have however been adjusted to be suitable for fog. Energy of the object is calculated as in the rain model where the original point energy is multiplied by a factor containing the extinction coefficient $E = E * e^{-2\alpha R_{Obj}}$. Energy of the drop is calculated using equations below which are adapted from (Hahner, Sakaridis, Dai, & Van Gool, 2021). It has been assumed that $\varepsilon\left(\mathrm{R_{Drop}}-\frac{\mathrm{ct}}{2}\right)=1$ and $\mathrm{U}\left(\mathrm{R_{Obj}}-\mathrm{R_{Drop}}+\frac{\mathrm{ct}}{2}\right)=1$.

$$E_{Drop} = C_A * E_{Peak} * \beta \int_0^{2T_H} \sin^2\left(\frac{\pi t}{2T_H}\right) \frac{e^{-2\alpha\left(R_{Drop}-\frac{ct}{2}\right)}}{\left(R_{Drop} - \frac{ct}{2}\right)^2} dt$$

$$C_A * E_{Peak} = E * \left(\frac{R_{Obj}^2}{\beta_0}\right)$$

Then E_{Drop}, E_{Obj}, and $E_{Threshold}$ can be compared or just E_{Drop} and $E_{Threshold}$ if there is no object point as in the rain model to determine what happens to the point. The process for comparing is the same as the one described in 5.1.2.

5.3.2 Point Clouds

Samples of the rain noise model applied to "ideal" point clouds in the CE PAVIN platform are shown in Figure 10. As for the rain, it is clearly visible that in both model and real foggy data, the number of points in the point cloud is significantly reduced with respect to the original 'ideal' point cloud, and the effect is more significant as the range of the points increases. However, in this case the simulated model seems to detect slightly less noise points than in the real noisy data. It is possible that the overall calculated attenuation of the model is slightly higher than the real attenuation in the CE chamber, and therefore the model can be further tweaked to better represent collected data.

Typically, the noise is expected to be a "dome" shape around the LiDAR sensor. However, the view presented in Figure 10 is limited to the front only due to the constraint of the indoor platform. As a false point is only present if the backscatter is larger than the intensity of the real point, only a limited range of fog is present for backscatter in the near range before hitting the side wall. Hence a "dome" shaped noise is not observed in the real or the simulated data.

Original "Dry" Point Cloud	Original Fog Point Cloud	Fog Model Point Cloud
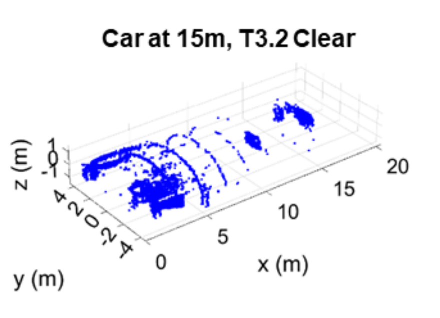	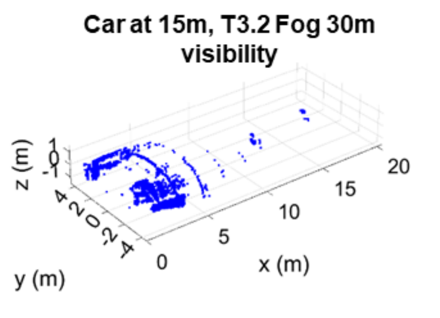	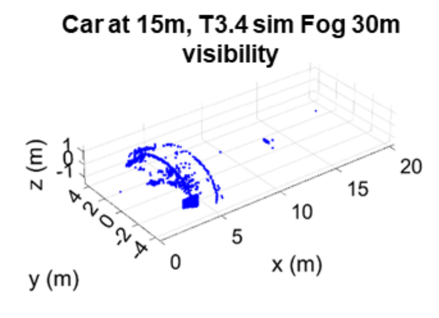

Figure 10: Comparison of emulated and physics-based simulated fog on LiDAR point cloud in the CE PAVIN platform

5.4 Snow

5.4.1 Key Equations

As with the rain model, intensity for the snow model is converted to energy in the same manner as above and for the same reasons (see section 5.1). The method of determining the number of snowflakes in the beam's path is the same as method used in the proposed rain model (see section 5.1.3) however the maximum and minimum droplet sizes and DSD have been changed to be representative of snow instead of rain. The exponential distribution has been used for snow as per (Rasshofer, Spies, & Spies, 2011), described in the equation for snow drop size distribution $N_{snow}(D)$

$$N_{snow}(D) = N_0 \exp{(\lambda D)}$$

$$N_0 = 7600 * R_I^{-0.87}$$
$$\lambda = 2.55 * R_I^{-0.48}$$

Where R_I is the precipitation rate measured in millimetres of equivalent liquid water per hour for snow fall. To convert the provided snowfall rate S_r into a precipitation rate we used a modified version of the equation for R_I in terms of S_r provided by the supplementary materials for the snow model from Hahner et al (Hahner, et al., 2022). In the equation for R_I below D_0 is set to 1mm and υ_s is set to 1.6m/s. The equation for the average snow density ρ_s was taken from Brandes et al (Brandes, Ikeda, Zhang, Schönhuber, & Rasmussen, 2007).

$$R_I = \sqrt[4]{\left(\frac{S_r}{487 * \rho_s * D_0 * \upsilon_s}\right)^3}$$

$$\rho_s = 0.178 * D_0^{-0.992}$$

The method for sampling snowflakes in the LiDAR beam is identical to the method seen in the proposed rain model (see chapter 5.2.1). For the calculation of the extinction coefficient as presented in chapter 5.2.1, we substitute the water refractive index for the ice refractive index. After sampling the snowflakes using the drop size distribution ($N_{snow}(D)$) for snow we obtain the maximum returned energy from all the returned energies of each sampled snowflake. The LiDAR returned energy equation used for the proposed snow model is shown below. R_{flake} is the range of the snowflake, $FlakeSize$ is the diameter of the sphere we are using to model the snowflake, ρ_0 is the snow reflectivity, $BeamRadius$ is the radius of the LiDAR beam, C_A is a system constant which is independent of time and range, c is the speed of light, T_H is the pulse width and R_{Obj} is the range of a point under consideration in the point cloud. The equations for E_{Flake} and C_A below have been adapted from Hahner et al. (Hahner, et al., 2022).

$$E_{Flake} = T_H * \frac{C_A \rho_s}{R_{flake}^2} \sin^2\left(\frac{\pi(R_{Obj} - R_{flake})}{c * T_H}\right) \min\left\{\left(\frac{FlakeSize}{2 * BeamRadius}\right)^2, 1\right\}$$

$$C_A = E_{Obj} {R_{Obj}}^2 / \rho_0$$

To modify the returned energy of the object if there are snowflakes present in the LiDAR beam, we attenuate the returned energy of the object point as shown in the equation below. $E_{Obj,modified}$ is the modified returned energy of the object point, E_{Obj} was the original returned energy of the point in the LiDAR point cloud and α is the extinction coefficient. It is calculated using the same method seen in chapter 5.2.1. If there are no snowflakes in the beam, when we set $E_{Obj,modified} = E_{Obj}$.

$$E_{Obj,modified} = E_{Obj} \cdot e^{-2\alpha R_{Obj}}$$

The energy of the snowflake is then compared to the modified energy of the object, and both are compared to the energy threshold to determine what happens to the original point in the point cloud. The logic used for this is shown below:

If $E_{Drop} > E_{Obj,modified}$

- Point is moved to position of snowflake - $I_{Drop} = (E_{Drop} / T_H)/A_{Receiver}$

Else If $E_{Obj,modified} < E_{Threshold}$ & $E_{Drop} < E_{Threshold}$:

- Point is removed from the point cloud – set point to position (0,0,0).
- Intensity value is set to zero.

Else If $E_{Obj,modified} < E_{Threshold}$ & $E_{Drop} \geq E_{Threshold}$:

- Point remains in the same position.
- Intensity value remains the same.

5.4.2 Point Clouds

We applied the proposed snow model to the WADS dataset, Figure 11, as it has snow point clouds with annotated snowflakes, and therefore it enables us to apply the model to ideal point clouds and compare them to the noisy ones (Kurup & Bos, 2021). The colour of the points is coloured based on the height of each point.

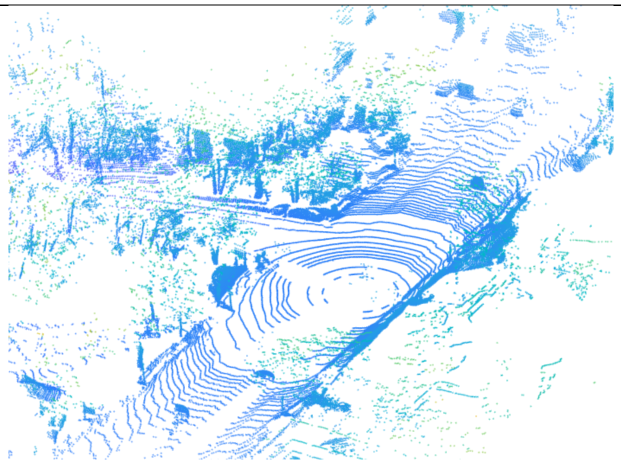

WADS Clear

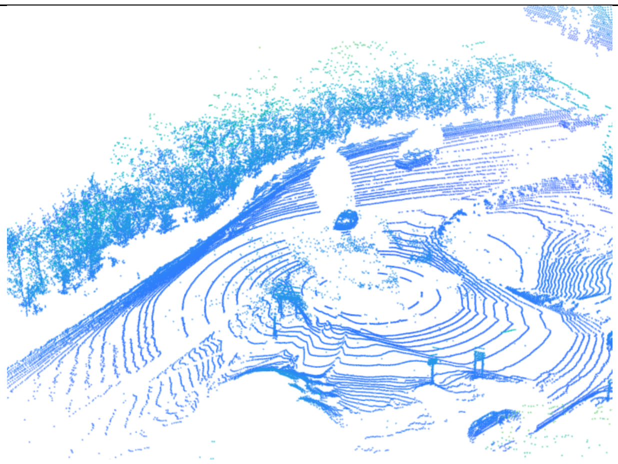

WADS Clear

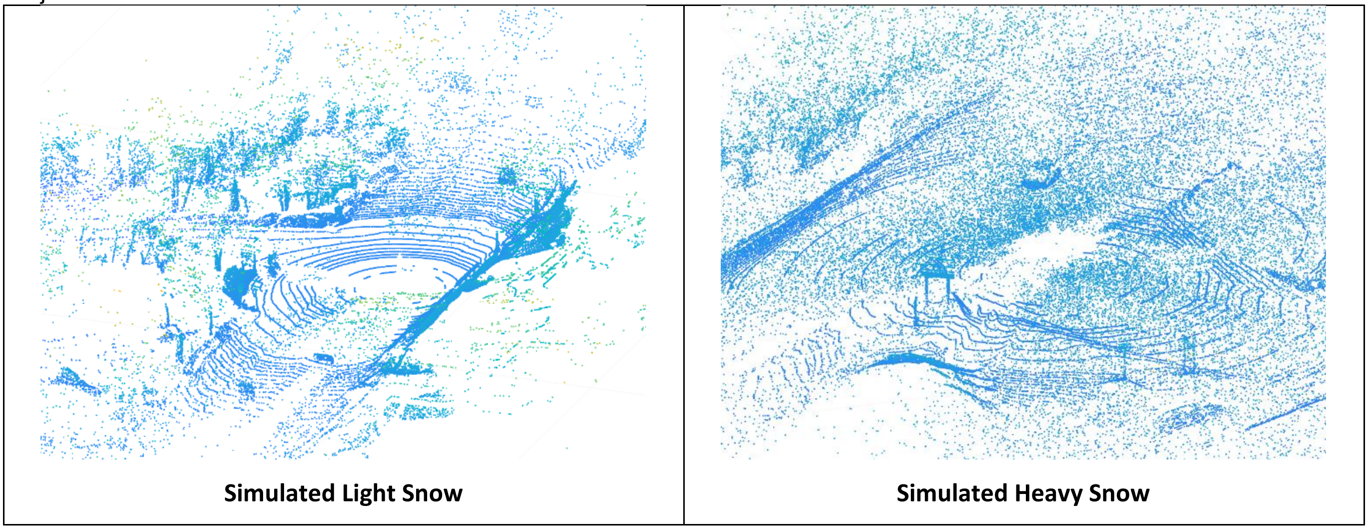

Figure 11: Comparison of the cleaned WADS point cloud against simulated snow using the T3.4 model

5.5 Model Innovation

The created ROADVIEW models contain key innovations with respect to existing work, as summarised below.

- Firstly, energy per beam is used instead of power in the LiDAR equations. Energy is based on photon count which is quantifiable, and makes the model adaptable to represent any real model/make of LiDAR.
- A core part of the ROADVIEW LiDAR model is that the LiDAR scanning pattern is considered.
- On top of adding noise to existing points in the original 'ideal' point cloud, the model also considers beams which had no return originally and evaluates if rain droplets are in that volume covered by that beam and can generate a detectable reflections, generating a false positive as a 'rain' point.

6 RADAR Model

The development of a 4D RADAR model to be used in this WP and specifically in this task, T3.5, and T3.7, as well as WP7. THI along with WMG's supervision have developed a simplified 4D RADAR model which will be used in ROADVIEW simulation environment (its integration with the CARLA platform is currently undergoing as a part of T3.7 and key to work package 7). No 4D RADAR models were available off the shelf to be used as a part of this project. In fact, most of the available RADAR models do not include the calculation of RADAR Cross Section (RCS) or Power, which are key to understand how to apply noise models.

Radio Detection and Ranging or RADAR is an active sensor which emits Electromagnetic (EM) waves into the free space. By measuring the time between emitting the EM wave/radio signal and its return to the sensor (round-trip time) it is possible to measure the distance by a simple distance calculation using

$$R = \frac{ct}{2}$$

where c is the speed of light, t is the round-trip time of the wave, and R is the distance. The direction of the object reflecting the EM wave can be estimated e.g. either by physically sweeping a narrow beam antenna, or by utilising an antenna array and calculations through digital beam forming based on the phase difference of the return signal at the different antenna array elements. Digital beam forming has the advantage of not needing any moving parts, but on the other hand places higher demands on the signal processing chain.

Depending on the used modulation technique, RADAR can also be able to calculate the target speed based on the Doppler effect. A common type of RADAR modulation in automotive applications is Frequency Modulated Continuous Wave (FMCW). It typically uses a saw tooth modulation, which is commonly referred to as chirping. Finally, the amplitude or power of the returned RADAR signal can provide information about the reflecting object. A common measure for this is the RADAR Cross Section (RCS or σ measured in squared meters), which is defined as (Skolnik, 2002)

$$\sigma = \frac{4\pi r^2 S_r}{S_t}$$

Above, r is the distance, S_r is the power density at the target, S_t is the power reflected from the target. The RCS is physically defined as the area that the target represents if it were to be measured as an area of a sphere of radius of 1m. In a more intuitive way, the RCS is defined below.

$$\sigma = \frac{\text{Reflected power/Unit of Solid Angle}}{\text{Power Density Incident}/4\pi}$$

It is important to note that RCS is not bound to the targeted object geometric size. Due to the target physical properties, its reflection may be stronger or weaker which in turn results in a greater or smaller RCS. Whilst in normal circumstances a bigger target usually means a greater RCS, in specific circumstances due to scattering the RCS of a bigger target may be lower than a smaller target. As the RCS influences the power of the returned signal it also has a strong influence on the RADAR detectability of an object.

Considering RCS, the returned power from a target with RCS σ is given by the RADAR power equation below.

$$P_e = \frac{P_s G^2 \lambda^2 \sigma}{r^4 (4\pi)^3},$$

Where P_e is Received power, P_s Emitted Power, G Antenna Gain, λ Wavelength, r is the range. This equation shows how the returned signal decreases rapidly with range. The Signal to Noise Ratio (SNR) thus also decreases with range, relating the detectability range to the RCS of any reflecting object.

Considering using the D3.2 data from the REHEARSE dataset, with a car at 45 degrees and at the same positions as the dataset (seen in Figure 12) it is possible to line cast the RADAR rays and get the respective triangle from the digital model (seen in Figure 13). With these triangles, it is possible to calculate the RCS from them using a discriminated RCS (σ) defined as (Pandey et al.) (Pandey & Ram, 2022)

$$\sigma_b = \eta 4\pi A_b^2 \cos^2\theta_b \sin^4 2\pi\lambda c d b \sin\theta b \lambda_c^2 \left(\frac{2\pi}{\lambda_c} d_b \sin\theta_b\right)^4,$$

where θ_b is the Aspect angle, λ is the wavelength, d_b is the dimension along the aspect angle, and A_b is the Area of the triangular facets. Which allows for the calculation of the RCS of a triangle considering it ray incident and normal directions.

With the RCS and distances from the targets, it is then possible to calculate the received signal at the ADC using

$$S_{\mathrm{Rx}}[i,:] = \sum_{k=0}^{M-1} \sqrt{\frac{A_{eff_{Rx}}[k] \cdot d_{tx_i} \cdot r_i}{\left(4\pi \cdot \left(d_i + v_i \cdot T_{adc} \cdot (i-1)\right)^2\right)^2}} \cdot \exp\left(1j \cdot \frac{4\pi \cdot \left(d_i + v_i \cdot T_{adc} \cdot (i-1)\right)}{\lambda}\right),$$

where, N_c is the Number of chirps, d_i is the Distance for the i-th chirp, r_i is the Radar Cross Section for the i-th chirp, v_i is the Velocity for the i-th chirp d_{tx_i} is the Transmission power coefficient for the i-th chirp, T_{adc} is the ADC sampling time, P_{Tx} is the Transmit power, $A_{eff_{Rx}}$, is the Effective receiving area matrix, λ is the wavelength of the transmitted signal S_{Rx} is the Received signal matrix. Then making a Fourier Transform of S_{Rx} it is possible to plot the range doppler plot of the detections under clear conditions as seen in Figure 14.

Figure 12: Top View 28m car 45deg, REHEARSE dataset on Carla

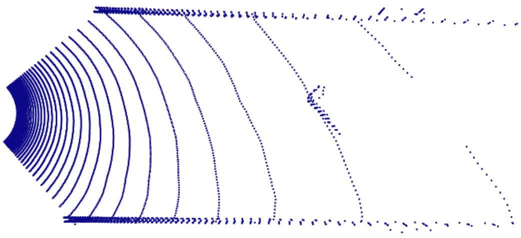

Figure 13: Line Casted RCS returns from the Carla Simulator.

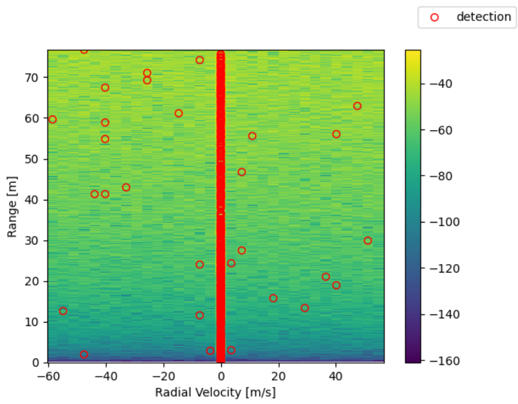

Figure 14: Range doppler detection under clear detections from simulated 4D RADAR

6.1 Rain

Rain causes attenuation on the RADAR received signal. This attenuation (γ) can be described as (Sander, 1975),

$$\gamma = ax^{b}(1 + ax^{-\beta}),$$

where γ is the rain attenuation in dB/km, x is the rain rate in mm/h, and a, b, β are constants. With a known rain rate the usage of the rain attenuation is added in the calculation of the returned signal.

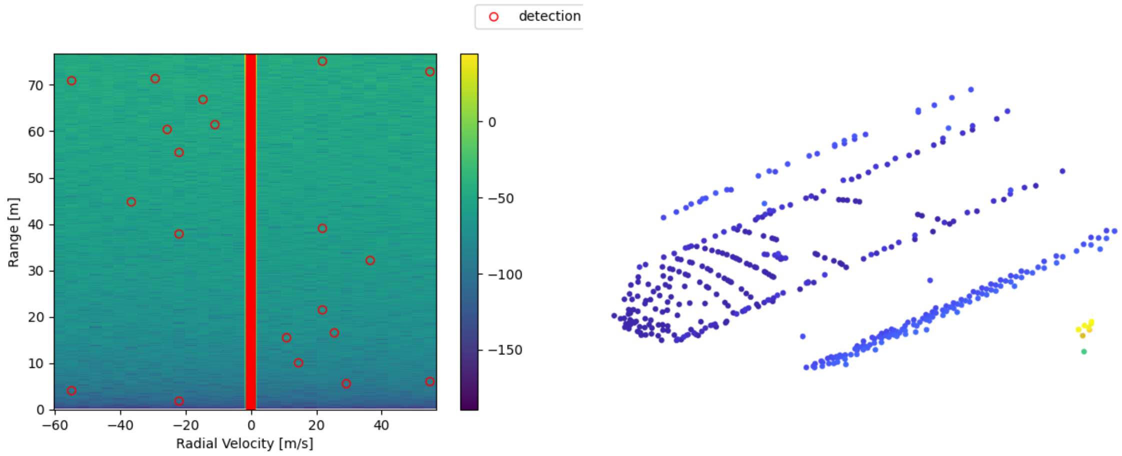

Figure 15: Range Doppler detections and RADAR point cloud (colour represents height of point) under rain

Figure 15 shows the Range Doppler graphic, of the RADAR model in rain conditions. When compared to the clear scenario, Figure 14: Range doppler detection under clear detections from simulated 4D RADAR, the noise has increased, denoted by the deeper shades of blue on the graph. In clear conditions, around 340 points were detected, whilst in rain conditions, 535 points were detected, demonstrating the increased noise cause more detections.

6.2 Fog

Li et al. shows that for RADAR from 0.1THz to 0.3 THz such as the simulated in this work (0.077THz), Mie Theory and Rayleigh approximation are close, in Meteorological Optical Range (MOR) from 30m to 200m (Li, et al., 2014). Above the 1THz threshold, the difference is quite significant. Therefore, Mie theory can also be used in for the RADAR attenuation calculations.

Using the normal distribution from D3.2 for fog DSD described by (Bernardin, Colomb, Egal, & Boreux, 2010), described as

$$n(r) = \frac{N}{r\sigma\sqrt{2\pi}} \exp\left(-\frac{(\ln r - \ln \tilde{r})^2}{2\sigma^2}\right),$$

allows the calculation of the liquid water content (LWC) which is described as

$$\mathrm{LWC} = \frac{4}{3}\pi \int_0^\infty r^3 n(r)\ dr,$$

then it is possible to specify the LWC for log-normal distribution as

$$\mathrm{LWC} = \frac{4}{3}\pi \int_0^\infty r^3 \frac{N}{r\sigma\sqrt{2\pi}} \exp\left(-\frac{(\ln r - \ln \tilde{r})^2}{2\sigma^2}\right) dr,$$

further developed as

$$\mathrm{LWC} = \frac{4}{3}\pi N \widetilde{r^3} \exp\left(\frac{9\sigma^2}{2}\right),$$

then with the usage of Liebe et al (Liebe, Manabe, & Hufford, 1989)

$$\gamma = \alpha \cdot LWC \cdot f^2,$$

where γ is the attenuation in dB/km, α as 0.1820 (Liebe, Manabe, & Hufford, 1989), and f is the frequency in GHz. Allows the calculation of the power attenuation for each target distance by the linearization of the attenuation and multiplication of the distance.

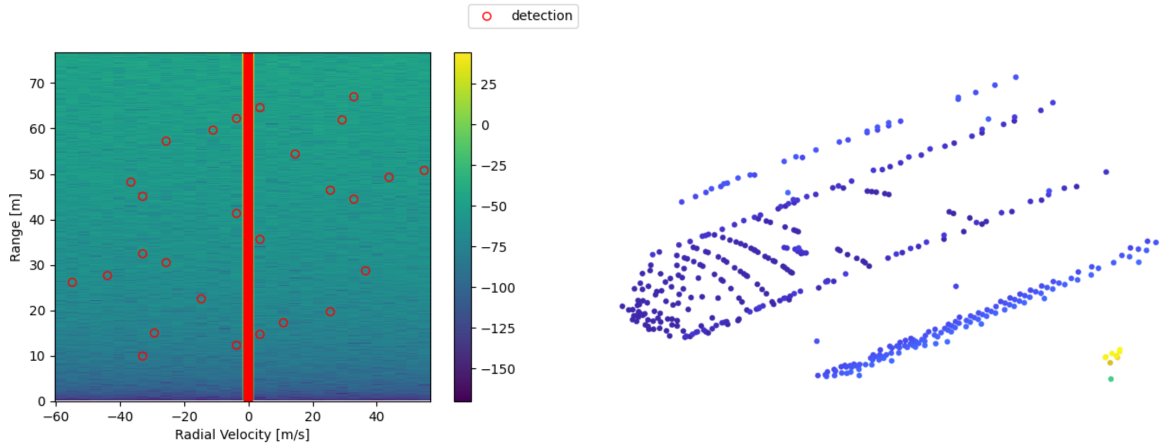

Figure 16: Range Doppler and RADAR point cloud (colour represent height of point) under heavy fog

6.3 Snow

Amarasinghe et al. shows that the snow attenuation is similar to the rain attenuation and makes special remarks on the snow attenuation, stating that at 77Ghz is significantly greater with a local maxima (Amarasinghe, Zhang, Zhang, & Mittleman, 2020). Amarasinghe et al. specifically points out that if the water content of wet snow is lower than 30% then most of the scattering effects are related to ice crystals on the snow (Amarasinghe, Zhang, Zhang, & Mittleman, 2020). The snow attenuation then can be calculated using the equation below.

$$\alpha_{\text{snow}} = 4.343 \times 10^3 \int_0^\infty \sigma_{\text{ext}}(m, r, \lambda) N(r)\ dr,$$

Where m is the refractive index of the particle, $N(r)$ is the snow size distribution (like the DSD but for snow), σ_{ext} is the extinction cross section. Norouziari et al. also shows a method for calculating the snow attenuation (Norouziari, et al., 2018).

Then with the usage of the attenuation on the RADAR power equation, it is possible to simulate the real snow effect, considering each of the distances to each detection.

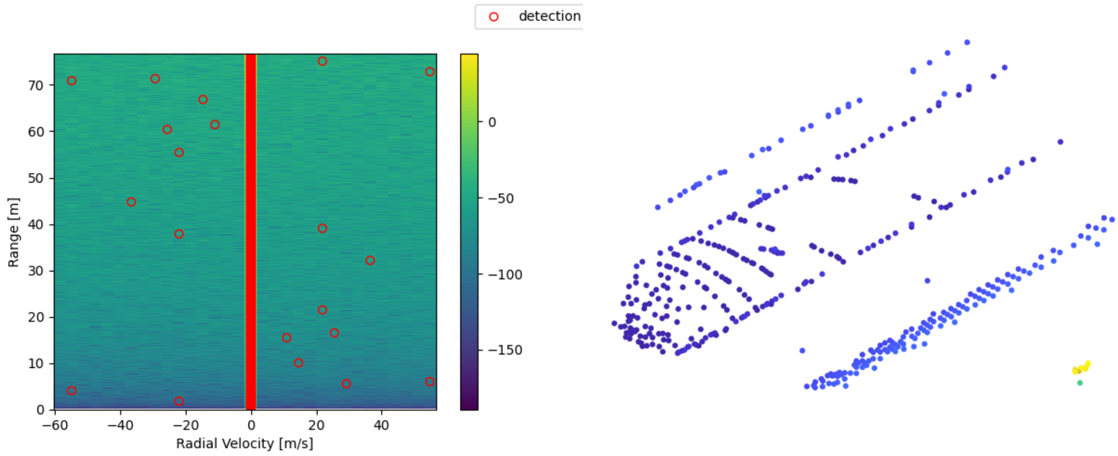

Figure 17: Range Doppler and RADAR point cloud (colour represent height of point) under snow

Figure 17 shows the Doppler Range graph under snow. The point cloud counted with 543 which is greater than the clear weather point cloud.

7 Evaluation, Comparison, and Validation of Created Models

The process of validating the sensor weather noise models created in T3.3 and T3.4 against the data captured in T3.2 will be described in this Chapter.

7.1 Validation of noise models

The process of validating noise models is not established, and as mentioned is very often based on qualitative evaluation and visual comparison of real to modelled data. Bearing in mind that one of the key outputs of T3.4 is to select the noise models to be integrated in X-i-L as a part of work package 7, as a part of ROADVIEW, we propose a validation/evaluation process, Figure 18, for the noise models based of the following steps:

- **Qualitative evaluation** of the noise generated, i.e. visually comparison of the noise applied to real 'clear' sensor data from the dataset to the 'noisy' data collected in rain, fog, and snow (see Chapters 4-5-6).
- **Quantitative evaluation** of the quality of 'noisy' frames, based on the metrics described in the next two sub-chapters.
- **Comparison of the metrics' values and variations** in real data and data generated with the models (see Chapter 7.4).
- **Comparison of the execution time of the models** for real time implementation (see Chapter Physics based model performance).

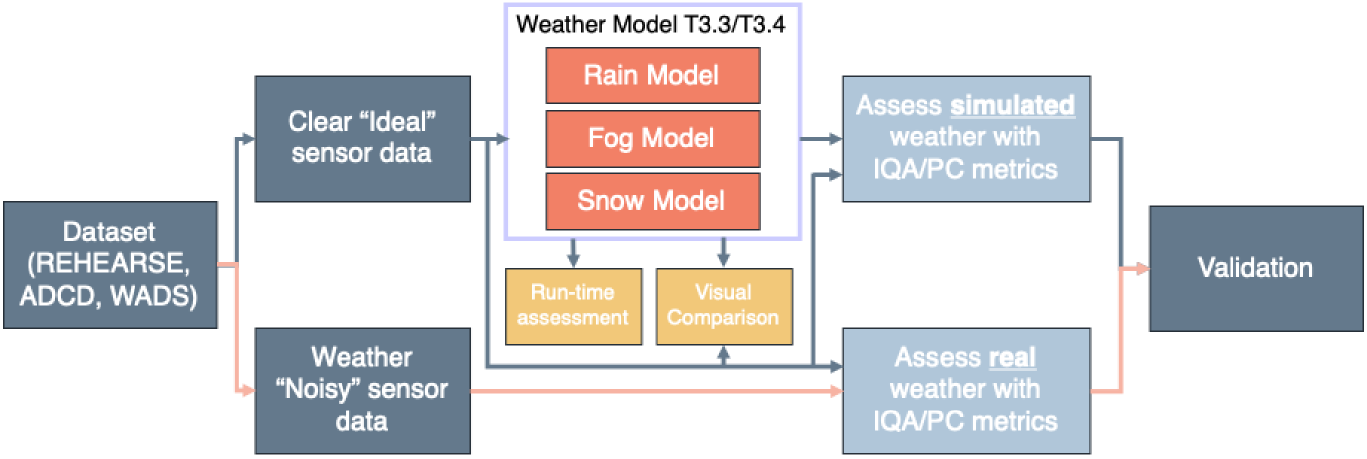

Figure 18: Methodology to assess the noise models (based on qualitative, quantitative and run-time) using the sensor data output, validated against weather data collected in the real world.

7.2 Metrics to evaluate and compare camera data

Traditional Image Quality Assessment (IQA) is based on trying to quantify the quality of images produced by digital cameras. IQA metrics are focused on establishing how 'good' or 'pleasant' is an image for a human consumer and therefore are tailored around the human visual system. Work in this field has generated two types of metrics, summarised below, and described in detail as a part of a ROADVIEW paper, currently under review (Gummadi, Chan, Wang, & Donzella, 2023).

- **Full-reference IQA (FR-IQA) metrics**, that generate a score by comparing a reference ('ideal', 'clear') image with another image under assessment.

- **No-reference IQA (NR-IQA) metrics**, based on extracting features from the image under assessment and mapping them based on hand-crafted mapping function or data-driven models.

As ROADVIEW aims to quantify the degradation of sensor data due to the noise models and compare it to the degradation in the real world of real automotive sensors, using FR-IQA is the best option, as it enables us to compare 'noisy' frames (either simulated or real) to the 'ideal' collected without any rain, fog, or snow. The image features assessed by the selected IQA metrics are presented in Table 10; as demonstrated in the table, we have selected a wide variety of metrics covering all the possible spatial and frequency features identified.

Moreover, we have studied the correlation of the above-mentioned metrics with Deep Neural Network (DNN) performance, and particularly object detection. The presented results show that of the 14 selected metrics 11 have high correlation with the perception performance, and in particular Information Content Weighted SSIM (IW-SSIM), Denoise Snow Score (DSS) and MS-SSIM are very accurate in predicting the DNN performance. The three metrics that have low correlation are PSNR, VIF, and MDSI (Gummadi, Chan, Wang, & Donzella, 2023).

Table 10: The 14 selected IQA metrics covering different assessment of image features. ↑ Score is higher if image is more similar to reference image. ↓ Score is lower if image is more similar to the reference image

IQA Metric	Frequency Features		Spatial Features				
	Fourier	Wavelet	Local Mean	Local Contrast	Edge Gradients	Chrominance	Visual Salience
1)PSNR↑ **Peak signal to noise ratio**							
2)SSIM↑ **Structural similarity index**			✓	✓			
3)CW-SSIM↑ **Complex wavelet SSIM**		✓					
4)DSS↑ **Discrete cosine transform subband similarity index**	✓						
5)HAAR-PSI↑ **Haar perceptual similarity index**		✓					
6)VIF↑ **Visual information fidelity**	✓						
7)VSI↑ **Visual saliency-induced index**					✓	✓	✓
8)MS-SSIM↑ **Multi scale SSIM**			✓	✓			
9)SR-SIM↑ **Spectral residual based similarity**					✓		✓
10)IW-SSIM↑ **Information content weighted SSIM**			✓	✓			
11)FSIM↑ **Feature similarity index measure**	✓				✓	✓	
12)GMSD↓ **Gradient magnitude similarity deviation**					✓		
13)MS-GMSD↓ **Multi scale GMSD**					✓		
14)MDSI↓ **Mean deviation similarity index**					✓	✓	

7.3 Metrics to compare LiDAR and 4D RADAR data

Concerning LiDAR and 4D RADAR, the work to evaluate the quality of data produced is scarce, if not nonexistent for 4D RADAR. However, this type of automotive RADAR produces data in a point cloud format (Chan, Shahbeigi, Ye, & Donzella, 2023), so we decided to apply the same metrics to LiDAR and 4D RADAR. For LiDAR the metrics have been traditionally created to understand how similar are point clouds, but in a way, they can be adapted to be used to measure the noise on a point cloud, with respect to an 'ideal' point cloud. Table 11 explains the significance of the selected point cloud (PC) metrics, i.e. metrics 2 to 6. Moreover, we have proposed a new metric, named SDM, metric 1 in Table, aimed particularly at evaluating the dissimilarity between point clouds, as fully discussed in our accepted ROADVIEW paper (Shahbeigi, Robinson, & Donzella, 2024). Recently, we have been also investigating the relationship between these PC metrics and semantic segmentation of point clouds, to propose a de-snow or de-noise score, the submitted paper is currently under review, and pre-prints are available here (Chan, Gummadi, Raisuddin, Aksoy, & Donzella, 2024). Moreover, we have demonstrated for the first time how to apply the above-mentioned metrics to 4D RADAR point cloud in (Chan, Shahbeigi, Ye, & Donzella, 2023), and they will be used in the following sections.

Finally, for the 4D RADAR, to add further information and evidence to our point cloud analysis, we have also evaluated number of points in the PC with and without noise, and in specific areas of the point clouds.

Table 11: Comparison of different PC comparison metrics. ↓ Score is lower (closer to 0) if PC is more similar to the reference PC

Metric	Importance	Pros	Cons
1)SDM↓ **Shahbeigi-Donzella metric**	PC shape signature and distance between signatures	View and size invariant	Can be computationally intensive
2)RMSE↓ **Root mean squared error**	Root Mean Squared Error (RMSE), point to point difference	Overall assessment of differences	Needs PCs of same size
3)MDE↓ **Mean distance error**	Euclidean distance between all nearest neighbour pairs	More robust to outliers than RMSE	More focused on spatial similarity
4)MMDE↓ **Maximum mean distance error**	Emphasise the maximum average distance between points	Emphasize detection of anomalies	Sensitivity to large differences
5)HD↓ **Hausdorff distance**	Maximum distance error of corresponding points	Anomaly detection	May introduce redundancy
6)HD95↓ **Hausdorff distance at 95th percentile**	Similar to HD, but assess the error of the 95th percentile	Robust outlier handling	May affect the sensitivity to certain outliers

7.4 Metric Comparison of Emulated and Simulated Weather

The REHEARSE dataset has methodologically captured paired frames from different scenarios (Poledna Y. , Drechsler, Donzella, & Chan, 2024) (Poledna Y. , et al., 2024). A subset of the scenarios was used to determine the baseline noise and used to post process application of the adverse weather using the IQA and PC metrics. To support the analysis of the snow model, additional datasets are explored, i.e. ACDC dataset and WADS dataset for camera and LiDAR respectively (Sakaridis, Dai, & Van Gool, ACDC: The Adverse Conditions Dataset with Correspondences for Semantic Driving Scene Understanding, 2021) (Kurup & Bos, 2021). Frames 51 to 70 and 251 to 270 were analysed when using the REHEARSE dataset for the IQA and PC metrics. For ACDC and WADS, specific sequences were deployed for analysis detailed in the following sections.

7.4.1 Camera

The fourteen metrics presented in Table 10 were adapted and then applied to quantify the noise present by comparing frames with real-world (T3.2) or simulated (T3.3 and T3.4) adverse weather conditions against the corresponding scene with clear weather. Three scenes were selected for rain and fog to evaluate the noise implemented with different test targets or distances see Table 12.

To quantify snow weather the ACDC dataset by Sakardis et al. has been used (Sakaridis, Dai, & Van Gool, ACDC: The Adverse Conditions Dataset with Correspondences for Semantic Driving Scene Understanding, 2021). This dataset provides matched frames of recorded sequences in the real world with and without the presence of snow. The falling snow rate was not provided with the images. To create the baseline dataset, some sequences were split into a heavy snow set (sequences GOPR0494, GP010494 and GP010496) and a light snow set (sequences GOPR0122, GP010176, GP020606 and GP030176) based on a visual inspection.

Table 12 summarises the number of IQA metrics that performed as expected for each scene, i.e. a decreasing or increasing trend when the amount of noise/degradation is increasing, see Table 12 for expected trends. There are very little correct metric trends (with many not showing a trend) coming from the **rainy** data collected in the real world T3.2, and simulated in data-driven methods from T3.3. For **fog**, the most metrics captured that as visibility reduces, the similarity to the clear scene is reduced. For these two weathers, the physics-based application of weather demonstrated the most expected trends. However, in the ACDC **snow**, the physics-based application did not match any expected trends. These aspects are further discussed in the following sections.

Comparisons of the SR-SIM scores and trends are presented in Figure 19, Figure 20 and Figure 21. The complete set of metric scores for camera is presented in Appendix 10.1.

Table 12: Number IQA metrics exhibiting expected trends with increasing adverse weather for different scenes. * dependent on definition of DSD for snow, see sec. 7.4.13.

Weather	Scene	Number of correct metric trends (out of 14)		
		REHEARSE (T3.2)	Data-Driven models (T3.3)	Physics-Based models (T3.4)
Rain	THI, Car, 28m	3	0	14
	THI, Car, 56m	2	0	14
	THI, Camera Target, 28m	0	3	14
Fog	CE, Car, 15m	13	11	13
	CE, Pedestrian + Bike, 15m	13	11	13
	CE, Sensor Targets, 15m	13	11	13
Snow	ACDC	11	-	0*
	THI, Car, 28m	-	14	-
	THI, Car, 56m	-	12	-
	THI, Camera Target, 28m	-	12	-

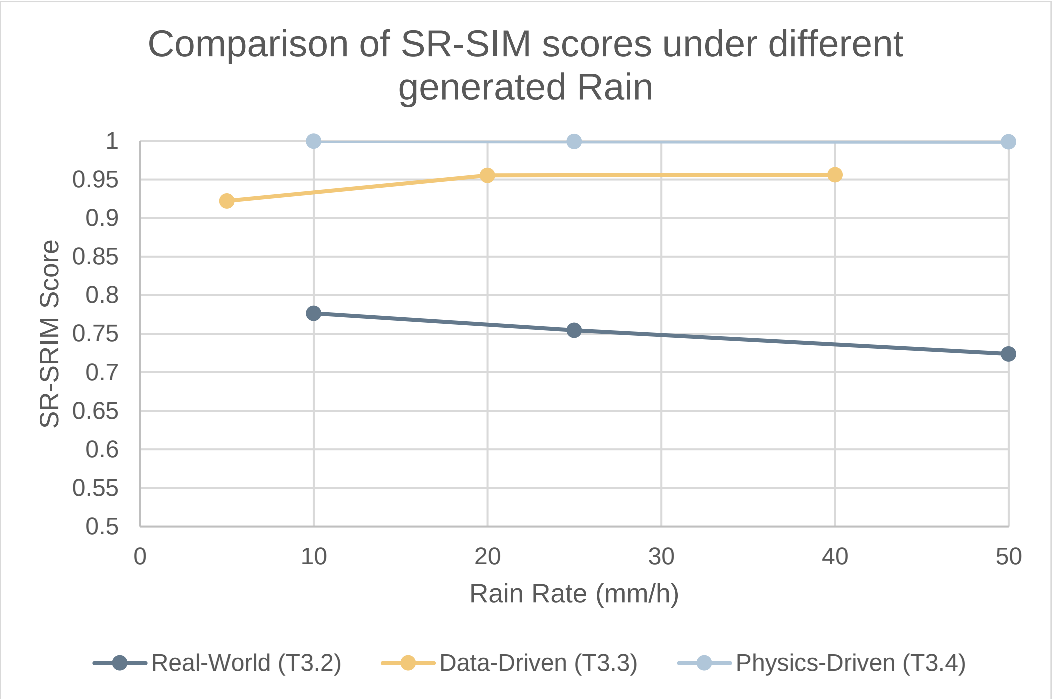

Figure 19: Comparison of SR-SIM for the different rain data from ROADVIEW

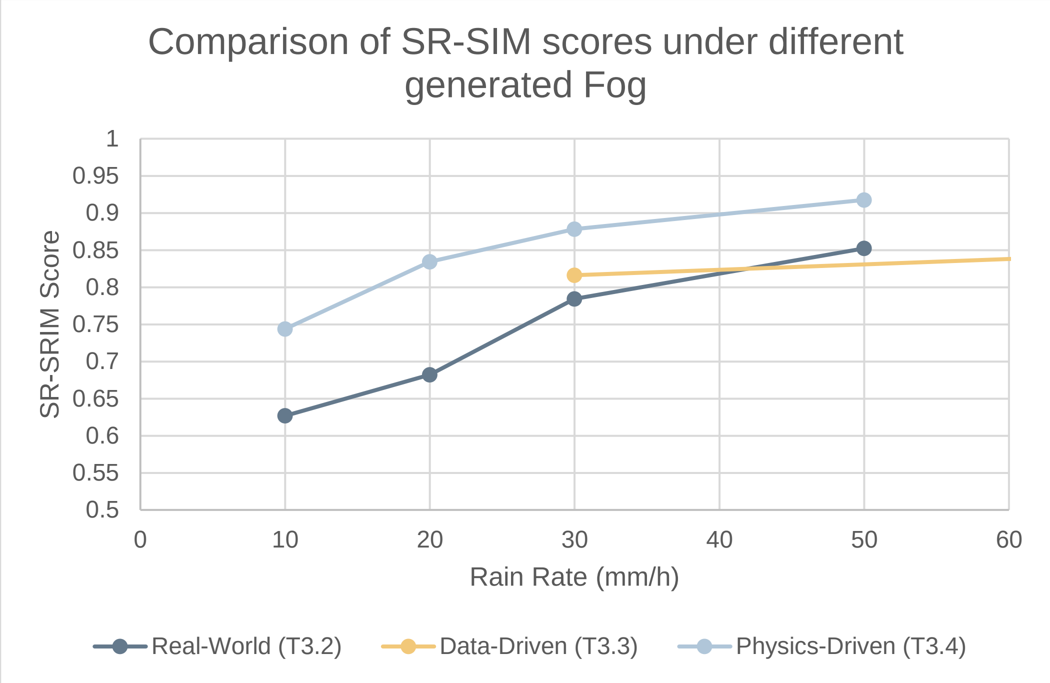

Figure 20: Comparison of SR-SIM for the different Fog data from ROADVIEW

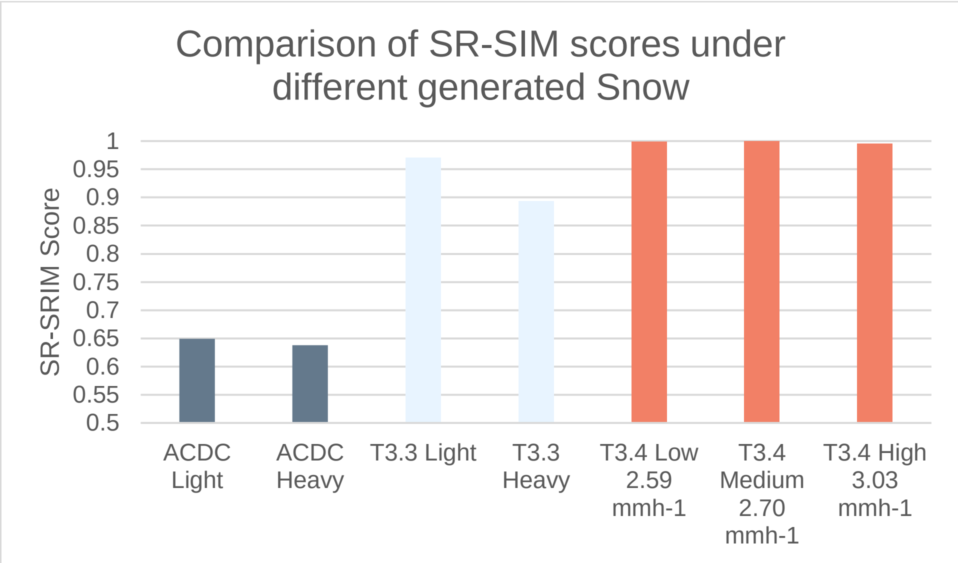

Figure 21: Comparison of SR-SIM for the for snow from ROADVIEW modelling compared against the ACDC snow dataset

7.4.1.1 Rain

In the REHEARSE real data with rain (T3.2), very little metrics exhibited the expected trend. At most, only 3 out of 14 IQA metrics follow the expected trend in the evaluated scenes. Visually inspecting the data, see Figure 22, there are a variety of lighting conditions (i.e. different time of day and sun position during the data capture) leading to difference in exposures. These lighting variations cause big fluctuations in the values of pixels between different frames, and are detected as 'degradation' by the metrics. Metrics like IW-SSIM and SR-SIM are less affected by the lighting conditions, perhaps because they enable a better analysis of the structural content of the frames.

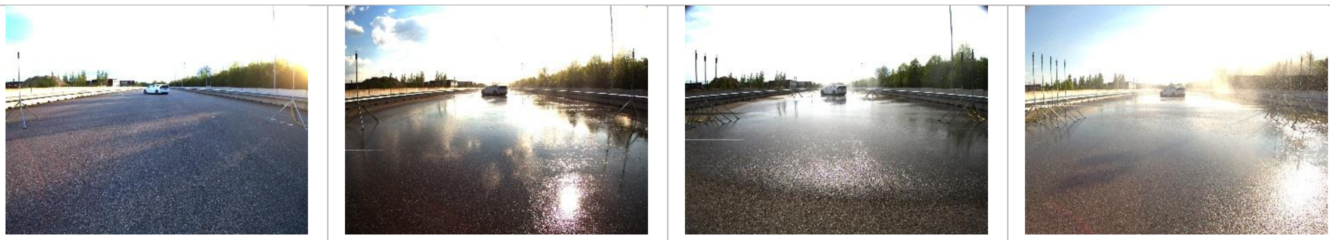

Clear Weather | Rain Rate = 10mm/h | Rain Rate = 25mm/h | Rain Rate = 50mm/h

Figure 22: Images of THI Data at different rain rates (Data Target = Car, Target Distance = 28m) and the corresponding clear image

In the data-driven model, there are no trends exhibited by the metrics in the compared data. This lack of trends might be due to two reasons: 1) generative models are difficult to control and overall the output rain rate is unpredictable; 2) the models used lower resolution frames and they were then upscaled to the original, input resolution. However, due to the small nature of raindrops and streaks, the generated effects may be reduced, or artefacts may be introduced from the upscaling technique.

In the physics-based model, all IQA metrics performed as expected. Based on the design of the model, the amount of noise from the rain added is based on the DSD. With the used Marshall-Palmer DSD, the number of droplets of different sizes increases as the rain rate increases, hence creating more noise as the rate increases. However, some metrics exhibited near perfect scores even with the added noise (indicating the 'noisy' image is almost exactly the same to the 'noisy' one). The only difference between the generated image and the reference image is only the applied rain noise (i.e. the output of the model is compared to the input of the model). Additionally, depending on the size and distance from the camera, many droplets only had a minor effect of the captured intensity per pixel and therefore had a minor effect on the metrics.

7.4.1.2 Fog

A comparison of the fog frames in the dataset and with simulated noise is shown in Figure 23. **In the emulated fog in the REHEARSE dataset** captured with the Lucid Triton camera, almost all metrics exhibited the expected trend, aside from VIF. The implementation of VIF is sensitive to the contrast of the image and was observed that a higher contrast image compared to a lower contrast image can have a score of above one (Photosynthesis Team, 2023). Within the Lucid Triton images, overexposure can be identified in the image with clear weather. As the visibility due to fog decreases, the area of overexposure increases due to the increased scattering of light across a wider area. Hence, as the visibility reduces (stronger fog), the contrast decreases, and the VIF metric trend is opposite to the initial assumption. In fact, the trend of VIF does increase as visibility decreases, and matches this theory.

The majority of the metrics does exhibit the expected trend for the **data driven fog model**. However, due to limitations in the data-driven techniques, the trends are presented based on visibility of 30m, 200m, and 400m compared to the REHEARSE emulated and physics-based simulated visibility of 10m, 20m, 30m, and 50m, so we cannot fully validate these models.

Table 13: Comparison of the attenuation coefficient computer per colour using Mie theory and Koschmieder's Theory

Fog Visibility (m)	Mie Theory (Wavelength)			Koschmieder Theory	Difference (%)		
	Blue (460 nm)	Green (530 nm)	Red (600 nm)		Blue	Green	Red
10	0.2889	0.2934	0.2989	0.3000	-3.7032	-2.1869	-0.6923
20	0.1457	0.1481	0.1504	0.1500	-2.8824	-1.2832	0.2675
30	0.1024	0.1043	0.1061	0.1000	2.4470	4.2750	6.0648
50	0.0705	0.0723	0.0740	0.0600	17.4307	20.4252	23.2552

In the physics-based model, the model's trend behaved the same as the data captured in the real world, again with VIF not following the expected trends. The model's attenuation was calculated based on Mie theory, applying the measured DSD provided by the data based on a different electromagnetic wavelength per colour channel (i.e. based on the Bayer data). This proved valuable as there are clear difference in the attenuation calculated with this method compared to the generalised Koschmieder's equation, used in many works, see Table 13. Whilst the attenuation coefficient using the approximation of Koschmieder's theory in this scenario is similar to the Mie theory at low visibility (i.e. 10 m and 20 m), this drastically changes at higher (better) visibility. At 50 m visibility, there is up to 23% difference between the attenuation coefficient between Mie theory and Koschmieder's theory. The attenuation calculated by Mie Theory is higher than Koschmieder's theory indicating that you will see less and hence would have less time to react. This timing is critical, especially at low ranges to detect hazards and hence is critical to model the weather properly. <u>Additionally, the difference in attenuation per colour channel also varies quite a lot at the same visibility, highlighting the importance of properly account for wavelength using Bayer input.</u>

REHEARSE collected images with fog	**Data-Driven Simulated Fog**	**Physics-Based Simulated Fog**

Figure 23: Comparison of 30m visibility fog in the collected data and ROADVIEW fog models

7.4.1.3 Snow

In the ACDC dataset (real-world data), the majority of the metrics exhibited the expected trend. Although the location was matched in the frames, there was a large time difference between the frames. This can be seen where there is mismatched construction in images but also difference in foliage condition, e.g. with green leaves in the clear frames and bare branches in the snow frames. These effects can have an impact of the metric scores with different severity based on the feature of the image being assessed.

The data-driven noise models performed well with many metrics exhibiting the expected trends. The generated snow images were resized through super resolution to match the original image size. In the generated images, see Figure 24, it is difficult to see indication of falling snow, reinforcing Rothmeier et al.'s work stating that it is difficult to generate falling snow using machine learning techniques (Rothmeier, Huber, & Knoll, 2024). However, in the heavy snow image, there are snow buildup generated on surfaces and also converting of the trees to branches similar to wintertime with no leaves.

Figure 24: Images generated by the data-driven snow model for validation. Left: light snow, Right: heavy snow

None of the expected trends in metric scores was observed for the physics-based model. Figure 8 presented the images from the output of the models. In the lowest simulated snow rate, there are several bright spots due to the snow. In the medium snow rate, there was very little effect on the image. With the heaviest snow rate, there are many patches with shifts in intensity towards white due to the modelled snow. A measured weather snow event DSD was used, but the parameterisation of the DSD equation individually modelled each rate. The three DSD models have led to the medium snow rate having far more small snowflake size compared the other rates, Figure 25. At the same distance, smaller snowflakes will have a lower impact on the pixel intensity than larger drops, hence the inconsistency in the effect on the final image. Indeed, if the medium snow was not accounted for, all the metrics show the expected trend. This model demonstrated the high importance of simulating the DSD alongside the weather rate as they both will determine the severity of the impact on the final image.

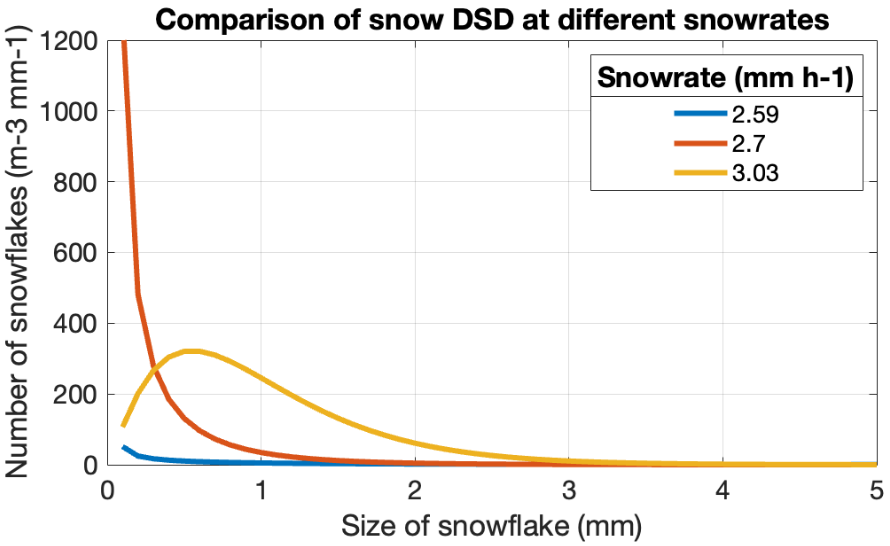

Figure 25: DSD of snowflakes using measured distribution from a Colorado snowstorm event

7.4.2 LiDAR

The six PC metrics were applied to the collected data from the Ouster LiDAR in the REHEARSE dataset and the 64 channel LiDAR in WADS to quantify the effect of the noise. The REHEARSE dataset provided the paired data for rain and fog, with the compared scenes presented in Table 14. Due to the method of emulating the rain in the REHEARSE dataset, there is only a limited region in space with emulated rain. To mitigate this, only this specific areas of the point clouds are evaluated.

There is a lack of directly paired datasets with snow for LiDAR. For this analysis, the WADS dataset which provided point clouds captured during snow events were used. Moreover, this dataset provides labelled snow points (Kurup & Bos, 2021), so we created a paired dataset to the best of our ability, i.e. removing snow points from the point clouds and using the resulting PC as the baseline 'clear' weather. Based on the number of snow points in the point clouds, we divided the sequences as light (i.e. sequences 35, 6% snow points) and heavy (i.e. sequences 26, 18% snow points) snow.

The number of expected trends for the applied PC metrics as the weather rate increases are summarised in Table 14. In the real data, less than half the metrics exhibited the expected metric. The data-driven models did not show trends, but the physics-based models worked a lot better at introducing increasing changes to the point cloud as the weather rate increased. Figure 26, Figure 27 and Figure 28 presents a comparison of the SDM scores on the different weather LiDAR data. The full list of metric scores is presented in Appendix 10.2.

The data-driven models are based on an statistical analysis on real data to remove points which would be attenuated by the weather. However, false points due to backscattering from the weather phenomena are not added, which could cause the lack of trends exhibited.

Table 14: Number PC metrics exhibiting expected trends with increasing adverse weather at different scenes for LiDAR.

Weather	Scene	Number of expected metric trends (out of 6)		
		Baseline (i.e. REHEARSE (T3.2))	Data-Driven (T3.3)	Physics-Based (T3.4)
Rain	THI, Car, 28m	2	0	4
	THI, Car, 56m	2	1	4
	THI, Cam Target, 28m	3	0	4
Fog	CE, Car, 15m	5	0	6
	CE, Pedestrian + Bike, 15m	3	2	6
	CE, Sensor Targets, 15m	4	0	6
Snow	WADS	5	-	6
	REHEARSE	-	-	-

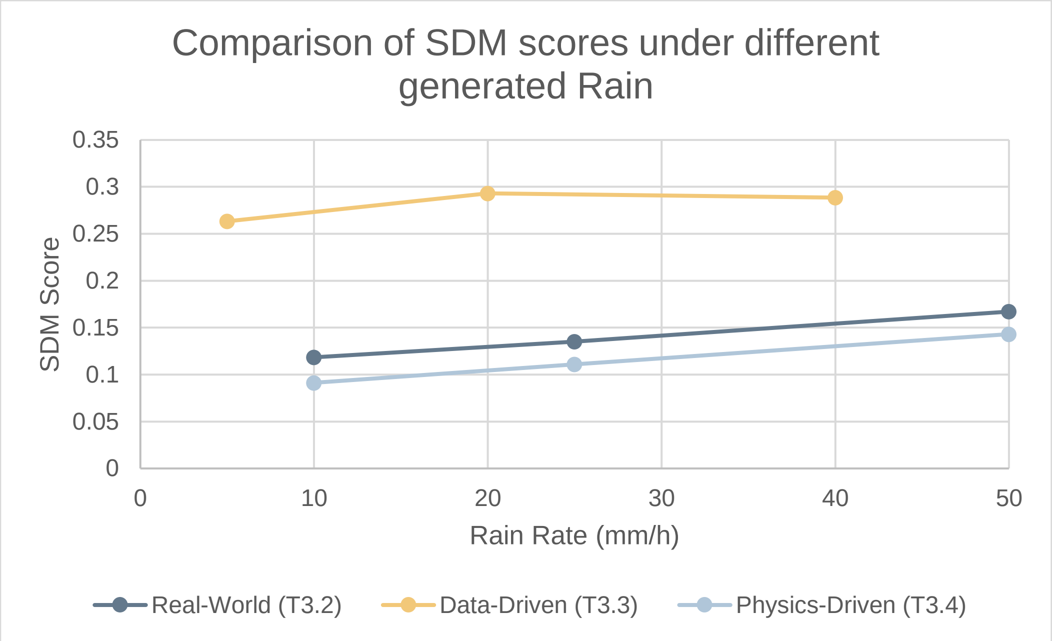

Figure 26: Comparison SDM for rain from ROADVIEW LiDAR data

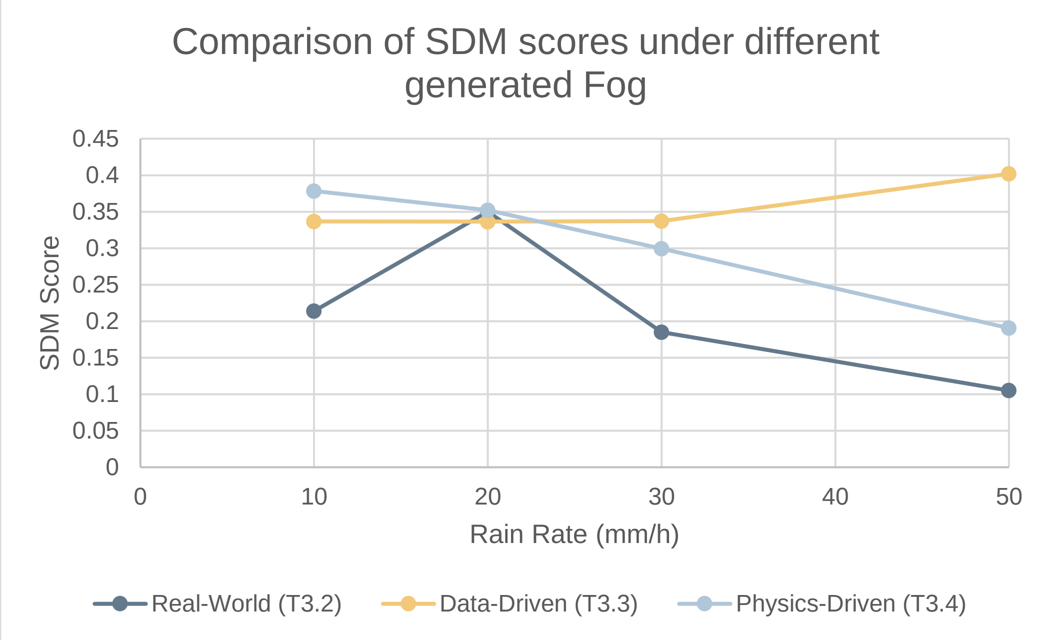

Figure 27: Comparison SDM for fog from ROADVIEW LiDAR data

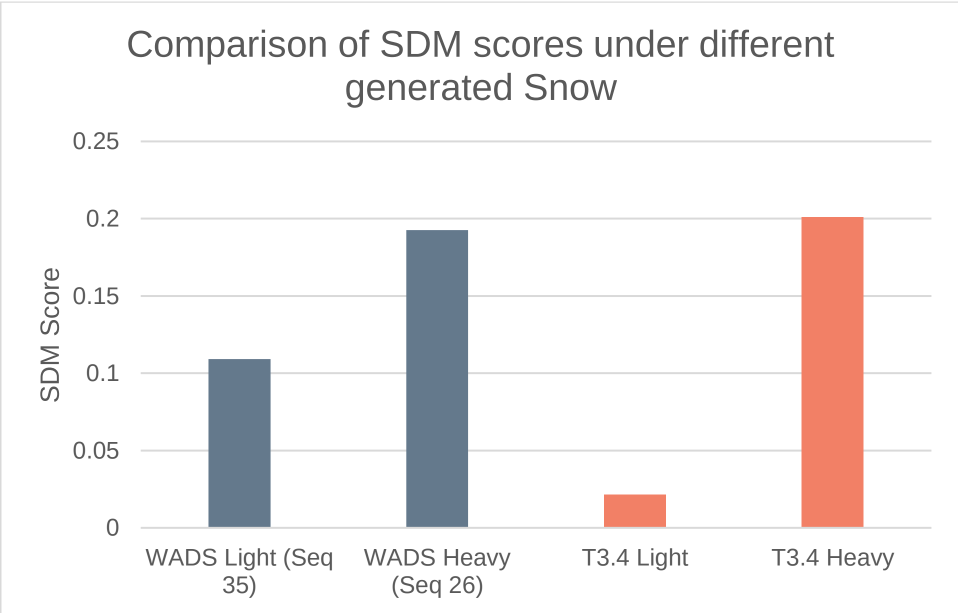

Figure 28: Comparison SDM for snow from ROADVIEW LiDAR snow model against the WADS snow dataset

7.4.2.1 Rain

In the capture of the rain in the REHEARSE dataset, the metrics had a poor performance with expected trends due to the low number of points captured in the emulated rain point clouds. A visualisation of the point clouds for comparison is presented in Figure 29. The target points along the far end of the x-axis start to diminish (i.e. attenuate due to increases in rain rates). However additional sprinklers detected by the LiDAR in the assessed area increase the number of points closer to the origin. Thus, adding unwanted noise to the structure of the point clouds and thereby altering the metric scores. The Ouster OS1 LiDAR conducts some data processing before providing the final point cloud, hence it appears that the false returns due to backscatter from the rain are filtered.

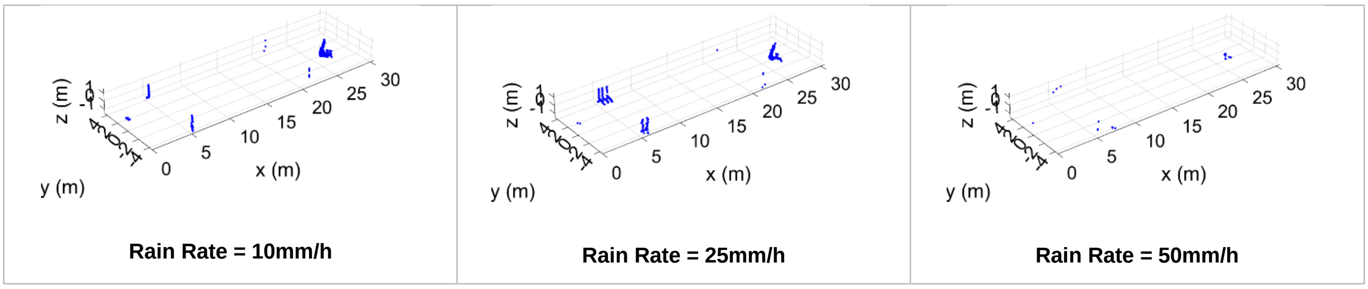

Figure 29: Point cloud regions assessed using PC metrics with point clouds of different rain rates from the REHEARSE dataset

The physics-based rain model consistently achieved 4 out of 6 expected trends. In all scenes, MMDE and HD95 does not follow the expected trends. These two metrics are designed to be less sensitive to outliers. The design of inserting false positive points per beam based on the DSD in the model can create many points which are distant from other points and classed as "outlier" in the metrics.

7.4.2.2 Fog

There are varying number of trends following the expected trend in the PC from the **REHEARSE dataset**. In the pedestrian and bike scene, demonstrating the lowest number of expected trends, it is observed that there are many newly introduced points in the near range from the fog at lower visibility in additional to the lower number of points in the far field, see Figure 30. These differences are causing some outliers which makes the metrics perform not as expected. This theory is reinforced by using HD95 which is more robust against outliers, with all three scenes demonstrating the expected trend with this metric. However, understanding the outlier is important as any false points due to fog is important and cannot be classified as an outlier. **The physics-based rain model consistently** achieved 6 out of 6 expected trends.

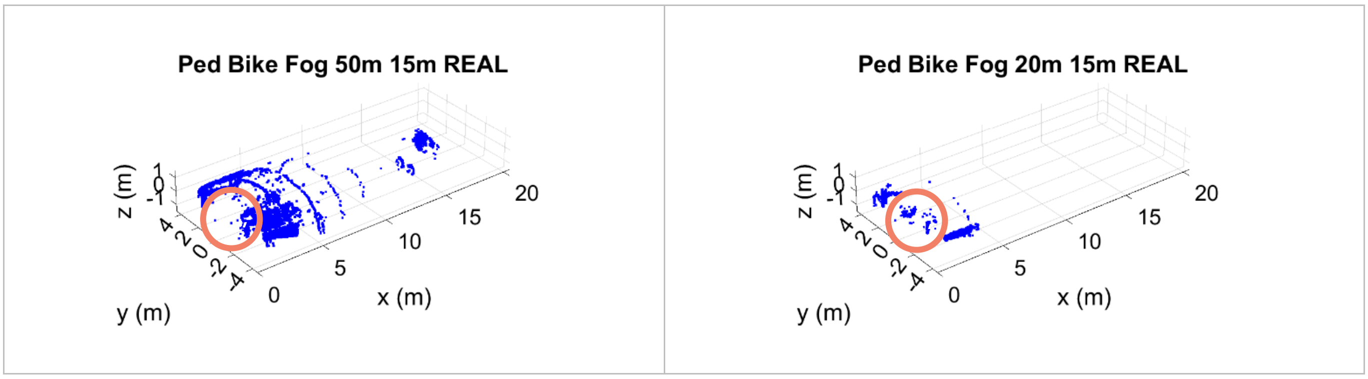

Figure 30: Sample point clouds from REHEARSE dataset under different visibility. The circle highlights an area which contains many more false points at lower visibility

7.4.2.3 Snow

From the WADS dataset, all but HD95 followed the expected trend, indicating that outliers are causing the core differences in the analysis. Due to the method of generating the ideal paired data, by removing snow points in the sequences, this could cause gaps in data where objects should be, particularly at heavier snow. Hence contributing to the higher number of outliers.

7.4.3 RADAR

The six defined PC metrics have been also applied to the REHEARSE 4D RADAR data and physics-based simulated 4D RADAR data. Due to the lack of conclusiveness from the data driven analysis, there was no 4D RADAR PC data available from the data-driven model (Duthon, Ouattara, Liandrat, & Poledna, 2024). For the physics based model, the 4D RADAR data in rain and fog are captured in the REHEARSE dataset. Using the same 4D RADAR, real snow events were captured at Puy De Dome (PDD). The scenes assessed and related PC trends are presented in Table 15.

The physics-based adverse weather models are applied to the PC generated by the ROADVIEW 4D RADAR model in Carla within the created THI and CE digital twins, delivered inT3.1 (Herranen & Kloek, 2023).

Figure 31, Figure 32 and Figure 33presents a comparison of the RMSE scores on the different weather 4D RADAR data. The full list of metric scores is presented in Appendix 10.3.

Table 15: Number PC metrics exhibiting expected trends with increasing adverse weather at different scenes with 4D RADAR PCs.

Weather	Scene	Number of expected metric trends (out of 6)		
		Baseline (i.e. REHEARSE (T3.2))	Data-Driven (T3.3)	Physics-Based (T3.4)
Rain	THI, Car, 28m	2	-	0
	THI, Car, 56m	4	-	0
	THI, RADAR Target, 28m	1	-	-
Fog	CE, Car, 15m	0	-	-
	CE, Pedestrian + Bike, 15m	0	-	-
	CE, Sensor Targets, 15m	0	-	-
	THI, Car, 28m	-	-	0
	THI, Car, 56m	-	-	0
Snow	PDD	3	-	-
	THI, Car, 28m	-	-	0
	THI, Car, 56m	-	-	3

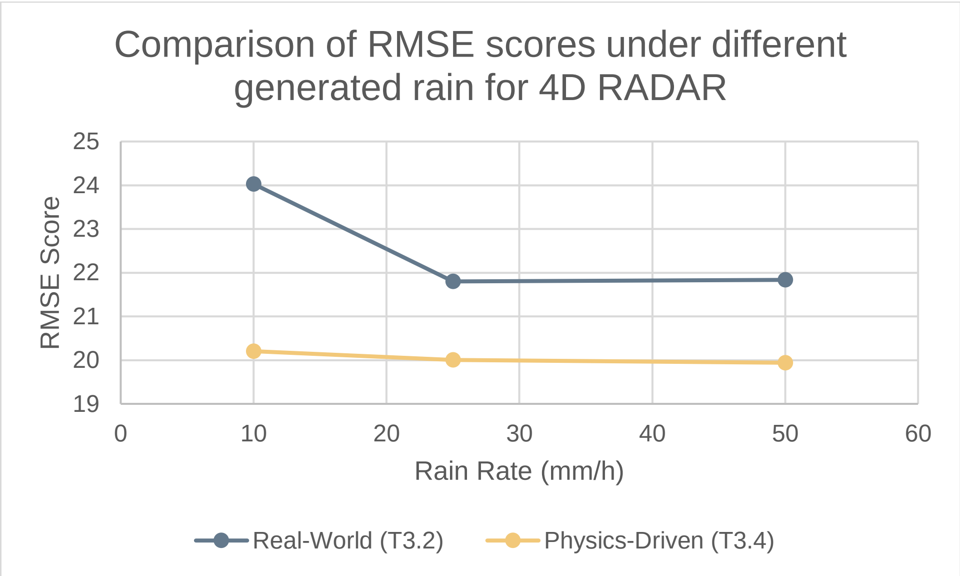

Figure 31: Comparison RMSE for rain from ROADVIEW 4D RADAR data

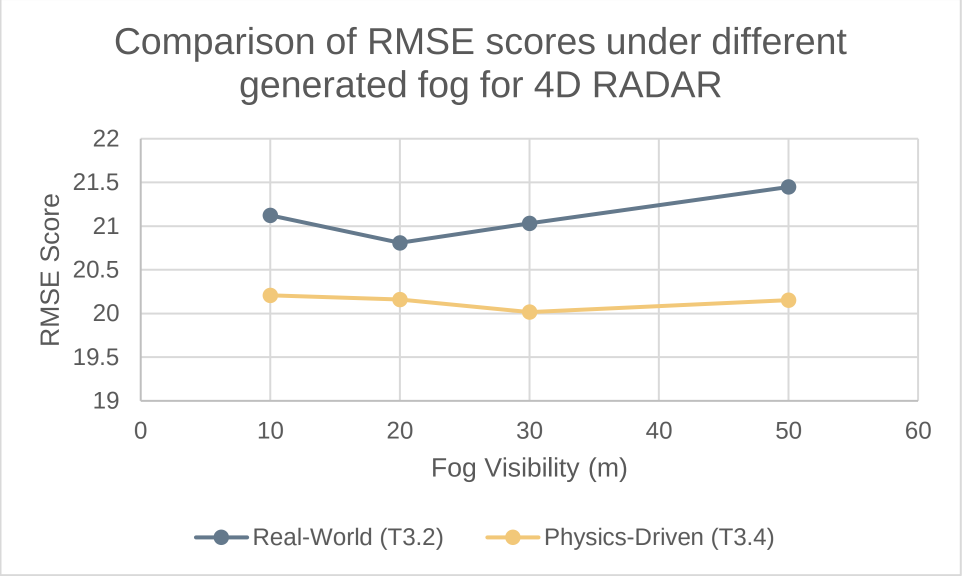

Figure 32: Comparison RMSE for fog from ROADVIEW 4D RADAR data

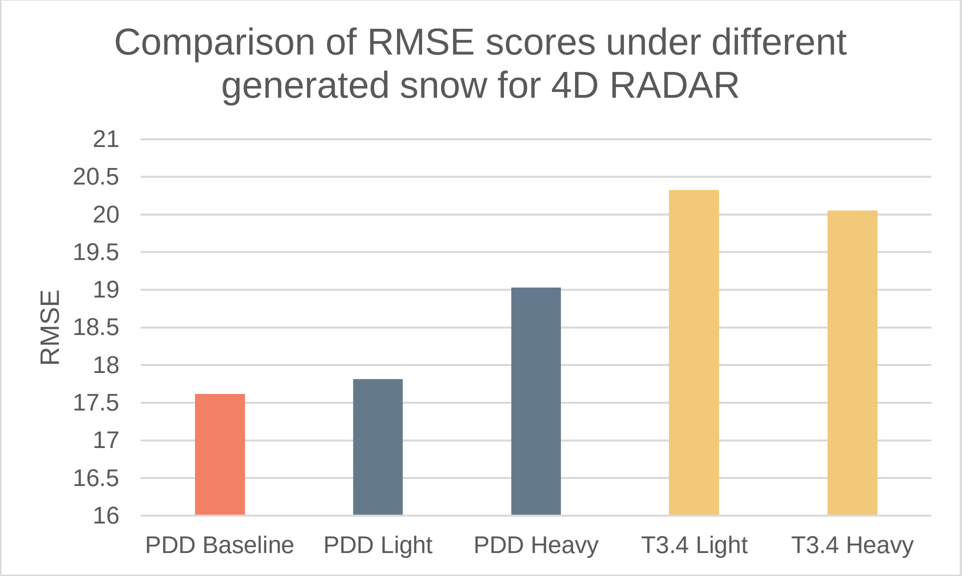

Figure 33: Comparison RMSE for snow from ROADVIEW 4D RADAR snow model against the snow data collected at PDD

In the REHEARSE dataset and the PDD data capture, there are a varying number of expected trends across the different weather conditions. The 4D RADAR data is inherently quite noisy, and comparing different 4D RADAR PCs collected in 'ideal' conditions, ~10% in the blue line in Figure 34, it was observed that the baseline variance is quite large. For most of the analysis with adverse weather, the average metric score falls within the standard deviation of the baseline clear-clear analysis. However, the average metric scores for adverse weather are always higher (worse) than the average for the baseline. This affirms literature that weather does not have a large effect of 4D RADAR, but there is still a minor effect.

The processing algorithms performed by commercial 4D RADAR are closely guarded, making it difficult to model and creating uncertainties in the effect of the noise. Similar to the real data, the number of points in the 'noisy' point clouds generated by the physics-based model does increase with respect to the pint clouds in clear weather. A lower level of random noise across frames collected/generated in similar conditions (lower variance across many similar frames) is exhibited in the simulated adverse weather data compared to the real world. This is likely due to a lower exposure to different sources of noise in the simulation.

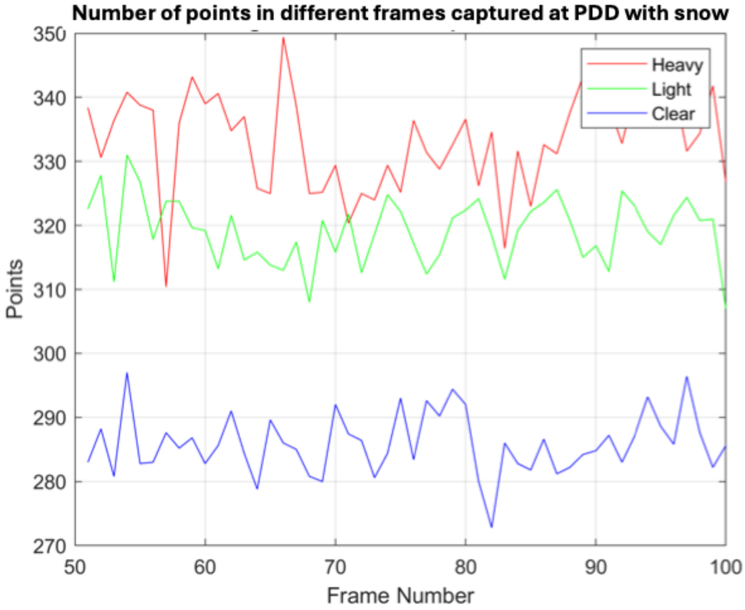

Figure 34: The number of 4D RADAR points present in the data capture at PDD under clear, light and heavy snow

7.4.3.1 4D RADAR point count analysis

The number of points was counted and averaged across 10 frames for each of the scenes in the REHEARSE dataset and the related scenes generated by the T3.4 RADAR noise model, Figure 35 and Figure 36. In the simulated adverse weather, Figure 35, there is a notable increase of detected points under the effect of adverse weather. Comparatively in the captured adverse weather, Figure 36, only fog increases in points by a small amount, with rain reducing the number of points as the weather increases. However, the effect of signal processing in the real collected 4D RADAR data is unknown, making a true comparison difficult.

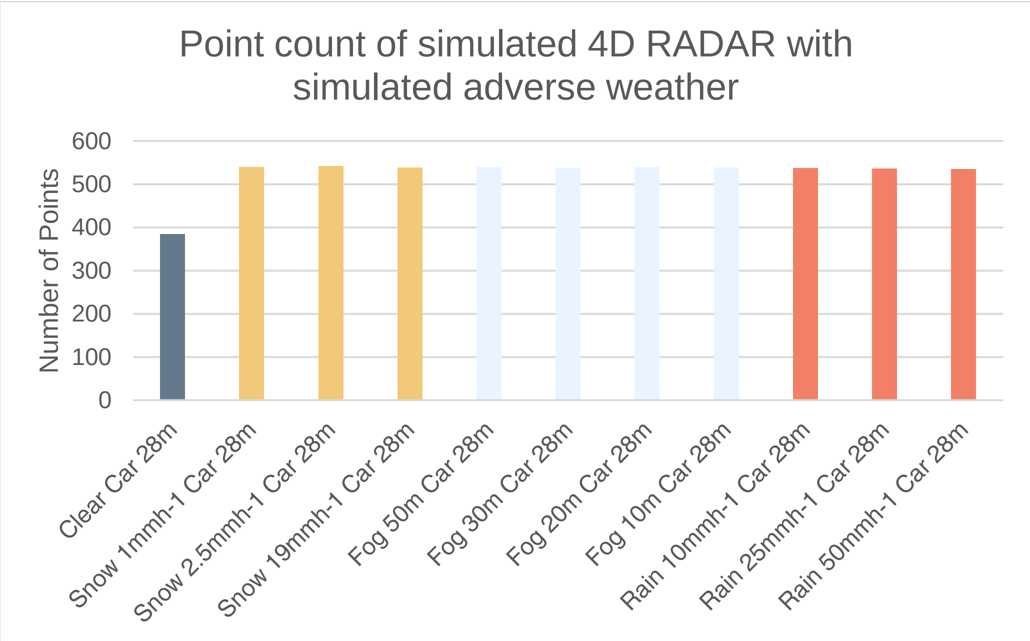

Figure 35: Average number of points in the simulated point clouds

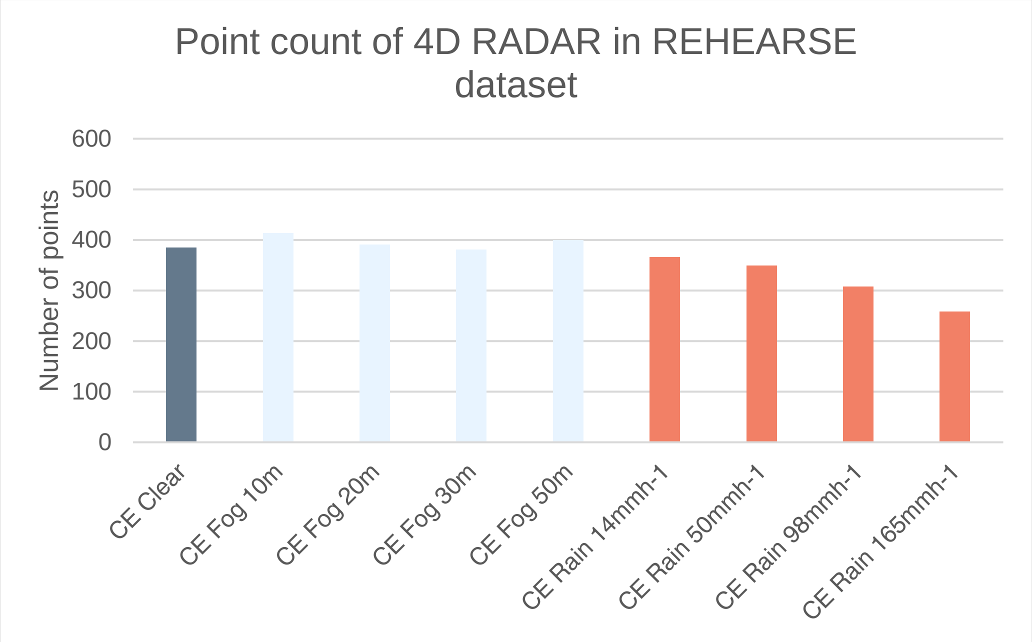

Figure 36: Average number of points in the 4D RADAR data captured in the REHEARSE dataset

7.5 Visual comparison of models

Table 16. Visual comparison of models

Model	REHEARSE (Clear/Input)	T3.3 Model	T3.4 Model
Camera (Rain)			
Camera (Fog) Lucid			
Camera (Snow)			
LiDAR (Rain)	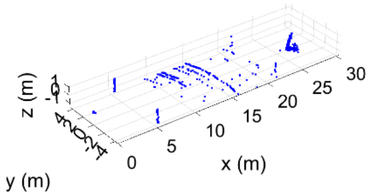	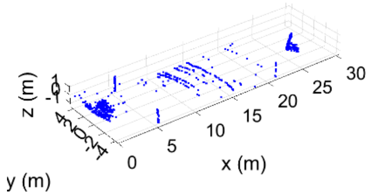	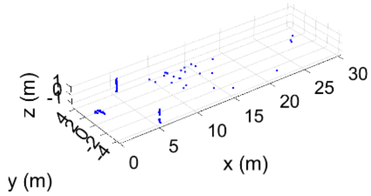
LiDAR (Fog)	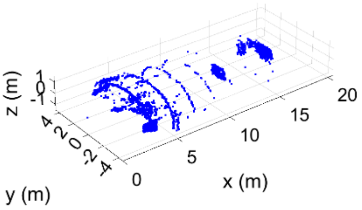	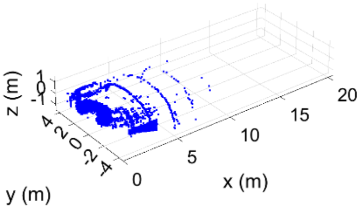	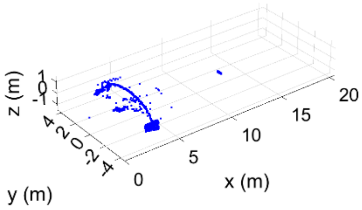
LiDAR (Snow)	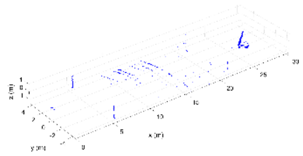	-	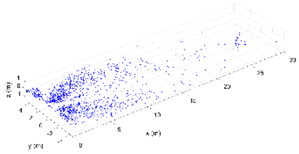

7.6 Physics based model performance

The developed **LiDAR noise models** was coded in MATLAB. The performance of the different noise models is presented in Table 17. Although the overall model time is not near real-time, the timing is based on the adaptation of the existing point clouds. In the ROADVIEW testing, the LiDAR model will be used to update the WMG LiDAR model in Carla, creating a WMG ROADVIEW LiDAR model delivered in T3.7 and used in WP7. This model has previously been demonstrated to operate in real time and the noise is calculated as the point is generated by the LiDAR model (Espineira, Robinson, Groenewald, Chan, & Donzella, 2021).

Table 17: Physics-based LiDAR weather model time performance

Rain	Fog	Snow
24.017 seconds per frame	17.899 seconds per frame	40.434 seconds per frame

The times taken to produce the **noisy camera frames** are presented in Table 18. The developed camera noise models are coded in python, running on single thread. The fog model can currently run at roughly 10 frames per second. With optimisations, the model will be able to perform at this rate consistently. For the particle model for rain and snow, it will be difficult to optimise for real-time whilst maintaining the model in its current form. With parallel processing, the particle model time can be drastically reduced. However, every particle's effect on the image within the FoV is individually considered to build up a mask used to apply the rain noise. The time taken for the particle model is also tied to the rain/snow rate. At lower rates, there are less particles to consider, and each frame can be generated quicker. To move towards the real time use of the model, it is suggested that the noise masks are pre-generated and combined with the output of the simulated camera image for real time testing.

Table 18: Physics-based camera weather model time performance

Rain 50 mmh-1	Fog 10 m	Snow 3.03 mmh-1
122.553 seconds per frame	0.092 seconds per frame	62.876 seconds per frame

The developed 4D RADAR model with integrated noise models requires roughly 60 seconds per frame. Steps are being taken to convert and integrate the 4D RADAR model inside Carla's C++ radar sensor and optimising the algorithm to achieve real-time performance.

8 Conclusions

In ROADVIEW T3.4, a series of physics-based weather noise models have been developed. These models are parametric and can be adapted based on the different perception sensors and weather parameters. Key contribution of the camera model is applying the noise at the Bayer level. For LiDAR, the energy of the beam is considered to ensure the model is agnostic to the sensor, and all possible beams (even if it was not in the input point cloud) are evaluated. For 4D RADAR, a novel ROADVIEW simulation model has been developed and the state-of-the-art models and collected data have been analysed and adapted to generate, for the first time, 4D RADAR noise models.

A series of IQA and PC metrics have been applied to the differently created adverse weather data, i.e. by real sensors (the REHEARSE dataset, T3.2), by data-driven models (T3.3), and by physics-based models (T3.4). The REHEARSE dataset provides the measured effect of noise on automotive perception sensors to be used as reference for the validation of the simulation models. However, even the collected data have non-ideal behaviours (e.g. unwanted variations of luminosity/saturation during the measurements due to sun position), causing unwanted variations in the IQA/PC metrics. Nonetheless, for the camera and LiDAR physics-based model, almost all metrics followed an expected trend, whilst the reasons for some trend not performing as expected have been provided.

Crucially, having accurate and validated sensor models is of utmost importance in testing. The camera fog demonstrates that using the physics-based Mie theory compared to the commonly used Koschmieder's theory resulted in up to 23% difference in attenuation at the visibility of 50 m, which drastically affects when the detection of objects can start occurring. This result demonstrates the importance of considering an accurate and measured drop size distributions in the model. This aspect is even further reinforced by the camera snow results. None of the applied metrics exhibited trends in this case, due to the metric value having unexpected values at the medium snow rate applied. However, there is a large difference in the size distribution of the snowflakes across the three snow rates used, resulting in the medium snow rate visibly looking less affected and with less snow flacks captured. A key takeaway is that the DSD should be considered alongside the weather rate when modelling adverse weather to properly capture the effects on sensor performance.

From the work performed in this task, there are several planned submissions. The SDM assessing point clouds was published in IEEE Access (Shahbeigi, Robinson, & Donzella, 2024). Two papers, deploying the used IQA and PC metrics have been submitted to top Tier IEEE journals (Gummadi, Chan, Wang, & Donzella, 2023) (Chan, Gummadi, Raisuddin, Aksoy, & Donzella, 2024). For the perception sensors, it is planned to submit three research articles to journals. In addition, the core findings to the validation process and in particular, the 4D RADAR's analysis will be planned to be submitted as a journal article. For 4D RADAR, we have already submitted a paper showing for the first time the application of a reduced set of PC metrics to establish the quality of RADAR point clouds (Chan, Shahbeigi, Ye, & Donzella, 2023).

The developed physics-based models from this task will be integrated into the testing pipeline of WP7 to simulate adverse weather. Additionally, the models will be considered in T3.5 alongside other sources of noise to provide a methodology to compound noise models. Finally, the models can be used to generate adverse weather data to support the tasks in WP4 and WP5.

9 References

Alexander, V., Volk, G., & Bringmann, O. (2019). imulating Photo-realistic Snow and Fog on Existing Images for Enhanced CNN Training and Evaluation . 2019 IEEE Intelligent Transportation Systems Conference (ITSC).

Amarasinghe, Y., Zhang, W., Zhang, R., & Mittleman, D. M. (2020). Scattering of Terahertz Waves by Snow. Journal of Infrared, Millimeter, and Terahertz Waves , 41, 215-224.

Ben-Daoued, A., Duthon, P., & Bernardin, F. (2023). Sweet: A realistic multiwavelength 3d simulator for automotive perceptive sensors in foggy conditions. Journal of Imaging, 9(2), 54.

Berk, M., Dura, M., Rivero, J. V., Schubert, O., Kroll, H.-M., Buschardt, B., & Straub, D. (2019). A Stochastic Physical Simulation Framework to Quantify the Effect of Rainfall on Automotive LiDAR. SAE Technical Paper.

Bernardin, F., Colomb, M., Egal, F. M., & Boreux, J.-J. (2010). Droplet distribution models for visibility calculation. 5th International Conference on Fog, Fog Collection and Dew. Munster.

Brandes, E. A., Ikeda, K., Zhang, G., Schönhuber, M., & Rasmussen, R. M. (2007). A Statistical and Physical Description of Hydrometeor Distributions in Colorado Snowstorms Using a Video Disdrometer. Journal of Applied Meteorology and Climatology, 46(5), 634-650.

Chan, P., Gummadi, D., Raisuddin, A., Aksoy, E. E., & Donzella, V. (2024). Chan, Pak Hung, et al. "LIDAR De-Snow Score (DSS): combining quality and perception metrics for optimised data filtering. Authorea Preprints.

Chan, P., Shahbeigi, S., Ye, X., & Donzella, V. (2023). A noise analysis of 4D RADAR: robust sensing for automotive? Authorea Preprints.

Chen, W.-T., Fang, H.-Y., Hsieh, C.-L., Tsai, C.-C., Chen, I., Ding, J.-J., & Kuo, S.-Y. (2021). using hierarchical dual-tree complex wavelet representation and contradict channel loss. Proceedings of the IEEE/CVF International Conference on Computer Vision.

Con Bernuth, A., Volk, G., & Bringmann, O. (2019). Simulating photo-realistic snow and fog on existing images for enhanced cnn training and evaluation. 2019 IEEE Intelligent Transportation Systems Conference (ITSC).

De Charette, R., Taburo, R., Barnum, P. C., & Rowe, A. (1-10). Fast reactive control for illumination through rain and snow . 2012 IEEE International Conference on Computational Photography (ICCP).

Du, H. (2024). Mie-scattering calculation. Applied optics, 43(9), 1951-1956.

Duthon, P., Ouattara, H., Liandrat, S., & Poledna, Y. (2024). D3.3 Library of validatied statistical noise models. ROADVIEW.

Espineira, J. P., Robinson, J., Groenewald, J., Chan, P., & Donzella, V. (2021). Realistic LiDAR With Noise Model for Real-Time Testing of Automated Vehicles in a Virtual Environment. IEEE Sensors Journal, 21(8), 9919-9926.

Garg, K., & Nayar, S. K. (2007). Vision and rain. International Journal of Computer Vision, 75, 3-27.

Grabner, M., & Kvicera, V. (2009). On the Relation between Atmospheric Visibility and the Drop Size Distribution of Fog for FSO Link Planning. 35th European Conference on Optical Communication. Vienna, Austria.

Gummadi, D., Chan, P., Wang, H., & Donzella, V. (2023). Correlating traditional image quality metrics and DNN-based object detection: a case study with compressed camera data. Authorea Preprints.

Gunn, K. L., & Marshall, J. S. (1958). The Distribution with Size of Aggregate Snowflakes. Journal of Meteorology(15), 453-455.

Hahner, M., Sakaridis, C., Bijelic, M., Heide, F., Yu, F., Dai, D., & Gool, L. V. (2022). LiDAR Snowfall Simulation for Robust 3D Object Detection. Conference on Computer Vision and Pattern Recognition (CVPR).

Hahner, M., Sakaridis, C., Dai, D., & Van Gool, L. (2021). Fog Simulation on Real LiDAR Point Clouds for 3D Object Detection in Adverse Weather. IEEE/CVF International Conference on Computer Vision (ICCV).

Haider, A., Pigniczki, M., Koyama, S., Köhler, M. H., Haas, L., Fink, M., . . . Koch, A. W. (2023). A Methodology to Model the Rain and Fog Effect on the Performance of Automotive LiDAR Sensors. Sensors, 23, 6891.

Hendrycks, D., & Dietterich, T. (2019). Benchmarking neural network robustness to common corruptions and perturbations. arXiv:1903.12261.

Herranen, T., & Kloek, A. (2023). D3.1 Implementation of digital twins. ROADVIEW.

Hospach, D., Mueller, S., Rosenstiel, W., & Bringmann, O. (2016). Simulation of falling rain for robustness testing of video-based surround sensing systems. Hospach, Dennis, Stefan Mueller, Wolfgang Rosenstiel, and Oliver Bringmann. "Simulation of falling rain for robustness testing of video-based surround sensing systems." In 2016 Design, Automation & Test in Europe Conference & Exhibition (DATE).

Kilic, V., Hegde, D., Sindagi, V., Cooper, A., Foster, M. A., & Patel, V. M. (2021). Lidar Light Scattering Augmentation (LISA): Physics-based Simulation of Adverse Weather Conditions for Object Detection. arXiv.

Kurup, A., & Bos, J. (2021). Dsor: A scalable statistical filter for removing falling snow from lidar point clouds in severe winter weather. arXiv:2109.07078.

Li, H., Wu, Z., Lin, L., ZHao, Z., Lu, C., & Zhang, X. (2014). The Analysis of Advection Fog Attenuation Algorithms in Terahertz Wave Band. 2014 XXXIth URSI General Assembly and Scientific Symposium (URSI GASS),. Beijing, China, 2014.

Li, Z., Lu, M., Zhang, X., Deng, X., Salman Asif, M., & Ma, Z. (2024). Efficient Visual Computing With Camera RAW Snapshots Publisher: IEEE Cite This . IEEE Transactions on Pattern Analysis and Machine Intelligence, 46(7), 4684-4701.

Liebe, H. J., Manabe, T., & Hufford, G. A. (1989). Millimeter-wave attenuation and delay rates due to fog/cloud conditions. IEEE Transactions on Antennas and Propagation, 37(12), 1617-1612.

Mai, N., Duthon Pierre, Khoudour, A., & Velastin, S. A. (2021). 3d object detection with sls-fusion network in foggy weather conditions. Sensors, 21(20), 6711.

Marshall, J. S., & Palmer, W. M. (1948). The distribution of raindrops with size. Journal of Atmospheric Sciences, 165-166.

Mpoeslund, T. b., Madsen, C. B., Aagaard, M., & Lerche, D. (2005). Modeling falling and accumulating snow. VVG.

Norouziari, F., Marchetti, M., Hoare, E., Gashinova, M., Constantinou, C., Gardner, P., & Cherniakov, M. (2018). Low-THz Wave Snow Attenuation. 2018 International Conference on Radar (RADAR). Brisbane.

Pandey, N., & Ram, S. S. (2022). Classification of Automotive Targets Using Inverse Synthetic. IEEE Transactions on Intelligent Vehicles 7.3, 674-689.

Pang, Z., Wang, H., Xiq, Q., Meng, D., & Xu, Z. (2024). Trg-net: An interpretable and controllable rain generator. arXiv:2403.09993.

Photosynthesis Team. (2023, July 4). Functional Interfaces. Retrieved July 25, 2024, from https://piq.readthedocs.io/en/latest/functions.html#visual-information-fidelity-vifp

pIXWLsHAM. (2020, December 26). Photography basics: Exposure Value vs Photographic Exposure vs Il/Luminance vs Pixel luminance measurements. Retrieved February 2024, from https://www.pixelsham.com/2020/12/26/exposure-value-measurements/

Poledna, Y., Drechsler, M. F., Duarte, L. C., Duthon, P., Henriksson, E., Ben-Daoued, A., . . . Donzella, V. (2024). D3.2 Reference dataset of measured weather characteristics. ROADVIEW.

Poledna, Y., Drechsler, M., Donzella, V., & Chan, P. (2024). Poledna, Y., Drechsler, M. F., Donzella, V., Chan, P. H., Duthon, P., & Huber, W. (2024, June). REHEARSE: adveRse wEatHEr datAset for sensoRy noiSe modEls. 2024 IEEE Intelligent Vehicles Symposium (IV). Jeju Island.

Rasshofer, R. H., Spies, M., & Spies, H. (2011). Influences of weather phenomena on automotive laser radar systems. Advances in Radio Science, 9, 49-60.

Rothmeier, T., Huber, W., & Knoll, A. C. (2024). Time to shine: Fine-tuning object detection models with synthetic adverse weather images. Proceedings of the IEEE/CVF Winter Conference on Applications of Computer Vision.

Sakaridis, C., Dai, D., & Van Gool, L. (2018). Semantic foggy scene understanding with synthetic data. International Journal of Computer Vision, 126, 973-992.

Sakaridis, C., Dai, D., & Van Gool, L. (2021). ACDC: The Adverse Conditions Dataset with Correspondences for Semantic Driving Scene Understanding. 2021 IEEE/CVF International Conference on Computer Vision (ICCV).

Sander, J. (1975). Rain attenuation of millimeter waves at λ = 5.77, 3.3, and 2 mm. IEEE Transactions on Antennas and Propagation, 23(2), 213-220.

Sekhon, R., & Srivastava, R. (1970). Snow size spectra and radar reflectivity. Journal of the Atmospheric Sciences, 27(2), 299-307.

Shahbeigi, S., Robinson, J., & Donzella, V. (2024). A Novel Score-based LiDAR Point Cloud Degradation Analysis Method. IEEE Access.

Shao, S., Oei, Z., Chen, W., Wu Xingming, & Li, Z. (2023). Nddepth: Normal-distance assisted monocular depth estimation. Proceedings of the IEEE/CVF International Conference on Computer Vision.

Skolnik, M. I. (2002). Introduction to Radar Systems. New York: McGraw-Hill Professional.

Teeti, I., Musat, V., Kahn, S., Rast, A., Cuzzolin, F., & Bradley, A. (2022). Vision in adverse weather: Augmentation using cyclegans with various object detectors for robust perception in autonomous racing. arXiv:2201.03246.

Teufel, S., Volk, G., Von Bernuth, A., & Bringmann, O. (2022). Simulating realistic rain, snow, and fog variations for comprehensive performance characterization of lidar perception. 2022 IEEE 95th Vehicular Technology Conference:(VTC2022-Spring).

Tremblay, M., Halder, S. S., De Charette, R., & Lalonde, J.-F. (2021). Rain rendering for evaluating and improving robustness to bad weather. International Journal of Computer VIsion, 129, 341-360.

Warg, F., Liandrat, S., Donzella, V., Lee, G., Chan, P., Viinanen, R., . . . Thorsén, A. (2024). D2.1: Definition of the complex environment conditions. ROADVIEW.

Wei, C., Wu, G., Barth, M., Chan, P., Donzella, V., & Huggett, A. (2023). Enhanced Object Detection by Integrating Camera Parameters into Raw Image-Based Faster R-CNN. 2023 IEEE 26th International Conference on Intelligent Transportation Systems (ITSC).

10 Appendix

10.1 Camera Metric Scores

10.1.1 T3.2 Rain

THI Rain Real Camera Data Metric Scores (Target = Car, Distance = 28m) (Green = Higher value equals better quality, Red = Lower value equals better quality) (Metric values showing expected trends are bold)

	PSNR	SSIM	MS-SSIM	CW-SSIM	IW-SSIM	DSS	VIF	VSI	FSIM	SR-SIM	HAAR-PSI	GMSD	MS-GMSD	MDSI
10mm/h	34.39	0.3677	0.4384	0.5981	**0.1416**	0.1948	**0.0125**	0.8931	0.6787	**0.7765**	0.2563	0.2512	0.2604	0.5198
25mm/h	35.43	0.3790	0.4476	0.6295	**0.1235**	0.2244	**0.0114**	0.9062	0.7185	**0.7546**	0.2704	0.2322	0.2422	0.4851
50mm/h	33.22	0.3662	0.4324	0.5994	**0.0773**	0.1590	**0.0087**	0.8819	0.6859	**0.7239**	0.2531	0.2519	0.2599	0.4952

THI Rain Real Camera Data Metric Scores (Target = Car, Distance = 56m) (Green = Higher value equals better quality, Red = Lower value equals better quality) (Metric values showing expected trends are bold)

	PSNR	SSIM	MS-SSIM	CW-SSIM	IW-SSIM	DSS	VIF	VSI	FSIM	SR-SIM	HAAR-PSI	GMSD	MS-GMSD	MDSI
10mm/h	34.40	0.3687	0.4454	0.6003	**0.1381**	0.2035	0.0119	0.8805	0.6835	**0.8075**	0.2698	0.2513	0.2597	0.4966
25mm/h	36.02	0.3871	0.4649	0.6272	**0.1302**	0.2384	0.0129	0.9078	0.7245	**0.7845**	0.2756	0.2324	0.2425	0.4702

Table 8: THI Rain Real Camera Data Metric Scores (Target = Camera Calibration Target, Distance = 28m) (Green = Higher value equals better quality, Red equals Lower value = better quality) (Metric values showing expect trends are bold)

	PSNR	SSIM	MS-SSIM	CW-SSIM	IW-SSIM	DSS	VIF	VSI	FSIM	SR-SIM	HAAR-PSI	GMSD	MS-GMSD	MDSI
10mm/h	32.29	0.3334	0.4223	0.5434	0.1940	0.1536	0.0364	0.8289	0.6233	0.7547	0.1888	0.2893	0.2943	0.4864
25mm/h	33.59	0.4009	0.4936	0.6008	0.3039	0.2192	0.0630	0.8682	0.6832	0.8219	0.2304	0.2464	0.2556	0.4558
50mm/h	33.88	0.3253	0.3984	0.5762	0.1550	0.1573	0.0132	0.8565	0.6584	0.7150	0.2215	0.2596	0.2673	0.4592

10.1.2 T3.2 Fog

CEREMA Fog Real Camera Data Metric Scores - Target = Car, Distance = 15m (Green = Higher value equals better quality, Red = Lower value equals better quality) (Metric values showing expected trends are bold)

Camera = Lucid Triton (SDR)

	PSNR	SSIM	MS-SSIM	CW-SSIM	IW-SSIM	DSS	VIF	VSI	FSIM	SR-SIM	HAAR-PSI	GMSD	MS-GMSD	MDSI
10m	**22.80**	**0.4992**	**0.5375**	**0.4588**	**0.2943**	**0.0676**	0.6902	**0.8602**	**0.6133**	**0.6268**	**0.2010**	**0.3076**	**0.3137**	**0.3753**
20m	**23.22**	**0.5298**	**0.5726**	**0.4991**	**0.3559**	**0.0825**	0.6711	**0.8695**	**0.6441**	**0.6823**	**0.2319**	**0.2888**	**0.2972**	**0.3723**
30m	**24.54**	**0.6459**	**0.7042**	**0.6506**	**0.5734**	**0.1893**	0.5866	**0.9064**	**0.7567**	**0.7845**	**0.3717**	**0.2190**	**0.2317**	**0.3584**
50m	**26.05**	**0.7387**	**0.7961**	**0.7536**	**0.7106**	**0.3587**	0.5396	**0.9351**	**0.8233**	**0.8523**	**0.5180**	**0.1634**	**0.1752**	**0.3401**

CEREMA Fog Real Camera Data Metric Scores - Target = Pedestrian + Bike, Distance = 15m (Green = Higher value equals better quality, Red = Lower value equals better quality) (Metric values showing expect trends are bold)														
Camera = Lucid Triton (SDR)														
	PSNR	SSIM	MS-SSIM	CW-SSIM	IW-SSIM	DSS	VIF	VSI	FSIM	SR-SIM	HAAR-PSI	GMSD	MS-GMSD	MDSI
10m	**22.01**	**0.4899**	**0.5286**	**0.4495**	**0.2736**	**0.0643**	0.7001	**0.8563**	**0.6079**	**0.6263**	**0.1899**	**0.3180**	**0.3234**	**0.3791**
20m	**22.42**	**0.5471**	**0.5834**	**0.5139**	**0.3679**	**0.0768**	0.6614	**0.8696**	**0.6486**	**0.6734**	**0.2338**	**0.2851**	**0.2951**	**0.3709**
30m	**23.36**	**0.6101**	**0.6596**	**0.6018**	**0.4961**	**0.1269**	0.6152	**0.8951**	**0.7219**	**0.7605**	**0.3158**	**0.2451**	**0.2572**	**0.3636**
50m	**26.21**	**0.7573**	**0.8219**	**0.7767**	**0.7491**	**0.4370**	0.5221	**0.9441**	**0.8528**	**0.8905**	**0.5657**	**0.1498**	**0.1613**	**0.3314**

CEREMA Fog Real Camera Data Metric Scores - Target = Camera Calibration Target, Distance = 15m (Green = Higher value equals better quality, Red = Lower value equals better quality) (Metric values showing expect trends are bold)														
Camera = Lucid Triton (SDR)														
	PSNR	SSIM	MS-SSIM	CW-SSIM	IW-SSIM	DSS	VIF	VSI	FSIM	SR-SIM	HAAR-PSI	GMSD	MS-GMSD	MDSI
10m	**22.28**	**0.5173**	**0.5553**	**0.4808**	**0.3093**	**0.0673**	0.6525	**0.8705**	**0.6255**	**0.6348**	**0.2039**	**0.3029**	**0.3107**	**0.3763**
20m	**22.80**	**0.5620**	**0.6029**	**0.5395**	**0.3881**	**0.0937**	0.6337	**0.8870**	**0.6680**	**0.7272**	**0.2534**	**0.2741**	**0.2847**	**0.3725**
30m	**24.04**	**0.6363**	**0.7009**	**0.6457**	**0.5615**	**0.1712**	0.5468	**0.9163**	**0.7554**	**0.7817**	**0.3534**	**0.2265**	**0.2387**	**0.3626**
50m	**25.43**	**0.7257**	**0.7812**	**0.7424**	**0.6842**	**0.2889**	0.5073	**0.9400**	**0.8098**	**0.8439**	**0.4682**	**0.1765**	**0.1887**	**0.3459**

10.1.3 ACDC Snow

ACDC Snow Real Camera data Metric Scores (Green = Higher value equals better quality, Red = Lower value equals better quality) (Metric values showing expect trends are bold)														
ACDC Camera														
	PSNR	SSIM	MS-SSIM	CW-SSIM	IW-SSIM	DSS	VIF	VSI	FSIM	SR-SIM	HAAR-PSI	GMSD	MS-GMSD	MDSI
Light	**58.66**	0.3302	0.2896	0.4971	**0.0886**	**0.0579**	**0.0136**	**0.8199**	**0.5690**	**0.6494**	**0.2009**	**0.3092**	**0.3150**	**0.5165**
Heavy	**58.60**	0.3573	0.3025	0.5022	**0.0878**	**0.0549**	**0.0125**	**0.8132**	**0.5632**	**0.6380**	**0.1942**	**0.3176**	**0.3228**	**0.5337**

10.1.4 T3.3 Rain

THI – CEREMA Rain Camera Model Metric Scores (Target = Car, Distance = 28m) (Green = Higher value equals better quality, Red = Lower value equals better quality) (Metric values showing expect trends are bold)														
	PSNR	SSIM	MS-SSIM	CW-SSIM	IW-SSIM	DSS	VIF	VSI	FSIM	SR-SIM	HAAR-PSI	GMSD	MS-GMSD	MDSI
5mm/h	16.7434	0.5011	0.6574	0.6027	0.4560	0.1389	0.1351	0.9421	0.7938	0.9222	0.3310	0.2781	0.2708	0.3834
20mm/h	19.9374	0.5106	0.6998	0.6618	0.5118	0.2913	0.1193	0.9716	0.8784	0.9553	0.3806	0.2242	0.2207	0.3501
40mm/h	21.7391	0.5179	0.6946	0.6262	0.4932	0.1877	0.1641	0.9615	0.8430	0.9561	0.3310	0.2644	0.2586	0.3685

THI – CEREMA Rain Camera Model Metric Scores (Target = Car, Distance = 56m) (Green = Higher value equals better quality, Red = Lower value equals better quality) (Metric values showing expect trends are bold)														
	PSNR	SSIM	MS-SSIM	CW-SSIM	IW-SSIM	DSS	VIF	VSI	FSIM	SR-SIM	HAAR-PSI	GMSD	MS-GMSD	MDSI
5mm/h	16.0927	0.4877	0.6468	0.5879	0.4465	0.1018	0.1491	0.9349	0.7607	0.9379	0.2836	0.2999	0.2913	0.3750
20mm/h	20.5174	0.5069	0.6920	0.6441	0.4948	0.2813	0.1280	0.9704	0.8635	0.9472	0.3673	0.2429	0.2392	0.3466
40mm/h	21.4600	0.5086	0.6941	0.6254	0.4913	0.1918	0.1508	0.9684	0.8549	0.9595	0.3470	0.2639	0.2604	0.3495

THI – CEREMA Rain Camera Model Metric Scores (Target = Camera Calibration Target, Distance = 28m) (Green = Higher value equals better quality, Red = Lower value equals better quality) (Metric values showing expect trends are bold)														
	PSNR	SSIM	MS-SSIM	CW-SSIM	IW-SSIM	DSS	VIF	VSI	FSIM	SR-SIM	HAAR-PSI	GMSD	MS-GMSD	MDSI
5mm/h	16.5364	0.3775	0.5228	0.5385	0.4082	0.1437	0.0857	**0.9005**	**0.7211**	0.8495	**0.2477**	0.2790	0.2798	0.4502
20mm/h	12.6993	0.3831	0.5218	0.4760	0.3259	0.0724	0.1853	**0.8983**	**0.6567**	0.8151	**0.1632**	0.3459	0.3365	0.3926
40mm/h	16.9173	0.4040	0.5430	0.4879	0.3471	0.0745	0.1884	**0.8870**	**0.6469**	0.8766	**0.1418**	0.3425	0.3324	0.4059

10.1.5 T3.3 Fog

CEREMA Data – CEREMA Fog Camera Model Metric Scores -Target = Car, Distance = 15m (Green = Higher value equals better quality, Red = Lower value equals better quality) (Metric values showing expect trends are bold)														
Camera = Lucid Triton (SDR)														
	PSNR	SSIM	MS-SSIM	CW-SSIM	IW-SSIM	DSS	VIF	VSI	FSIM	SR-SIM	HAAR-PSI	GMSD	MS-GMSD	MDSI
30m	16.6938	0.4471	**0.5583**	**0.4943**	**0.3425**	**0.1229**	0.1845	**0.9003**	**0.7112**	**0.8162**	**0.2384**	**0.3211**	**0.3150**	**0.3746**
200m	17.9210	0.4637	**0.6509**	**0.6301**	**0.4754**	**0.2690**	0.1075	**0.9575**	**0.8674**	**0.9399**	**0.3733**	**0.2477**	**0.2455**	**0.3516**
400m	16.0760	0.4506	**0.6543**	**0.6683**	**0.4924**	**0.3140**	0.0863	**0.9667**	**0.8874**	**0.9519**	**0.4039**	**0.2246**	**0.2235**	**0.3441**

CEREMA Data – CEREMA Fog Camera Model Metric Scores -Target = Pedestrian + Bike, Distance = 15m (Green = Higher value equals better quality, Red = Lower value equals better quality) (Metric values showing expect trends are bold)														
Camera = Lucid Triton (SDR)														
	PSNR	SSIM	MS-SSIM	CW-SSIM	IW-SSIM	DSS	VIF	VSI	FSIM	SR-SIM	HAAR-PSI	GMSD	MS-GMSD	MDSI
30m	16.8506	0.4439	**0.5535**	**0.4949**	**0.3334**	**0.1116**	0.1763	**0.9012**	**0.7071**	**0.8215**	**0.2300**	**0.3298**	**0.3238**	**0.3783**
200m	17.8527	0.4615	**0.6405**	**0.6228**	**0.4583**	**0.2466**	0.1059	**0.9562**	**0.8561**	**0.9343**	**0.3634**	**0.2554**	**0.2541**	**0.3570**
400m	16.8379	0.4579	**0.6570**	**0.6731**	**0.4922**	**0.3442**	0.0838	**0.9686**	**0.8907**	**0.9488**	**0.4103**	**0.2199**	**0.2202**	**0.3447**

CEREMA Data – CEREMA Fog Camera Model Metric Scores -Target = Camera Calibration Target, Distance = 15m (Green = Higher value equals better quality, Red = Lower value equals better quality) (Metric values showing expect trends are bold)

Camera = Lucid Triton (SDR)														
	PSNR	**SSIM**	**MS-SSIM**	**CW-SSIM**	**IW-SSIM**	**DSS**	**VIF**	**VSI**	**FSIM**	**SR-SIM**	**HAAR-PSI**	**GMSD**	**MS-GMSD**	**MDSI**
30m	17.0179	0.4451	**0.5500**	**0.4871**	**0.3208**	0.1048	0.1886	**0.9037**	**0.6919**	**0.8062**	**0.2188**	**0.3347**	**0.3279**	**0.3795**
200m	18.3709	0.4654	**0.6402**	**0.6165**	**0.4517**	0.2350	0.1103	**0.9527**	**0.8496**	**0.9333**	**0.3553**	**0.2616**	**0.2598**	**0.3592**
400m	17.6063	0.4648	**0.6625**	**0.6716**	**0.4945**	0.3432	0.0865	**0.9666**	**0.8875**	**0.9485**	**0.4048**	**0.2219**	**0.2216**	**0.3447**

10.1.6 T3.3 Snow

THI – CEREMA Snow Camera Model Metric Scores (Target = Car, Distance = 28m) (Green = Higher value equals better quality, Red = Lower value equals better quality) (Metric values showing expect trends are bold)														
	PSNR	**SSIM**	**MS-SSIM**	**CW-SSIM**	**IW-SSIM**	**DSS**	**VIF**	**VSI**	**FSIM**	**SR-SIM**	**HAAR-PSI**	**GMSD**	**MS-GMSD**	**MDSI**
0mm/h	**21.8347**	**0.5227**	**0.7205**	**0.7006**	**0.5512**	**0.4187**	**0.1010**	**0.9817**	**0.9208**	**0.9741**	**0.4634**	**0.1903**	**0.1901**	**0.3271**
10mm/h	**15.7129**	**0.5021**	**0.6632**	**0.6691**	**0.4803**	**0.2687**	**0.0964**	**0.9362**	**0.7872**	**0.8544**	**0.3654**	**0.2253**	**0.2273**	**0.3953**

THI – CEREMA Snow Camera Model Metric Scores (Target = Car, Distance = 56m) (Green = Higher value equals better quality, Red = Lower value equals better quality) (Metric values showing expect trends are bold)														
	PSNR	**SSIM**	**MS-SSIM**	**CW-SSIM**	**IW-SSIM**	**DSS**	**VIF**	**VSI**	**FSIM**	**SR-SIM**	**HAAR-PSI**	**GMSD**	**MS-GMSD**	**MDSI**
0mm/h	**22.0188**	**0.5063**	**0.7005**	**0.6862**	**0.5223**	0.2659	0.0896	**0.9756**	**0.8976**	**0.9709**	**0.4322**	**0.2099**	**0.2110**	**0.3427**
10mm/h	**16.4111**	**0.4967**	**0.6721**	**0.6729**	**0.4915**	0.3094	0.0929	**0.9470**	**0.8102**	**0.8931**	**0.3786**	**0.2200**	**0.2217**	**0.3834**

THI – CEREMA Snow Camera Model Metric Scores (Target = Camera Calibration Target, Distance = 28m) (Green = Higher value equals better quality, Red = Lower value equals better quality) (Metric values showing expect trends are bold)														
	PSNR	**SSIM**	**MS-SSIM**	**CW-SSIM**	**IW-SSIM**	**DSS**	**VIF**	**VSI**	**FSIM**	**SR-SIM**	**HAAR-PSI**	**GMSD**	**MS-GMSD**	**MDSI**
0mm/h	**16.4633**	**0.4143**	**0.6138**	**0.5947**	**0.4769**	**0.2188**	0.1075	**0.9187**	**0.7838**	**0.8573**	**0.3051**	**0.2603**	**0.2592**	0.4608
10mm/h	**15.4696**	**0.3995**	**0.5436**	**0.5162**	**0.3616**	**0.1101**	0.1246	**0.8622**	**0.6779**	**0.7995**	**0.1695**	**0.3131**	**0.3067**	0.4109

10.1.7 T3.4 Rain

THI – WMG Rain Camera Model Metric Scores (Target = Car, Distance = 28m) (Green = Higher value equals better quality, Red = Lower value equals better quality) (Metric values showing expect trends are bold)														
	PSNR	**SSIM**	**MS-SSIM**	**CW-SSIM**	**IW-SSIM**	**DSS**	**VIF**	**VSI**	**FSIM**	**SR-SIM**	**HAAR-PSI**	**GMSD**	**MS-GMSD**	**MDSI**
10mm/h	**41.42**	**0.9841**	**0.9947**	**0.9918**	**0.9941**	**0.9889**	**0.7818**	**0.9998**	**0.9993**	**0.9997**	**0.9814**	**0.0065**	**0.0068**	**0.1080**
25mm/h	**41.09**	**0.9828**	**0.9939**	**0.9894**	**0.9930**	**0.9798**	**0.7725**	**0.9996**	**0.9988**	**0.9994**	**0.9774**	**0.0111**	**0.0108**	**0.1207**
50mm/h	**40.56**	**0.9810**	**0.9927**	**0.9860**	**0.9907**	**0.9653**	**0.7611**	**0.9994**	**0.9979**	**0.9990**	**0.9713**	**0.0169**	**0.0164**	**0.1371**

THI – WMG Rain Camera Model Metric Scores (Target = Car, Distance = 56m) (Green = Higher value equals better quality, Red = Lower value equals better quality) (Metric values showing expect trends are bold)

	PSNR	SSIM	MS-SSIM	CW-SSIM	IW-SSIM	DSS	VIF	VSI	FSIM	SR-SIM	HAAR-PSI	GMSD	MS-GMSD	MDSI
10mm/h	**40.73**	**0.9827**	**0.9939**	**0.9895**	**0.9940**	**0.9831**	**0.7692**	**0.9995**	**0.9988**	**0.9992**	**0.9782**	**0.0088**	**0.0087**	**0.1163**
25mm/h	**39.72**	**0.9801**	**0.9924**	**0.9851**	**0.9913**	**0.9679**	**0.7534**	**0.9991**	**0.9976**	**0.9980**	**0.9709**	**0.0151**	**0.0145**	**0.1339**

THI – WMG Rain Camera Model Metric Scores (Target = Camera Calibration Target, Distance = 28m) (Green = Higher value equals better quality, Red = Lower value equals better quality) (Metric values showing expect trends are bold)														
	PSNR	SSIM	MS-SSIM	CW-SSIM	IW-SSIM	DSS	VIF	VSI	FSIM	SR-SIM	HAAR-PSI	GMSD	MS-GMSD	MDSI
10mm/h	**38.83**	**0.9816**	**0.9942**	**0.9930**	**0.9981**	**0.9874**	**0.7526**	**0.9998**	**0.9994**	**0.9997**	**0.9771**	**0.0066**	**0.0078**	**0.0942**
25mm/h	**38.74**	**0.9808**	**0.9938**	**0.9919**	**0.9977**	**0.9828**	**0.7484**	**0.9997**	**0.9991**	**0.9995**	**0.9753**	**0.0089**	**0.0096**	**0.1020**
50mm/h	**38.57**	**0.9797**	**0.9932**	**0.9904**	**0.9969**	**0.9751**	**0.7431**	**0.9996**	**0.9985**	**0.9991**	**0.9722**	**0.0127**	**0.0129**	**0.1139**

10.1.8 T3.4 Fog

CEREMA – WMG Fog Camera Model Metric Scores -Target = Car, Distance = 15m (Green = Higher value equals better quality, Red = Lower value equals better quality) (Metric values showing expect trends are bold)														
Camera = Lucid Triton														
	PSNR	SSIM	MS-SSIM	CW-SSIM	IW-SSIM	DSS	VIF	VSI	FSIM	SR-SIM	HAAR-PSI	GMSD	MS-GMSD	MDSI
10m	**10.3433**	**0.614**	**0.659**	**0.638**	**0.507**	**0.1682**	1.4065	**0.9063**	**0.6957**	**0.7438**	**0.3432**	**0.2264**	**0.2397**	**0.3726**
20m	**13.6245**	**0.7884**	**0.8229**	**0.8221**	**0.7558**	**0.3584**	1.0964	**0.9513**	**0.8138**	**0.8343**	**0.57**	**0.1395**	**0.1545**	**0.3329**
30m	**15.7217**	**0.8587**	**0.8854**	**0.8885**	**0.8458**	**0.5046**	1.0063	**0.9673**	**0.869**	**0.8785**	**0.7023**	**0.1017**	**0.1159**	**0.3082**
50m	**18.1597**	**0.9115**	**0.9317**	**0.9356**	**0.911**	**0.6648**	0.9422	**0.9782**	**0.917**	**0.9176**	**0.8228**	**0.0673**	**0.0797**	**0.2797**

CEREMA – WMG Fog Camera Model Metric Scores -Target = Pedestrian& Bike, Distance = 15m (Green = Higher value equals better quality, Red = Lower value equals better quality) (Metric values showing expect trends are bold)														
Camera = Lucid Triton														
	PSNR	SSIM	MS-SSIM	CW-SSIM	IW-SSIM	DSS	VIF	VSI	FSIM	SR-SIM	HAAR-PSI	GMSD	MS-GMSD	MDSI
10m	**10.7613**	**0.6438**	**0.6864**	**0.6681**	**0.5467**	**0.1827**	1.2745	**0.9121**	**0.7154**	**0.7715**	**0.3664**	**0.2168**	**0.2303**	**0.3706**
20m	**14.1883**	**0.8127**	**0.8436**	**0.8418**	**0.7839**	**0.3898**	1.0335	**0.9555**	**0.8335**	**0.8632**	**0.6014**	**0.1303**	**0.1445**	**0.3278**
30m	**16.3425**	**0.8765**	**0.9004**	**0.9018**	**0.8657**	**0.5382**	0.9613	**0.9698**	**0.8853**	**0.9024**	**0.7316**	**0.0934**	**0.1067**	**0.3018**
50m	**18.8299**	**0.9231**	**0.9413**	**0.9435**	**0.9236**	**0.6938**	0.9089	**0.9792**	**0.9287**	**0.9355**	**0.8437**	**0.0607**	**0.0721**	**0.2725**

CEREMA – WMG Fog Camera Model Metric Scores -Target = Sensor Target, Distance = 15m (Green = Higher value equals better quality, Red = Lower value equals better quality) (Metric values showing expect trends are bold)														
Camera = Lucid Triton (SDR) (NEW DATA MAY)														
	PSNR	SSIM	MS-SSIM	CW-SSIM	IW-SSIM	DSS	VIF	VSI	FSIM	SR-SIM	HAAR-PSI	GMSD	MS-GMSD	MDSI

10m	10.5828	0.6347	0.6811	0.6596	0.5314	0.1813	1.3168	0.8987	0.7119	0.7553	0.357	0.2202	0.2333	0.3726
20m	13.9357	0.8051	0.8392	0.8359	0.7739	0.3798	1.0518	0.9516	0.8301	0.8471	0.5864	0.1335	0.1474	0.3285
30m	16.0614	0.8709	0.8968	0.8975	0.8582	0.5243	0.9745	0.9693	0.8817	0.8869	0.7153	0.0971	0.1101	0.3024
50m	18.5239	0.9194	0.9387	0.9406	0.9185	0.6789	0.9186	0.9818	0.9254	0.9229	0.8314	0.0643	0.0758	0.2735

10.1.9 T3.4 Snow

ACDC – WMG Snow Camera Model Metric Scores (Green = Higher value equals better quality, Red = Lower value equals better quality) (Metric values showing expect trends are bold)														
GOPR0604_frame_000619_rgb_anon														
	PSNR	SSIM	MS-SSIM	CW-SSIM	IW-SSIM	DSS	VIF	VSI	FSIM	SR-SIM	HAAR-PSI	GMSD	MS-GMSD	MDSI
2.59 mm/h	88.66	0.9830	0.9929	0.9899	0.9892	0.9231	0.8074	0.9992	0.9969	0.9986	0.9579	0.0329	0.0318	0.1711
2.70 mm/h	91.22	0.9852	0.9956	0.9923	0.9959	0.9813	0.8162	0.9997	0.9986	0.9995	0.9708	0.0167	0.0159	0.1316
3.03 mm/h	84.11	0.9502	0.9787	0.9562	0.9673	0.8649	0.6211	0.9976	0.9897	0.9953	0.8987	0.0593	0.0559	0.2112
GOPR0604_frame_000672_rgb_anon														
	PSNR	SSIM	MS-SSIM	CW-SSIM	IW-SSIM	DSS	VIF	VSI	FSIM	SR-SIM	HAAR-PSI	GMSD	MS-GMSD	MDSI
2.59 mm/h	88.72	0.9821	0.9926	0.9887	0.9897	0.9280	0.7969	0.9991	0.9965	0.9987	0.9552	0.0322	0.0311	0.1707
2.70 mm/h	91.11	0.9845	0.9952	0.9915	0.9962	0.9835	0.8083	0.9996	0.9985	0.9995	0.9682	0.0153	0.0149	0.1332
3.03 mm/h	84.22	0.9531	0.9812	0.9563	0.9723	0.8911	0.6149	0.9975	0.9896	0.9960	0.8957	0.0533	0.0504	0.2028

10.2 LiDAR Metric Scores

10.2.1 T3.2 Rain

THI Rain Real LiDAR Data Metric Scores (Target = Car, Distance = 28m) (Red = Lower value equals better quality) (Metric values showing expect trends are bold)						
	SDM	**RMSE**	**MDE**	**MMDE**	**HD**	**HD95**
10mm/h	**0.1184**	21.1463	20.7944	20.0665	63.8943	**2.5402**
25mm/h	**0.1352**	19.8247	19.2585	18.6678	62.2677	**2.6536**
50mm/h	**0.1671**	21.5485	18.1560	12.1519	99.8371	**8.9147**

THI Rain Real LiDAR Data Metric Scores (Target = Car, Distance = 56m) (Red = Lower value equals better quality) (Metric values showing expect trends are bold)						
	SDM	**RMSE**	**MDE**	**MMDE**	**HD**	**HD95**
10mm/h	**0.0631**	20.8378	20.9919	20.8445	53.2722	**2.5486**
25mm/h	**0.0810**	19.7697	19.6749	18.4951	43.9195	**2.8051**

THI Rain Real LiDAR Data Metric Scores (Target = LiDAR Calibration Targets, Distance = 28m) (Red = Lower value equals better quality) (Metric values showing expect trends are bold)						
	SDM	**RMSE**	**MDE**	**MMDE**	**HD**	**HD95**
10mm/h	**0.0347**	19.4678	18.9200	17.4289	**29.3720**	**1.0952**
25mm/h	**0.0928**	18.6041	18.3829	18.0913	**32.4197**	**1.2385**
50mm/h	**0.2343**	18.4369	15.1789	10.6449	**103.6870**	**10.1207**

10.2.2 T3.2 Fog

CEREMA Fog Real LiDAR Data Metric Scores - Target = Car, Distance = 15m (Red = Lower value equals better quality) (Metric values showing expect trends are bold)						
	SDM	**RMSE**	**MDE**	**MMDE**	**HD**	**HD95**
10m	0.2139	**1.5832**	**0.4773**	**0.4773**	**14.0512**	**11.0215**
20m	0.3501	**1.5610**	**0.4287**	**0.4287**	**13.4899**	**9.8773**
30m	0.1853	**1.4589**	**0.3600**	**0.3600**	**3.8995**	**0.9581**
50m	0.1051	**1.3478**	**0.3456**	**0.3456**	**2.7276**	**0.5153**

CEREMA Fog Real LiDAR Data Metric Scores - Target = Pedestrian + Bike, Distance = 15m (Red = Lower value equals better quality) (Metric values showing expect trends are bold)						
	SDM	**RMSE**	**MDE**	**MMDE**	**HD**	**HD95**
10m	**0.3217**	1.3790	0.5420	0.5420	**13.8556**	**2.5649**
20m	**0.3099**	1.4348	0.6335	0.6335	**13.2973**	**2.1129**
30m	**0.1496**	1.3894	0.5732	0.5732	**5.0212**	**1.0931**
50m	**0.0892**	1.4254	0.5692	0.5692	**3.3366**	**0.8755**

CEREMA Fog Real LiDAR Data Metric Scores - Target = LiDAR Calibration Targets, Distance = 15m (Red = Lower value equals better quality) (Metric values showing expect trends are bold)						
	SDM	**RMSE**	**MDE**	**MMDE**	**HD**	**HD95**
10m	0.4269	**1.7084**	**0.6890**	**0.6890**	41.5985	**11.6410**
20m	0.3264	**1.6700**	**0.6385**	**0.6385**	29.5226	**2.0850**
30m	0.3956	**1.5448**	**0.5102**	**0.5101**	37.0063	**1.4309**
50m	0.3804	**1.4913**	**0.4971**	**0.4971**	29.7519	**0.9577**

10.2.3 WADS Snow

Table 23: WADS Real LiDAR Data Metric Scores - (Red = Lower value equals better quality) (Metric values showing expect trends are bold)						
	SDM	**RMSE**	**MDE**	**MMDE**	**HD**	**HD95**
0.250 mm/h (Sequence 35)	**0.1091**	**24.830**	**19.0487**	**18.5981**	**4.9060**	2.8202
0.835 mm/h (Sequence 26)	**0.1926**	**35.8030**	**27.5533**	**25.8981**	**6.0135**	1.7922

10.2.4 T3.3 Rain

THI – CEREMA Rain LiDAR Model Metric Scores (Target = Car, Distance = 28m) (Red = Lower value equals better quality) (Metric values showing expect trends are bold)						
	SDM	**RMSE**	**MDE**	**MMDE**	**HD**	**HD95**
10mm/h	0.2633	5.5847	1.6143	1.6143	106.9676	2.9403
25mm/h	0.2931	5.4893	1.5496	1.5496	106.9676	1.9088
50mm/h	0.2887	5.5106	1.5577	1.5577	106.9676	1.7063

THI – CEREMA Rain LiDAR Model Metric Scores (Target = Car, Distance = 56m) (Red = Lower value equals better quality) (Metric values showing expect trends are bold)						
	SDM	**RMSE**	**MDE**	**MMDE**	**HD**	**HD95**
10mm/h	**0.1852**	5.8282	1.8013	1.8013	75.7452	2.7772
25mm/h	**0.2091**	5.7554	1.7468	1.7468	75.7452	1.8293

THI – CEREMA Rain LiDAR Model Metric Scores (Target = LiDAR Calibration Target, Distance = 28m) (Red = Lower value equals better quality) (Metric values showing expect trends are bold)						
	SDM	**RMSE**	**MDE**	**MMDE**	**HD**	**HD95**
10mm/h	0.2936	5.2321	1.8176	1.8176	81.8098	1.9225
25mm/h	0.3138	5.2166	1.8011	1.8011	81.8098	1.5885
50mm/h	0.2996	5.1839	1.7809	1.7809	81.8098	1.6003

10.2.5 T3.3 Fog

CEREMA Data - CEREMA Fog Model Metric Scores - Target = Car, Distance = 15m (Red = Lower value equals better quality) (Metric values showing expect trends are bold)						
	SDM	**RMSE**	**MDE**	**MMDE**	**HD**	**HD95**
10m	0.3368	1.8676	1.5383	1.5383	7.3149	3.7043
20m	0.3365	1.8679	1.5388	1.5388	7.3149	3.7043
30m	0.3370	1.8681	1.5391	1.5391	7.3149	3.7043
50m	0.4020	1.8523	1.5103	1.5103	2.3551	1.0805

CEREMA Data - CEREMA Fog Model Metric Scores - Target = Pedestrian + Bike, Distance = 15m (Red = Lower value equals better quality) (Metric values showing expect trends are bold)						
	SDM	**RMSE**	**MDE**	**MMDE**	**HD**	**HD95**
10m	0.2801	1.7023	**1.5312**	**1.5312**	7.4407	1.0571
20m	0.2803	1.7026	**1.5311**	**1.5311**	7.4407	1.0575
30m	0.2811	1.7022	**1.5309**	**1.5309**	7.4407	1.0595
50m	0.4205	1.6594	**1.4185**	**1.4185**	2.4787	1.0562

CEREMA Data - CEREMA Fog Model Metric Scores - Target = LiDAR Calibration Target, Distance = 15m (Red = Lower value equals better quality)						
	SDM	**RMSE**	**MDE**	**MMDE**	**HD**	**HD95**
10m	0.1678	1.9197	1.5966	1.5966	33.0160	4.0573
20m	0.1676	1.9197	1.5971	1.5971	33.0160	4.0573
30m	0.1672	1.9199	1.5969	1.5969	33.0160	4.0573
50m	0.2820	1.9062	1.5636	1.5636	26.2892	1.0755

10.2.6 T3.4 Rain

THI – WMG Rain LiDAR Model Metric Scores (Target = Car, Distance = 28m) (Red = Lower value equals better quality) (Metric values showing expect trends are bold)						
	SDM	**RMSE**	**MDE**	**MMDE**	**HD**	**HD95**
10mm/h	**0.0913**	**7.4512**	**6.2487**	4.5384	**2.5269**	0.9237
25mm/h	**0.1108**	**8.8674**	**7.0836**	4.2041	**3.4383**	0.5096
50mm/h	**0.1431**	**10.1911**	**7.6929**	3.7144	**4.6461**	0.7723

THI – WMG Rain LiDAR Model Metric Scores (Target = Car, Distance = 56m) (Red = Lower value equals better quality) (Metric values showing expect trends are bold)						
	SDM	**RMSE**	**MDE**	**MMDE**	**HD**	**HD95**
10mm/h	**0.1045**	**6.1117**	**5.4242**	3.8620	**3.6452**	0.9901
25mm/h	**0.1080**	**6.6586**	**5.6440**	3.2888	**4.8029**	0.5225

THI – WMG Rain LiDAR Model Metric Scores (Target = LiDAR Calibration Target, Distance = 28m) (Red = Lower value equals better quality) (Metric values showing expect trends are bold)						
	SDM	**RMSE**	**MDE**	**MMDE**	**HD**	**HD95**
10mm/h	**0.2402**	**9.5801**	**7.0919**	5.2508	**5.7080**	4.4715
25mm/h	**0.2533**	**10.6026**	**7.3841**	4.5780	**6.9570**	2.5112
50mm/h	**0.2652**	**12.1296**	**8.1306**	4.0669	**7.8321**	0.7644

10.2.7 T3.4 Fog

CEREMA - WMG Fog Model Metric Scores - Target = Car, Distance = 15m (Red = Lower value equals better quality) (Metric values showing expect trends are bold)						
	SDM	**RMSE**	**MDE**	**MMDE**	**HD**	**HD95**
10m	**0.3785**	**2.0321**	**0.6605**	**0.6605**	**14.6616**	**14.4958**
20m	**0.3521**	**1.9084**	**0.5037**	**0.5037**	**4.5296**	**4.0607**
30m	**0.2996**	**1.7692**	**0.3408**	**0.3408**	**4.2206**	**2.9209**
50m	**0.1906**	**1.5615**	**0.2049**	**0.2049**	**2.7027**	**0.2969**

CEREMA - WMG Fog Model Metric Scores - Target = Pedestrian + Bike, Distance = 15m (Red = Lower value equals better quality) (Metric values showing expect trends are bold)						
	SDM	**RMSE**	**MDE**	**MMDE**	**HD**	**HD95**
10m	**0.4889**	**2.1605**	**0.7367**	**0.7367**	**14.8421**	**14.5842**
20m	**0.3054**	**2.0706**	**0.6053**	**0.6053**	**5.8617**	**2.2007**
30m	**0.2398**	**1.9073**	**0.4226**	**0.4226**	**4.8277**	**2.0340**
50m	**0.1974**	**1.7172**	**0.2604**	**0.2604**	**3.4547**	**0.5068**

CEREMA - WMG Fog Model Metric Scores - Target = LiDAR Calibration Target, Distance = 15m (Red = Lower value equals better quality) (Metric values showing expect trends are bold)						
	SDM	**RMSE**	**MDE**	**MMDE**	**HD**	**HD95**
10m	**0.4688**	**2.1625**	**0.7574**	**0.7574**	**14.6986**	**12.9380**
20m	**0.3292**	**2.0075**	**0.6047**	**0.6047**	**5.8478**	**2.0287**
30m	**0.2785**	**1.8440**	**0.4248**	**0.4248**	**4.7502**	**1.8485**
50m	**0.1734**	**1.5943**	**0.2476**	**0.2476**	**3.0160**	**0.4409**

10.2.8 T3.4 Snow

WADS Simulated Snow LiDAR Data Metric Scores - (Red = Lower value equals better quality) (Metric values showing expect trends are bold)						
	SDM	**RMSE**	**MDE**	**MMDE**	**HD**	**HD95**
0.250 mm/h (Sequence 35)	**0.021515**	**30.37925**	**27.18993**	**21.81859**	**31.00348**	**3.278101**
0.835 mm/h (Sequence 26)	**0.201155**	**37.82021**	**34.7185**	**29.01104**	**40.28281**	**4.370519**

10.3 4D RADAR Metric Scores

10.3.1 T3.2 Rain

THI Rain Real 4D RADAR Data Metric Scores (Target = Car, Distance = 28m) (Red = Lower value equals better quality) (Metric values showing expect trends are bold)						
	SDM	**RMSE**	**MDE**	**MMDE**	**HD**	**HD95**
10mm/h	**0.0960**	24.0276	24.7886	22.7935	**34.4317**	7.4839
25mm/h	**0.1030**	21.7996	23.1031	22.1339	**35.8017**	7.2546
50mm/h	**0.1102**	21.8348	23.2531	22.6334	**38.2687**	8.0810

THI Rain Real 4D RADAR Data Metric Scores (Target = Car, Distance = 56m) (Red = Lower value equals better quality) (Metric values showing expect trends are bold)						
	SDM	**RMSE**	**MDE**	**MMDE**	**HD**	**HD95**
10mm/h	0.1012	**21.7706**	**22.6511**	**21.6649**	33.6681	**7.4314**
25mm/h	0.0856	**22.2279**	**23.3089**	**22.1810**	31.8613	**7.6230**

THI Rain Real 4D RADAR Data Metric Scores (Target = RADAR Calibration Targets, Distance = 28m) (Red = Lower value equals better quality) (Metric values showing expect trends are bold)						
	SDM	**RMSE**	**MDE**	**MMDE**	**HD**	**HD95**
10mm/h	0.1028	23.1067	24.6511	23.7887	34.0010	**7.6026**
25mm/h	0.0859	22.9136	24.0359	23.3059	33.1591	**8.3530**
50mm/h	0.0894	23.8409	25.6005	24.7130	35.4813	**8.4902**

10.3.2 T3.2 Fog

CEREMA Fog Real 4D RADAR Data Metric Scores - Target = Car, Distance = 15m (Red = Lower value equals better quality) (Metric values showing expect trends are bold)						
	SDM	**RMSE**	**MDE**	**MMDE**	**HD**	**HD95**
10m	0.0687	21.2467	21.7609	21.0076	21.1666	7.0854
20m	0.0681	20.6692	21.0828	20.4844	21.7615	7.1443
30m	0.0673	20.8993	21.2416	20.4612	21.4534	7.0866
50m	0.0831	21.2274	21.9808	21.5132	24.2974	8.0446

CEREMA Fog Real 4D RADAR Data Metric Scores - Target = Pedestrian + Bike, Distance = 15m (Red = Lower value equals better quality) (Metric values showing expect trends are bold)						
	SDM	**RMSE**	**MDE**	**MMDE**	**HD**	**HD95**
10m	0.0605	20.6561	21.2630	20.2728	20.7718	7.3712
20m	0.0671	20.3231	21.1241	20.3063	23.3454	7.4493
30m	0.0559	20.6440	21.0377	19.9803	21.9281	7.2849
50m	0.0524	20.8737	21.1230	20.1565	23.1149	7.4436

CEREMA Fog Real 4D RADAR Data Metric Scores - Target = RADAR Targets, Distance = 15m (Red = Lower value equals better quality) (Metric values showing expect trends are bold)						
	SDM	**RMSE**	**MDE**	**MMDE**	**HD**	**HD95**
10m	0.0604	19.3141	19.7053	19.1108	24.4032	7.6214
20m	0.0668	19.8310	20.2655	19.2738	23.9622	7.7500
30m	0.0582	20.4321	20.7456	19.2425	25.7862	7.6988
50m	0.0667	20.3895	20.6103	19.4091	24.6774	7.3913

10.3.3 PDD Snow

PDD Snow Real 4D RADAR Data Metric Scores (Red = Lower value equals better quality) (Metric values showing expect trends are bold)						
	SDM	**RMSE**	**MDE**	**MMDE**	**HD**	**HD95**
Baseline (No Snow)	0.1124	17.6163	19.1400	18.6303	20.3441	4.9212
Light Snow	**0.1048**	**17.8141**	**18.2038**	15.7833	26.3578	6.7144
Heavy Snow	**0.1102**	**19.0295**	**19.1069**	15.6033	23.6963	6.1131

10.3.4 T3.4 Rain

THI – WMG Rain 4D RADAR Model Metric Scores (Target = Car, Distance = 28m) (Red = Lower value equals better quality) (Metric values showing expect trends are bold)						
	SDM	**RMSE**	**MDE**	**MMDE**	**HD**	**HD95**
10mm/h	0.0280	20.2037	18.3911	15.7693	5.1652	1.7404
25mm/h	0.0280	20.0033	18.1682	15.5828	5.1652	1.7404
50mm/h	0.0280	19.9401	18.1866	15.6252	5.1652	1.7404

THI – WMG Rain 4D RADAR Model Metric Scores (Target = Car, Distance = 56m) (Red = Lower value equals better quality) (Metric values showing expect trends are bold)						
	SDM	**RMSE**	**MDE**	**MMDE**	**HD**	**HD95**
10mm/h	0.0280	20.2037	18.3911	15.7693	5.1652	1.7404
25mm/h	0.0280	20.0033	18.1682	15.5828	5.1652	1.7404
50mm/h	0.0280	19.9401	18.1866	15.6252	5.1652	1.7404

10.3.5 T3.4 Fog

THI – WMG Rain 4D RADAR Model Metric Scores (Target = Car, Distance = 28m) (Red = Lower value equals better quality) (Metric values showing expect trends are bold)						
	SDM	**RMSE**	**MDE**	**MMDE**	**HD**	**HD95**
10m	0.0280	20.2080	18.3403	15.6949	5.1652	1.7404
20m	0.0280	20.1612	18.3293	15.6788	5.1652	1.7404
30m	0.0280	20.0158	18.1397	15.5437	5.1652	1.7404
50m	0.0280	20.1512	18.2858	15.6288	5.1652	1.7404

THI – WMG Rain 4D RADAR Model Metric Scores (Target = Car, Distance = 56m) (Red = Lower value equals better quality) (Metric values showing expect trends are bold)						
	SDM	**RMSE**	**MDE**	**MMDE**	**HD**	**HD95**
10m	0.0351	20.8822	19.2400	16.1377	3.1937	1.5851
20m	0.0351	20.8850	19.1815	16.0301	3.1937	1.5851
30m	0.0351	20.9530	19.2223	16.0454	3.1937	1.5851
50m	0.0351	20.7848	19.1014	16.0026	3.1937	1.5851

10.3.6 T3.4 Snow

THI – WMG Snow 4D RADAR Model Metric Scores (Target = Car, Distance = 28m) (Red = Lower value equals better quality) (Metric values showing expect trends are bold)						
	SDM	**RMSE**	**MDE**	**MMDE**	**HD**	**HD95**
1mm/h	0.0280	20.3241	18.4969	15.8059	5.1652	1.7404
19mm/h	0.0280	20.0513	18.2272	15.6013	5.1652	1.7404

THI – WMG Snow 4D RADAR Model Metric Scores (Target = Car, Distance = 56m) (Red = Lower value equals better quality) (Metric values showing expect trends are bold)

	SDM	RMSE	MDE	MMDE	HD	HD95
1mm/h	0.0351	**20.7359**	**19.1456**	**16.0574**	3.1937	1.5851
19mm/h	0.0351	**20.8454**	**19.1885**	**16.0944**	3.1937	1.5851

10.4 Camera depth estimation

A depth map is needed for the camera models. For real world collected images, a modified nddepth algorithm is used (Shao, Oei, Chen, Wu Xingming, & Li, 2023). For the Carla simulation, a depth sensor model is deployed alongside the simulated camera model.

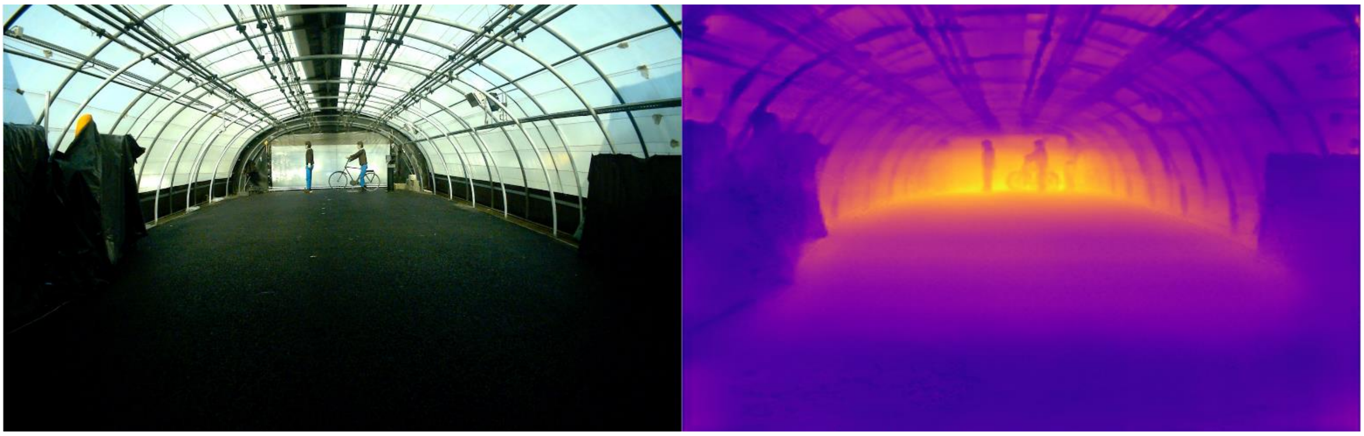

Figure 37: Depth estimated from a real image using nddepth network

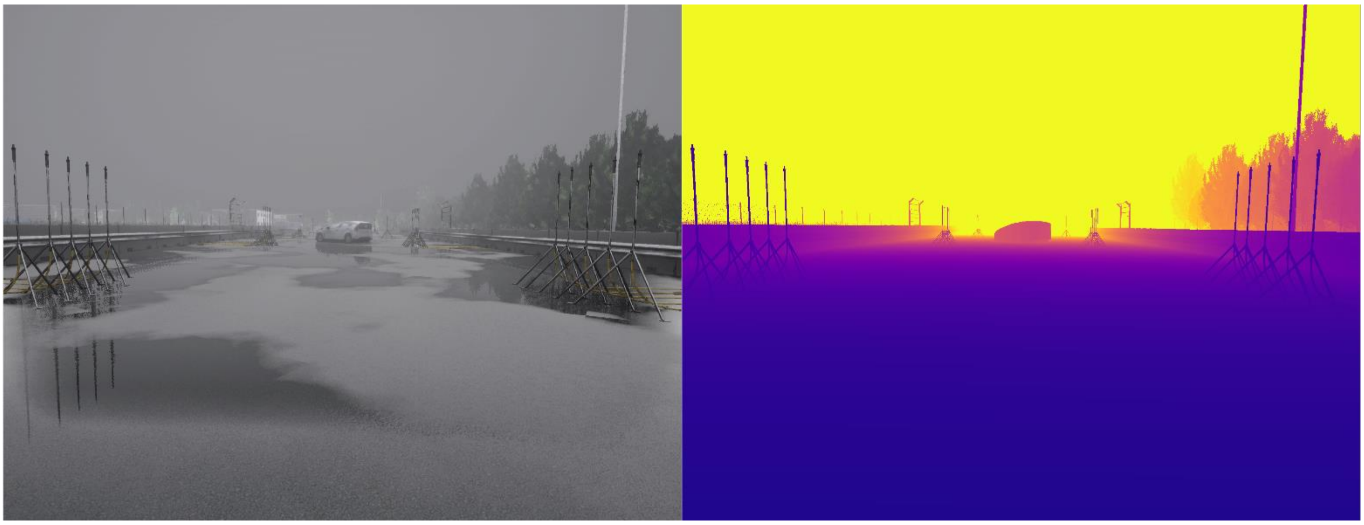

Figure 38: Depth from a depth camera sensor in Carla deployed with the Carla camera sensor